BEDLOAD TRANSPORT IN GRAVEL-BED STREAMS UNDER A WIDE RANGE OF SHIELDS STRESSES

Jaber H. Almedeij

Dissertation submitted to the Faculty of the
Virginia Polytechnic Institute and State University
in partial fulfillment of the requirements for the degree of

Doctor of Philosophy
in
Civil Engineering

Dr. Panayiotis Diplas, Chair
Dr. Clinton Dancey
Dr. G. V. Loganathan
Dr. Yuriko Renardy
Dr. Joseph Schetz

March 28, 2002
Blacksburg, Virginia

Keywords: sediment entrainment, segregation, flow, rivers, mode, pavement

BEDLOAD TRANSPORT IN GRAVEL-BED STREAMS UNDER A WIDE RANGE OF SHIELDS STRESSES

Jaber H. Almedeij

ABSTRACT

Bedload transport is a complicated phenomenon in gravel-bed streams. Several factors account for this complication, including the different hydrologic regime under which different stream types operate and the wide range of particle sizes of channel bed material. Based on the hydrologic regime, there are two common types of gravel-bed streams: perennial and ephemeral. In terms of channel bed material, a gravel bed may have either unimodal or bimodal sediment.

This study examines more closely some aspects of bedload transport in gravel-bed streams and proposes explanations based on fluvial mechanics. First, a comparison between perennial and ephemeral gravel-bed streams is conducted. This comparison demonstrates that under a wide range of Shields stresses, the trends exhibited by the bedload transport data of the two stream types collapse into one continuous curve, thus a unified approach is warranted. Second, an empirical bedload transport relation that accounts for the variation in the make-up of the surface material within a wide range of Shields stresses is developed. The accuracy of the relation is tested using available bedload transport data from streams with unimodal sediment. The relation is also compared against other formulae available in the literature that are commonly used for predicting bedload transport in gravel-bed streams. Third, an approach is proposed for transforming the bimodal sediment into two independent unimodal fractions, one for sand and another for gravel. This transformation makes it possible to carry out two separate computations of bedload transport rate using the bedload relation developed in this study for unimodal sediment. The total bedload transport rate is estimated by adding together the two contributions.

ACKNOWLEDGMENTS

I would like to express my deep gratitude to my advisor, Dr. Panayiotis Diplas, for his contributions, discussions, and critical comments. Without his patience and support, it would not have been possible to complete this research.

I would like also to thank Dr. Clinton Dancey, Dr. G. V. Loganathan, Dr. Yuriko Renardy, and Dr. Joseph Schetz for serving on my committee and giving their encouragement.

I would like also to extend my thanks to Dr. Michael Renardy, who provided valuable comments.

The financial support of this work by Kuwait University is gratefully acknowledged.

I dedicate this work to my parents, my wife Tahani Alrumaidhi, and my children Raghad and Fawaz. I am indebted to them for their unlimited support, sacrifices, patience, and unwavering love throughout the course of this work.

TABLE OF CONTENTS

LIST OF TABLES

LIST OF FIGURES

Chapter 1: Introduction

Gravel-bed streams have features that distinguish them from sand-bed streams and create challenging problems for their analysis. One of the main features is the channel bed material. In sandy streams, the bed material tends to be more uniform in size, while in gravel-bed streams it is typically poorly sorted. Furthermore, the channel bed material in the former does not exhibit any vertical segregation in terms of grain size, but gravel-bed streams typically have a surface material overlying a finer subsurface. Although the surface layer contains all the grain sizes available in the subsurface material, the larger grains are present in significantly higher proportions.

Gravel-bed streams can be classified in terms of stream type and channel bed material. There are two common types of gravel-bed streams: perennial and ephemeral. Perennial streams, typical of humid environments, convey water throughout the year, while ephemeral streams, commonly found in arid and semiarid environments, discharge water infrequently, during flood events. In terms of channel bed material, a gravel bed may have either unimodal or bimodal sediment. The former has a grain size distribution with only one mode, but the latter has two prominent modes, one of sand size and the other of gravel size.

This variability in gravel-bed streams makes the prediction of bedload transport rates a difficult task. Despite the plethora of available bedload transport relations, there is still considerable controversy over their performance. For example, the choice of the representative grain size parameter in a gravel bedload transport relation is still a subject of debate. Whether the median or any other statistical parameter is used, the choice is questionable if no distinction is made between the bed surface and subsurface materials. The bimodal distribution found in some bed materials complicates the problem even further because of the presence of two sediment fractions, sand and gravel, both of which might be described with a representative particle size.

This study focuses on bedload transport in gravel-bed streams under a wide range of Shields stresses. The study examines the behavior of the transported material on a gravel bed under conditions starting from a low water discharge, typically found in perennial streams, to the much higher discharges found during infrequent flood events common to ephemeral streams. Furthermore, this study explores bedload transport data from gravel-bed streams with unimodal and bimodal sediments.

1.1 Objectives

This study has the following main objectives:

- Investigate bedload transport in perennial and ephemeral gravel-bed streams, propose an explanation based on fluvial mechanics for the observed differences between them, and attempt to unify their bedload data into a general trend of bedload transport;
- Investigate bedload transport in gravel-bed streams with unimodal sediment, and propose a new bedload transport relation; and
- Investigate bedload transport in gravel-bed streams with bimodal sediment, and propose an approach for predicting their transport rates.

1.2 Dissertation Outline

The dissertation is organized into three main chapters that are separate papers focusing in detail on the various issues involved in gravel bedload transport. In the first paper (Chapter 2: *Streambed structure and bedload transport: A unified approach for perennial and ephemeral gravel-bed streams*), apparent differences between perennial and ephemeral gravel-bed streams are classified into streambed structure and bedload transport efficiency. The bed structure of perennial streams is segregated by grain size into a surface that is coarser than the subsurface material, while in some ephemeral streams the reverse phenomenon occurs, with a layer of finer material overlying a coarser sediment. An explanation for the formation of the finer surface layer is given with reference to a mechanical process. On the other hand, available bedload transport data sets indicate that the two stream types exhibit a different bedload transport efficiency, which is attributed to the difference found in channel bed structure. Notwithstanding this, the study demonstrates that in terms of a dimensionless presentation of the data, the lower magnitudes of flows in some ephemeral channels overlap with the higher magnitudes of flows in perennial channels, thus suggesting that bedload transport data from both stream types might form a continuum.

In the second paper (Chapter 3: *Bedload transport in gravel-bed streams with unimodal sediment*), an empirical bedload transport relation for gravel-bed streams is proposed. It is suggested that the choice of the mode as the representative grain size of bed material provides better calculations for bedload transport rates. Available bedload data sets from gravel-bed streams with unimodal sediment are used to test the accuracy of the relation. A comparison with other bedload transport relations commonly used for gravel-bed streams is also considered.

The third paper (Chapter 4: *Bedload transport analysis in gravel-bed streams with bimodal sediment*) shows that the presence of the two modes in a bimodal sediment complicates the bedload transport rate predictions even further, because one mode may have influence on the mobility of the other. An approach is proposed for rendering the bimodal sediment into two independent unimodal fractions, of sand and gravel. This is a possible approach to calculate bedload transport rates for each sediment fraction separately. The total bedload transport rate can be estimated by adding together the two computations.

Chapter 2: Streambed Structure and Bedload Transport: A Unified Approach for Perennial and Ephemeral Gravel-Bed Streams

2.1 Abstract

Perennial gravel-bed streams typically possess a surface bed layer that is coarser than the subsurface material. Recent observations have indicated that this coarser surface layer is absent from some ephemeral gravel-bed streams and that in some other cases the reverse phenomenon occurs, with a layer of finer material overlying coarser sediment. Another difference is the considerably higher efficiency exhibited by the ephemeral in transporting sediment. This study provides an explanation for the formation of the finer surface layer of ephemeral streams with reference to a mechanical process of grain size segregation and suggests a unified approach to bedload transport for both stream types. It is advocated that the mechanisms responsible for these features distinguishing ephemeral from perennial streams are interrelated and that they are triggered by the significantly different hydrologic regime under which the two stream types operate.

2.2 Introduction

Perennial gravel-bed streams typically possess a surface layer that is coarser than the immediate subsurface material [*Parker and Klingeman*, 1982; *Andrews and Parker*, 1987; *Sutherland*, 1987]. Although the coarser surface layer, called pavement [*Parker*, 1980], contains all the grain sizes available in the subsurface, the larger grains are present in significantly higher proportions [*Parker et al.*, 1982; *Diplas*, 1987]. This vertical segregation of grain sizes causes problems regarding the choice of the appropriate layer to be used as a basis for sediment transport rate calculations [e.g., *Parker*, 1990]. Recent observations from ephemeral gravel-bed streams have complicated the picture even further. In some cases, the reverse phenomenon occurs, with a layer of finer material overlying coarser sediment [*Reid et al.*, 1995; *Laronne et al.*, 1994]. Ephemeral streams are commonly found in arid and semiarid zones; high intensity and short duration thunderstorms often result in rapid and short-lived runoff in these locations [e.g., *Wheater et al.*, 1991]. Since the groundwater table is below the streambed, they do not experience any recharge to support a base flow; instead, they suffer transmission losses. As a result, ephemeral streams remain dry except for brief periods of time, during flood events.

Several researchers have emphasized the differences between perennial and ephemeral gravel-bed streams and have suggested that both stream types exhibit different behavior [e.g., *Laronne and Reid*, 1993; *Reid and Laronne*, 1995]. *Reid and Laronne* [1995] observed that, under the same flow conditions, the ephemeral stream has significantly higher unit bedload transport rates than other stream types. *Reid et al.* [1996] compared a number of bedload transport equations, derived using data obtained mainly from perennial streams and laboratory experiments, against a set of field data collected during flash floods from Nahal Yatir, an ephemeral stream in Israel [*Reid et al.*, 1995]. They found that the Meyer-Peter and Muller equation is the only one that performs well, while the other formulas exhibit trends that are not in agreement with the trend shown by the Nahal Yatir data. This was related to the apparent abundance of sediment supply typically found within the ephemeral channel system. *Laronne and Reid* [1993], *Reid et al.* [1997], and *Powell et al.* [1998] have suggested that the increased sediment supply in ephemeral streams discourages the formation of a pavement layer and, instead, causes fining of the bed surface material. This process of surface fining suggested for ephemeral streams is basically similar to that experienced by perennial streams, where coarsening of the surface develops from the local imbalance of sediment input and ability of the stream to transport higher amounts of bedload [*Dietrich et al.*, 1989]. However, given the different hydrologic conditions under which the two stream types operate, it might be expected that the processes responsible for the finer surface material in ephemeral streams are not similar to the processes that coarsen the surface bed material in perennial streams.

The present study examines closely the apparent differences between perennial and ephemeral gravel-bed streams in terms of streambed structure and bedload transport. The streambed structure is investigated using a dimensionless expression for stream power, while the bedload transport is examined using the Shields stress parameter. An explanation for the formation of the finer surface layer of ephemeral streams is provided with reference to a mechanical process of particle size segregation. This study also suggests that in terms of dimensionless parameters, bedload data from both stream types might actually be parts of the same overall curve relating bedload transport rate to increasing bed shear stress. The change in the dimensionless parameters, of stream power and shear stress, is responsible for the differences observed in the field.

2.3 Streambed Structure

2.3.1 Pavement in perennial streams

Observations from field studies and laboratory experiments indicate that the pavement layer in perennial gravel-bed streams is typically as thick as the diameter of the D_{90} particle size [e.g., *Petrie and Diplas*, 2000] (Figure 2.1a). Owing to their higher inertia, the coarse grains of the pavement protect the subsurface material during low to medium strength bed shear stresses. Also, in some cases, the coarse surface grains form clusters, which further enhance the stability of the pavement layer and, therefore, provide additional protection for the subsurface material [e.g., *Brayshaw et al.*, 1983]. As shear stress increases, however, the coarser grains of the surface material are entrained and, for sufficiently high shear stress values, the surface will eventually approach the composition of the subsurface material [*Diplas*, 1992]. However, shear stresses in perennial gravel-bed streams modestly exceed the critical shear stress value [e.g., *Parker et al.*, 1982; *DeVries*, 2000]. It is only during very infrequent flood events that the shear stresses experienced by the channel bed become two to three times as high as the critical value [*Parker et al.*, 1982].

There are two main mechanisms involved in the development of the pavement layer of perennial gravel-bed streams: vertical winnowing and selective transport of particle sizes [*Parker and Klingeman*, 1982]. Vertical winnowing is the mechanism of segregating the finer grains located on the surface layer into the subsurface, by falling through the crevices created by the larger particles of the pavement, thus resulting in a subsurface material that is rich in fine grains [*Parker and Klingeman*, 1982; *Diplas and Parker*, 1992]. This mechanism resembles the mechanical shaking or vibration of a bucket filled with a material of different particle sizes, a phenomenon termed the "Brazil nuts effect" [*Rosato et el.*, 1987]. Herein, owing to their larger size, the Brazil nuts remain on top, while the smaller nuts find their way to the bottom of a can containing mixed sizes of nuts.

Selective transport of particle sizes is a response to the imbalance between sediment supply from upstream and stream sediment transport capacity [*Dietrich et al.*, 1989]. If the sediment supply is less than the ability of the stream to transport bedload, the balance of the sediment load has to be provided from the bed itself. Owing to the nonuniformity of bed materials, for low to moderate shear stresses, the finer particles are transported at a higher proportion than the coarser particles [*Parker and Klingeman*, 1982; *Diplas*, 1987]. This increases the proportion of the coarser grains on the surface and results in a pavement layer coarser than the subsurface material. As sediment supply from upstream continues to decrease, the pavement layer coarsens further, until it eventually reaches an ultimate coarsening state of the surface material. This upper limit behavior has been suggested by *Chin* [1985], who showed that the degree of the surface coarsening has a limiting value equal to $D_{\max} / D_{50s} = 1.8$; where $D_{\max}$ is the coarsest particle size, and D_{50s} is the median grain size of the surface material.

At shear stresses capable of mobilizing the coarser grains, the pavement layer tends to become finer. Based on the model suggested by *Dietrich et al.* [1989], the finest possible state of the surface material is attained when $D_{50s} / D_{50sub} = 1$ [see Figure (3) in *Dietrich et al.*, (1989)]; where D_{50sub} is the median grain size of the subsurface material. This state is reached during high bedload transport rates when the condition of equal mobility prevails—the condition at which all particle sizes are transported at rates proportional to their presence in the bed material [*Parker et al.*, 1982; *Diplas*, 1992]. This is the behavior at the other limit of perennial gravel-bed streams during the passage of rare floods.

An example of a perennial stream possessing a well-developed pavement layer is Oak Creek in Oregon [*Milhous*, 1973]. Oak Creek is a small, steep mountain stream with D_{50s} / D_{50sub} equal to 2.7 (Table 2.1). It is worth mentioning that among the 66 filed measurements of bedload transport rates reported by *Milhous* [1973], only few of them were obtained at Shields stress values exceeding 0.03. Below this value, the process of selective transport dominates, with the finer particle sizes being transported through the reach at a higher rate than the coarser grains [*Diplas*, 1987].

2.3.2 Segregation in ephemeral streams

Field observations from some ephemeral gravel-bed streams depict a bed material with the opposite particle size segregation found in perennial gravel-bed streams, i.e., the coarser sediment located underneath a finer surface layer (Figure 2.1b). For example, in Nahal Yatir, which drains a catchment of 19 km^2 [*Reid et al.*, 1995], the D_{50s} / D_{50sub} ratio is equal to 0.6 (Table 2.1).

Attempts have been made to explain the existence of the finer surface layer of ephemeral streams by extending the *Dietrich et al.* model [e.g., *Laronne and Reid*, 1993; *Powell et al.*, 1998]. However, mass balance arguments can be used to demonstrate that such an approach requires that the coarser grains must be transported in proportions that are higher than those available in the bed material. This bedload transport pattern violates the presently accepted condition of equal mobility during very high shear stresses [*Parker et al.*, 1982; *Diplas*, 1987]. Another difference between ephemeral and perennial streams mentioned here is the thickness of the top layer. In the latter case, the coarser surface layer is typically considered to be as thick as D_{90}, while the thickness of the finer surface layer found in some ephemeral streams typically scales with the maximum scour depth. For example, the measured thickness of the surface layer in Nahal Yatir was reported to be closer to $3\,D_{90}$ [*Reid et al.*, 1995]. This thickness coincides with the maximum depth of scour determined through the use of chains [*Reid et al.*, 1995]. Consequently, it can be surmised that this observed bed structure of ephemeral streams might have resulted from a different mechanism than that responsible for the pavement development in perennial streams.

The most likely interpretation comes from another mechanism of particle size segregation. As mentioned earlier, when a material of different particle sizes is shaken, the coarse particles are found near the top, but the finer particles near the bottom. However, the reverse size stratification occurs when simply pouring the material onto a pile [e.g., *Makse et al.*, 1997]. In this case, the fine particles are found near the top of the pile, while the coarser particles near the bottom. As reported by *Makse et al.* [1997], this segregation mechanism is controlled by the angle of repose of sediment particles. The angle of repose is larger for more angular and for larger grains. The particle with the larger angle of repose will have the tendency to settle closer to the bottom.

It is proposed here that the same mechanism is responsible for the bed structure observed in some ephemeral gravel-bed streams. During flood events, the flood rises very quickly and similarly it drops quickly to very low water discharges. In Nahal Eshtemoa, for instance, an ephemeral stream in Israel, *Reid et al.* [1994] reported that the flood bore generated during a rainfall event reached a depth of 0.9 m within three minutes, then the bore declined for about an hour, and after that the flow depth increased dramatically by up to $0.25\ \text{m min}^{-1}$ to a maximum depth of 2.5 m. Here, the high shear stresses result in massive sediment transport and considerable scour and fill of the riverbed. Scour typically occurs during the rising limb of the hydrograph and filling during the falling limb [*Leopold et al.*, 1966]. This process resembles the removal and depositing of a large amount of bed material. Given that the sediment particles of natural streambeds have nearly the same particle shape [*Bagnold*, 1973], it can be expected that the grain size will trigger the segregation process, with the larger grains located near the bottom of the entrained layer.

The mechanism of size segregation can be investigated using stream power

$$\omega = \frac{\rho g Q S}{B} = \tau_0 U \tag{2.1}$$

in which ω is the specific stream power per unit width, ρ is the water density, g is the gravitational acceleration, Q is the water discharge, S is the energy slope, B is the channel width, τ_0 is the bed shear stress, and U is the average water velocity. As shear stress, water velocity, or both increase, more stream power becomes available for rearranging the channel bed material. This most likely influences both the amount of the segregated material in the channel bed and the burial depth of coarse grains.

Hassan [1990] placed magnetically-tagged coarse particles, with sizes ranging from 45 to 180 mm, in Nahal Hebron and Nahal Og (Table 2.2), two ephemeral gravel-bed streams in Israel, and traced their location following the passage of several floods. The percent of tagged particles that was found buried within the bed material is plotted in Figure (2.2a) against the stream power of the corresponding flood event. For both streams, the tagged particles are coarser than the median grain sizes of the surface and subsurface materials. It can be seen that as the stream power increases, the percent of buried particles increases until it approaches 70% and 90% of the tagged particles for Nahal Hebron and Nahal Og, respectively. However, if the stream power is relatively low, then the coarse grains will remain on the surface. It is interesting to mention that the median grain size of the surface material, as well as of the subsurface, is almost identical in these two streams [*Hassan*, 1990]. The fact that the bed surface material in Nahal Hebron is well packed, filled with fine matrix, while the packing in Nahal Og is poor, could possibly explain the consistently higher percentage of buried particles observed in Nahal Og. This condition allows the riverbed in Nahal Og to be scoured more easily and the loose particles of the material to segregate according to size, with the coarser grains located near the bottom of the entrained layer. Figure (2.2b) shows the influence of the stream power on the burial depth of the coarse tracers in Nahal Og. As can be seen, the burial depth is a good estimate of the depths of streambed scour and fill.

2.3.3 Stream power and streambed structure

Observations and measurements of scour depth from ephemerals discussed in the previous section suggest that stream power could be used as a means of describing the bed structure of streams. The well-paved Oak Creek and the unpaved Nahal Yatir can be used to perform this comparison since they represent two extreme cases [*Reid and Laronne*, 1995]. Using Equation (2.1), the range of stream power for Oak Creek is estimated to be between $\omega \approx 3.54$ and 93.77 $\mathrm{kg\,s^{-3}}$, and for Nahal Yatir between 7.15 and 105.75 $\mathrm{kg\,s^{-3}}$. The dimensional form of stream power is suitable for comparing two streams possessing the same bed material; However, for streams having different bed composition, a dimensionless form of stream power that takes into consideration the size and specific gravity of the particles present in the material will be more appropriate. One way to express such a dimensionless parameter is the following:

$$\omega^* = \frac{\tau_0 U}{\gamma_s \sqrt{R_s g D_{50s}^3}} = \frac{\omega}{\gamma_s \sqrt{R_s g D_{50s}^3}} \tag{2.2}$$

where ω^* is the dimensionless stream power, γ_s is the specific weight of sediment, and R_s is the submerged specific gravity of the sediment. While simpler expressions for the denominator, such as $(\gamma_s - \gamma)\sqrt{gD_{50s}^3}$, could be used to nondimensionalize ω, the expression in Equation (2.2) is more appropriate for unifying the data for the various forms of stream power found in the literature. The range of dimensionless stream power values for Oak Creek becomes 0.002188 to 0.058 and for Nahal Yatir 0.158 to 2.336. These results suggest that the flash floods in some ephemeral streams generate much higher values of dimensionless stream power, compared to those encountered in most perennial streams.

Based on the limited number of data sets obtained from the literature, a conceptual model that describes the variation of the bed structure of perennial and ephemeral gravel-bed streams in terms of ω^* is proposed here (Figure 2.3). As can be seen, a plethora of coarse particles populate the surface layer during very low ω^* values, when the sediment supply from upstream is limited, resulting in $D_{50s} / D_{50sub} > 1$ (from A to C). As ω^* increases, coarser grains are entrained, and the surface material becomes finer. However, in perennial streams, D_{50s} is not expected to become finer than D_{50sub}. D_{50s} reaches its minimum value of $D_{50s} / D_{50sub} = 1$, when eventually the condition of equal mobility prevails under relatively high bedload discharges (from C to D). In some ephemeral gravel-bed streams, the surface layer is expected to approach the subsurface material first [*Powell et al.*, 2001], as seen from B to D ($D_{50s} / D_{50sub} \geq 1$), before considerable scouring of the bed occurs. The scour depth increases as ω^* increases, and coarser grains are removed and re-deposited on the channel bed. This encourages the coarser particles to segregate into the subsurface; therefore, D_{50s} / D_{50sub} decreases until it becomes < 1 (from D to E). As the scour depth continues to increase, the coarse grains deposit deeper into the channel bed.

2.4 Bedload Transport

Once a streambed is paved, the subsurface material becomes protected from entrainment until the pavement layer is broken up. In the process, the pavement influences the rate and the composition of the transported material. This section provides an analysis of the complex response of pavement material to changes in hydraulic conditions during this process.

2.4.1 Median bedload grain size variation

The influence of the pavement material on bedload transport can be investigated by considering the variation of the median grain size of bedload, D_{L50}, within a wide range of Shields stresses. The Shields stress based on the median diameter of subsurface material, τ_{50}^*, is obtained from the following well-known expression:

$$\tau_{50}^{*}=\frac{\tau_0}{(\gamma_s-\gamma)D_{50sub}} \tag{2.3}$$

where, γ is the specific weight of water. τ_{50}^{*} is normalized by dividing it by the reference Shields stress τ_{r50}^{*}

$$\phi_{50}=\frac{\tau_{50}^{*}}{\tau_{r50}^{*}} \tag{2.4}$$

where ϕ_{50} is the normalized Shields stress, $\tau_{r50}^{*}=\tau_r/(\gamma_s-\gamma)D_{50sub}$, and τ_r is a reference shear stress. τ_{r50}^{*} corresponds to a specified, very low sediment transport rate below which the bedload transport rate is of no practical importance [*Paintal*, 1971; *Parker et al.*, 1982].

The bedload data of Oak Creek [*Milhous*, 1973] is used here to investigate the variation of D_{L50} with ϕ_{50}. For this data set, *Diplas* [1987] suggested that $\tau_{r50}^{*}=0.0873$. In Figure (2.4), the median grain size of the subsurface material of Oak Creek, a constant, is divided by the median grain size of bedload, D_{50sub}/D_{50L}, and plotted as a function of the normalized Shields stress ϕ_{50}. As can be seen, when the normalized Shields stress is less than 0.6, the pavement material remains in place, with transported sediment dominated by the finer grains. As a result, the median grain size of bedload material is approximately constant and considerably smaller than the median grain size of subsurface material. At $\phi_{50}\approx 0.6$, the pavement material starts dismantling and D_{50L} becomes gradually coarser until it eventually matches the value of D_{50sub} at $\phi_{50}\approx 1.2$. Here, the condition of equal mobility with regard to the subsurface material is reached. Owing to the lack of field data, it is difficult to know the behavior of D_{50L} for higher values of ϕ_{50}. Based on a hypothetical model that he proposed, *Diplas* [1987] suggested that if the normalized Shields stress exceeds 1.2, then D_{50L} would become coarser than D_{50sub}. D_{50L} would reach its coarsest value at $\phi_{50}\approx 2.0$, and then gradually decline until it again matches the subsurface value for $\phi_{50}\geq 4.0$. Here, the pavement is expected to be entirely broken and D_{50L} will be equal to D_{50sub} and D_{50s}, which is the condition of equal mobility with regard to both surface and subsurface materials. The implication is that beyond this point, and before ϕ_{50} becomes very high, there is no pavement present.

In some ephemeral gravel-bed streams, the Shields stress values generated during flood events significantly exceed the value that represents the upper equal mobility condition ($\phi_{50} \approx 4.0$). Based on the model proposed in Figure (2.3), the coarser grains will be deposited deeper into the subsurface, and the finer grains will be exposed on the surface layer. It follows that the finer surface material will be transported efficiently downstream, and D_{50L} will be equal to D_{50s}. In Nahal Yatir, for example, *Reid et al.* [1995] found that the bedload grain size distribution during the passage of four effective floods did not change and that the D_{50L} value was equal to exactly that of the surface material.

2.4.2 General trend of bedload transport

A comparison between the data of Oak Creek and Nahal Yatir reveals more clearly the influence of the pavement layer on the bedload transport rate. The bedload data are plotted in Figure (2.5) as a function of the bed shear stress, τ_0,

$$\tau_0 = \rho g d S \tag{2.5}$$

where d is the flow depth. Undoubtedly, for the same range of shear stresses, Nahal Yatir has much higher bedload transport rates than Oak Creek. However, in the latter stream, the rate of change of bedload transport with increasing shear stress is higher than that in the former. Curves fitted to groups of data points provide more details (Figure 2.5). It can be seen that the beginning (ending) slope of the Oak Creek data is about four (two) times greater than the beginning slope of the Nahal Yatir data. This result suggests that the two streams exhibit completely different behavior, which coincides with the opinion of various authors [e.g., *Laronne and Reid*, 1993; *Reid and Laronne*, 1995; *Powell et al.*, 2001]. However, given the difference in the structure of bed material, it seems that a comparison based on dimensionless plots of bedload and shear stress will constitute a more suitable basis for comparison.

Figure (2.6) includes the same measured bedload transport rates shown in Figure (2.5) but in dimensionless form

$$q_B^* = \frac{q_B}{\sqrt{R_s g D_{50s}^3}} \tag{2.6}$$

where q_B^* is the Einstein bedload parameter, and q_B is the volumetric bedload transport rate per unit channel width. The bed shear stress is expressed as

$$\tau^* = \frac{\tau_0}{(\gamma_s - \gamma) D_{50s}} \tag{2.7}$$

where τ^* is the Shields stress parameter based on the surface material. It appears that the data points of Oak Creek and Nahal Yatir might be parts of the same overall curve relating the bedload transport rate to shear stress. The Oak Creek data represents the lower end of this relation, while the Nahal Yatir data covers conditions at much higher Shields stresses.

To demonstrate the trends, two different empirical equations are presented as follows:

$$q_B^* = 10^{9.7} \ \tau^{*\ 9.6063} \tag{2.8}$$

and

$$q_B^* = 10^{0.85333(D_{50s}/D_{50sub})^{2.437}} \ \tau^{*\ \ 1.85(D_{50s}/D_{50sub})^{1.642}} \tag{2.9}$$

Equation (2.8) was fitted by log-linear regression using only the Oak Creek data with a constant value of D_{50s}, equal to 54 mm (Table 2.1). This assumption of a constant D_{50s} value is not appropriate for a wide range of Shields stresses ($\phi_{50} \geq 1.2$) because of the variation of D_{50s} with increasing values of τ^*. Therefore, Equation (2.8) does not match the Nahal Yatir data, as seen in Figure (2.6). On the other hand, Equation (2.9), which was fitted by log-linear regression using both data sets of Oak Creek and Nahal Yatir, takes into account the variation of D_{50s} with respect to D_{50sub} and τ^*. This relationship can adequately describe both data sets. The implication here is that accounting for the variation of D_{50s}/D_{50sub} within a wide range of Shields stresses has the potential of unifying bedload data from different gravel-bed streams, even those operating under different hydrologic conditions.

2.4.3 *Bedload transport efficiency*

Given the measured bedload transport and stream power values, the bedload transport efficiency, e_b, of Oak Creek and Nahal Yatir can be examined. This provides the opportunity to investigate the bedload data using the suggested dimensionless expression of stream power, ω^*, (Equation 2.2).

The transport efficiency is calculated using *Bagnold's* [1973] equation

$$e_b = \frac{100 q_B}{(\omega / \tan\alpha)} \tag{2.10}$$

where both q_B and ω are presented here in the above equation in terms of mass per unit channel width and unit time, and α is the angle of internal friction; $\tan\alpha$ is considered a constant equal to 0.63 [*Bagnold*, 1973]. This equation can be rewritten using the parameters ω^* and q_B^* as

$$e_b = \frac{100 \dfrac{q_B}{\sqrt{R_s g D_{50s}^3}}}{\dfrac{(\omega / \tan\alpha)}{\gamma_s \sqrt{R_s g D_{50s}^3}}} = \frac{100 q_B^*}{(\omega^* / \tan\alpha)} \tag{2.11}$$

Figure (2.7a) presents the bedload data of the two streams in terms of ω and q_B, similar to the way that was plotted by *Reid and Laronne* [1995]. Figure (2.7b) presents the same comparison, but in terms of ω^* and q_B^*. Obviously, either plot provides the same range of efficiency values for Oak Creek and for Nahal Yatir and shows that the latter stream is more efficient than the former (Table 2.1). However, Figure (2.7a) suggests that both streams exhibit completely different behavior, while Figure (2.7b) suggests that the two data sets form a continuum. Obviously, the advantage is similar to that plotting bedload data against dimensional and dimensionless shear stress.

2.5 Conclusion

Available data from perennial and ephemeral gravel-bed streams were used to highlight apparent differences between them and propose explanations based on fluvial mechanics. The study has discussed two main differences: streambed structure and bedload transport. The bed structure in perennial gravel-bed streams has a pavement layer overlying a finer subsurface material, while in some ephemeral gravel-bed streams the reverse phenomenon occurs, with coarse material buried under finer sediment. This type of segregation in ephemeral streams may be resulted from the considerable scour and fill reported in these locations. A dimensionless expression for stream power, ω^*, has been suggested to account for this difference.

Comparing the bedload transport rates of Oak Creek and Nahal Yatir has revealed that the two stream types exhibit different bedload transport efficiency, attributed to the difference found in bed structure. Notwithstanding this, it has been suggested that the two data sets might actually be parts of the same overall curve relating bedload transport rate to increasing bed shear stress. Consideration should be given to the variation of D_{50s} / D_{50sub} within a wide range of Shields stresses.

References

Andrews, E. D., and G. Parker, Formation of a coarse surface layer as the response to gravel mobility, in *Sediment Transport in Gravel-Bed Rivers*, edited by C. R. Thorne, J. C. Bathurst, and R. D. Hey, pp. 269-300, John Wiley, New York, 1987.

Bagnold, R. A., The nature of saltation and of bed-load transport in water, *Proc. Roy. Soc.*, *Ser.*, *A332*, 473-504, 1973.

Brayshaw, A. C., L. E. Frostick, and I. Reid, The hydrodynamics of particle clusters and sediment entrainment in coarse alluvial channels, *Sedimentol.*, *30*, 137-143, 1983.

Chin, C. O., Stream bed armouring, *Rep. No. 403*, Dept. Civ. Eng., Univ. of Auckland, New Zealand, 1985.

DeVries, P. E., Scour in low gradient gravel bed rivers: Patterns, processes, and implications for the survival of salmonid embryos, unpublished Ph.D. thesis, Univ. of Washington, Seattle, 2000.

Dietrich, W. E., J. W. Kirchner, H. Ikeda, and F. Iseya, Sediment supply and the development of the coarse surface layer in gravel-bedded rivers, *Nature*, *340*, 215-217, 1989.

Diplas, P., Bedload transport in gravel-bed streams, *J. Hydraul. Engng., Am. Soc. Civ. Eng.*, *113*(3), 277-291, 1987.

Diplas, P., Equal mobility versus changing bedload grain sizes in gravel-bed streams, Discussion, in *Dynamics of Gravel-Bed Rivers*, edited by P. Billi, R. D. Hey, C. R. Thorne, and P. Tacconi, pp. 131-135, John Wiley, New York, 1992.

Diplas, P., and G. Parker, Deposition and removal of fines in gravel-bed streams, in *Dynamics of Gravel-Bed Rivers*, edited by P. Billi, R. D. Hey, C. R. Thorne, and P. Tacconi, pp. 313-329, John Wiley, New York, 1992.

Hassan, M. A., Scour, fill, and burial depth of coarse material in gravel bed streams, *Earth Surf.* Processes Landforms, 15, 341-356, 1990.

Laronne, J. B., and I. Reid, Very high rates of bedload sediment transport by ephemeral desert rivers, *Nature*, *366*, 148-150, 1993.

Laronne, J. B., I. Reid, Y. Yitshak, and L. E. Frostick, The non-layering of gravel streambeds under ephemeral flood regimes, *J. Hydrol.*, *159*, 353-363, 1994.

Leopold, L. B., W. W. Emmett, and R. R. Myrick, Channel and hillslope processes in a semiarid area, New Mexico, U.S. Geol. Surv. Prof. Pap., 352, 1966.

Makse, H. A., S. Havlin, P. R. King, and H. E. Stanley, Spontaneous stratification in granular mixtures, *Nature*, *386*, 379-382, 1997.

Milhous, R. T., Sediment transport in a gravel-bottomed stream, unpublished Ph.D. thesis, Oregon State Univ., Corvallis, 1973.

Paintal, A. S., Concept of critical shear stress in loose boundary open channels, *J. Hydraul. Res.*, *9*(1), 91-113, 1971.

Parker, G., Armored versus paved gravel beds, Discussion, *J. Hydraul. Div. Am. Soc. Civ. Eng.*, *106*(HY11), 1120-1121, 1980.

Parker, G., Surface-based bedload transport relation for gravel rivers, *J. Hydraul. Res.*, *28*(4), 417-436, 1990.

Parker, G., and P.C. Klingeman, On why gravel bed streams are paved, *Water Resour. Res.*, *18*(5), 1409-1423, 1982.

Parker, G., P. C. Klingeman, and D. G. McLean, Bedload and size distribution in paved gravel bed streams, J. Hydraul. Div. Am. Soc. Civ. Eng., 108(HY4), 544-569, 1982.

Petrie, J., and P. Diplas, Statistical approach to sediment sampling accuracy, *Water Resour. Res.*, *36*(2), 597-605, 2000.

Powell, D. M., I. Reid, J. B. Laronne, and L. E. Frostick, Cross-stream variability of bedload flux in narrow and wider ephemeral channels during desert flash floods, in *Gravel-Bed Rivers in the Environment*, edited by P. C. Klingeman, R. L. Beschta, P. D. Komar, and J. B. Bradley, pp. 177-196, Water Resources Publications, Colorado, 1998.

Powell, D. M., I. Reid, and J. B. Laronne, Evolution of bed load grain size distribution with increasing flow strength and the effect of flow duration on the caliber of bed load sediment yield in ephemeral gravel bed rivers, *Water Resour. Res.*, *37*(5), 1463-1474, 2001.

Reid, I., and J. B. Laronne, Bed load sediment transport in an ephemeral stream and a comparison with seasonal and perennial counterparts, *Water Resour. Res.*, *31*(3), 773-781, 1995.

Reid, I., D. M. Powell, J. B. Laronne, and C. Garcia, Flash floods in desert rivers: studying the unexpected, *EOS Trans. AGU*, *75*(39), 452, 1994.

Reid, I., J. B. Laronne, and D. M. Powell, The Nahal Yatir bedload database: sediment dynamics in a gravel-bed ephemeral stream, *Earth Surf. Processes Landforms*, *20*, 845-857, 1995.

Reid, I., D. M. Powell, and J. B. Laronne, Prediction of bed-load transport by desert flash floods, *J. Hydraul. Eng.*, *122*(3), 170-173, 1996.

Reid, I., J. C. Bathurst, P. A. Carling, D. E. Walling, and B. W. Webb, Sediment erosion, transport and deposition, in *Applied Fluvial Geomorphology for River Engineering and Management*, edited by C. R. Thorne, R. D. Hey, and M. D. Newson, pp. 95-135, John Wiley, New York, 1997.

Rosato, A., K. J. Strandburg, F. Prinz, and R. H. Swendsen, Why the Brazil nuts are on top: size segregation of particulate matter by shaking, *Phs. Rev. Lett.*, *58*(10), 1038-1040, 1987.

Sutherland, A. J., Static armour layers by selective erosion, in *Sediment Transport in Gravel-Bed Rivers*, edited by C. R. Thorne, J. C. Bathurst, and R. D. Hey, pp. 243-267, John Wiley, New York, 1987.

Wheater, H. S., A. P. Butler, E. J. Stewart, and G. S. Hamilton, A multivariate spatial-temporal model of rainfall in southwest Saudi Arabia. I. spatial rainfall characteristics and model formulation, *J. Hydrol.*, *125*, 175-199, 1991.

Notation

B	Channel width, [L]
D_{50sub}	Median grain size of the subsurface, [L]
D_{90}	Particle grain size for which 90 percent of all particles are smaller, [L]
D_{50L}	Median grain size of the bedload, [L]
$D_{\max}$	Coarsest particle size of the surface, [L]
D_{50s}	Median grain size of the surface, [L]
d	Flow depth, [L]
e_b	Bedload transport efficiency
g	Gravitational acceleration, [L/T^2]
Q	Water discharge, [L^3/T]
q_B	Volumetric bedload transport rate per unit channel width, [L^2/T]
q_B^*	Einstein bedload parameter
R_s	Submerged specific gravity of the sediment
S	Energy slope
U	Average water velocity, [L/T]
α	Angle of internal friction
γ	Specific weight of water, [M/L^{2}T^2]
γ_s	Specific weight of sediment, [M/L^{2}T^2]
ρ	Water density, [M/L^3]
τ_0	Bed shear stress, [M/LT^2]
τ_r	Reference value of shear stress, [M/LT^2]
τ^*	Shields stress for grain size D_{50s}
τ_{50}^*	Shields stress for grain size D_{50sub}
τ_{r50}^*	Reference Shields stress for grain size D_{50sub}
ϕ_{50}	Normalized Shields stress

ω	Stream power per unit width, [M/T^3]
ω^*	Dimensionless stream power

Table 2.1 Characteristics of Gravel-Bed Streams.

Characteristics	Oak Creek	Nahal Yatir
Stream type	Perennial	Ephemeral
[a]Number of samples	66	74
Surface median grain size D_{50s} (mm)	54	6
Subsurface median grain size D_{50sub} (mm)	20	10
Slope S	[b]0.0083-0.0108	[c]0.007-0.0101
Flow depth d (m)	0.11-0.45	0.10-0.47
Shear stress τ_0 (N m^{-2}) (Eq. 2.5)	8.93-43.22	8.67-36.92
Shields stress τ^* (Eq. 2.7)	0.00877-0.0424	0.092-0.39
Bedload transport rate q_B (kg m^{-1} s^{-1})	1.26 x 10^{-7}- 0.115	0.20 - 7.05
Froude Number	0.28-0.66	0.75-1.30
Specific stream power ω (kg s^{-3}) (Eq. 2.1)	3.54-93.77	7.15-105.75
Dimensionless specific stream power ω^* (Eq. 2.2)	2.19 x 10^{-3}-0.058	0.158-2.336
Bedload transport efficiency e_b (%) (Eq. 2.10)	1.37 x 10^{-5}- 1.07	7.30 - 57.79

[a]Number of measurements of bedload discharge during different flows
[b]Channel bed slope
[c]Water surface slope

Table 2.2 Characteristics of Nahal Hebron and Nahal Og.

Characteristics	Nahal Hebron	Nahal Og
Stream type	Ephemeral	Ephemeral
Number of tagged particles	282	250
Size range of tagged particles (mm)	45-180	45-180
Average bed slope S	0.016	0.014
Channel width B (m)	3-5	5-12
Bed shear stress τ_0 (N m^{-2}) (Eq. 2.5)	3.9-15.2	1.4-16.6
Specific stream power ω (kg s^{-3}) (Eq. 2.1)	215.8-1954	15.7-1440

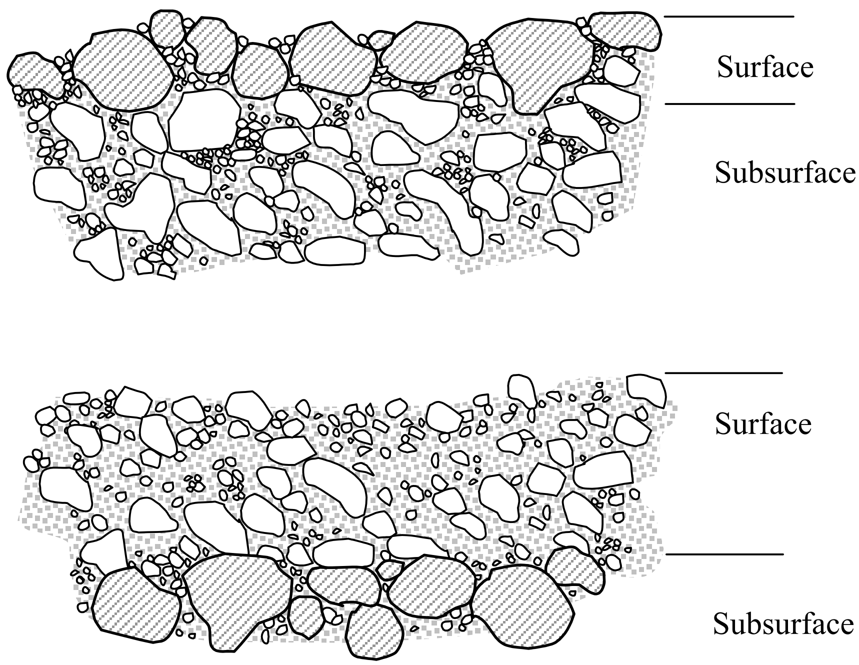

Figure 2.1 Bed structure in perennial and ephemeral gravel-bed streams. (a) Segregation in perennial streams; (b) segregation in ephemeral streams.

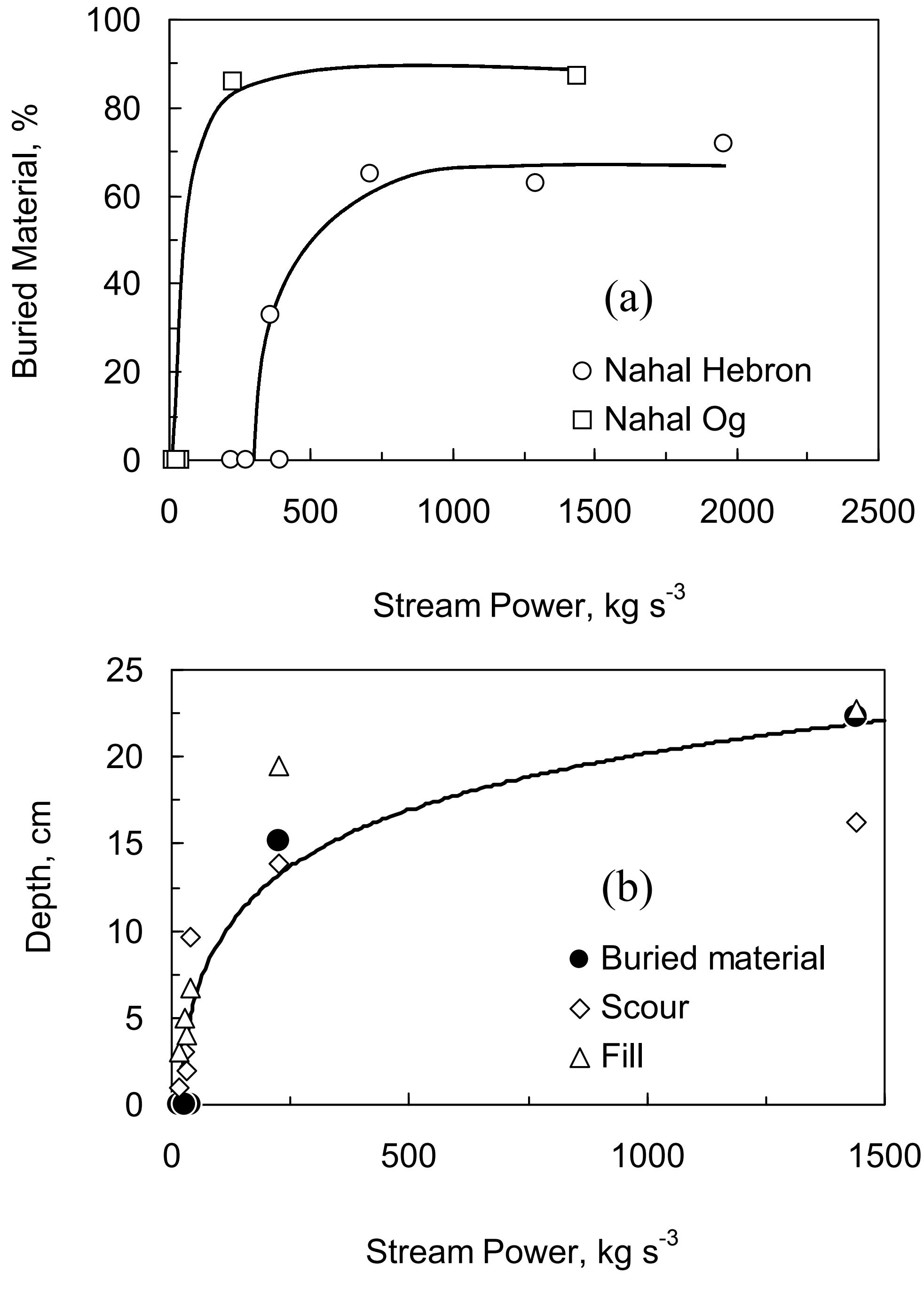

Figure 2.2 Influence of stream power on bed structure. (a) Stream power versus buried material for Nahal Hebron and Nahal Og; (b) stream power versus burial depth for Nahal Og. Data source is *Hassan* [1990].

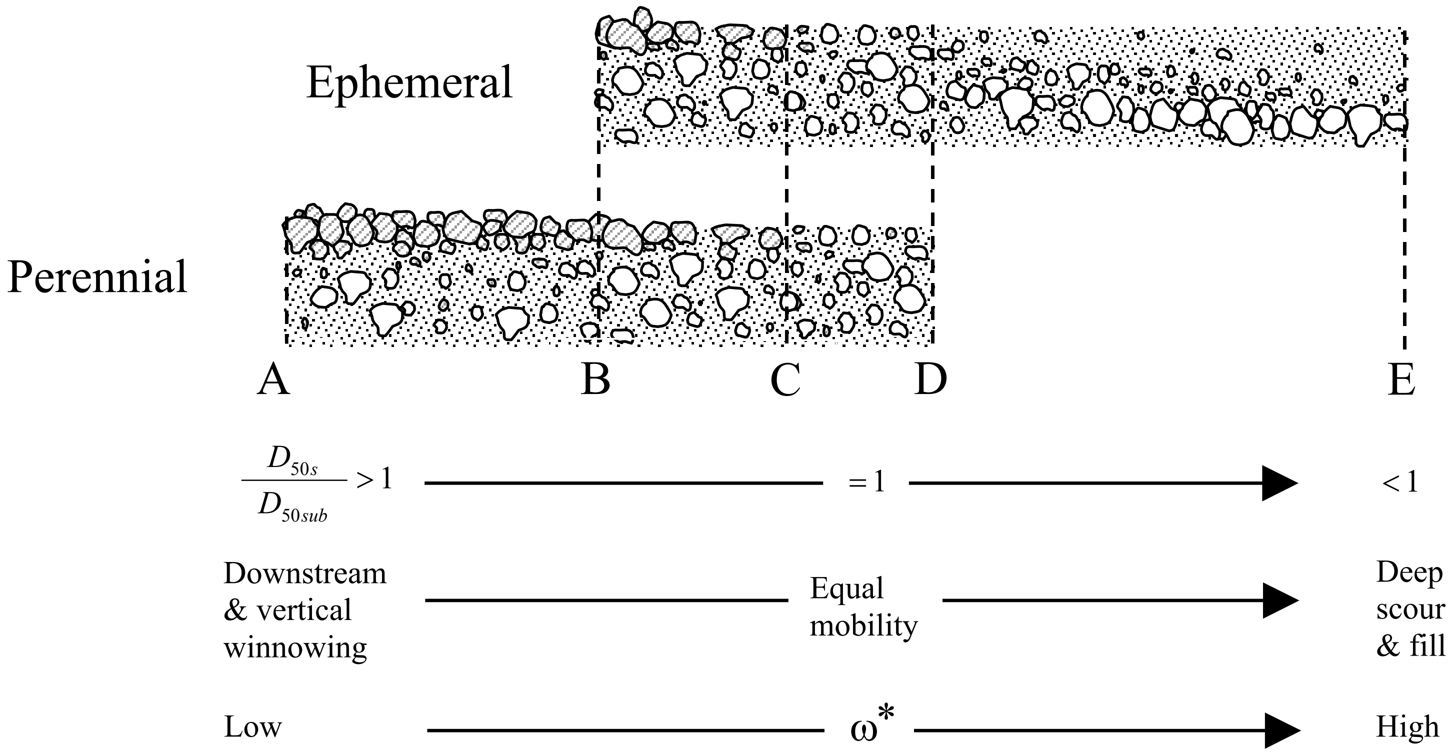

Figure 2.3 Conceptual model describing the variation of the bed structure of perennial and ephemeral gravel-bed streams in terms of dimensionless specific stream power, ω^*.

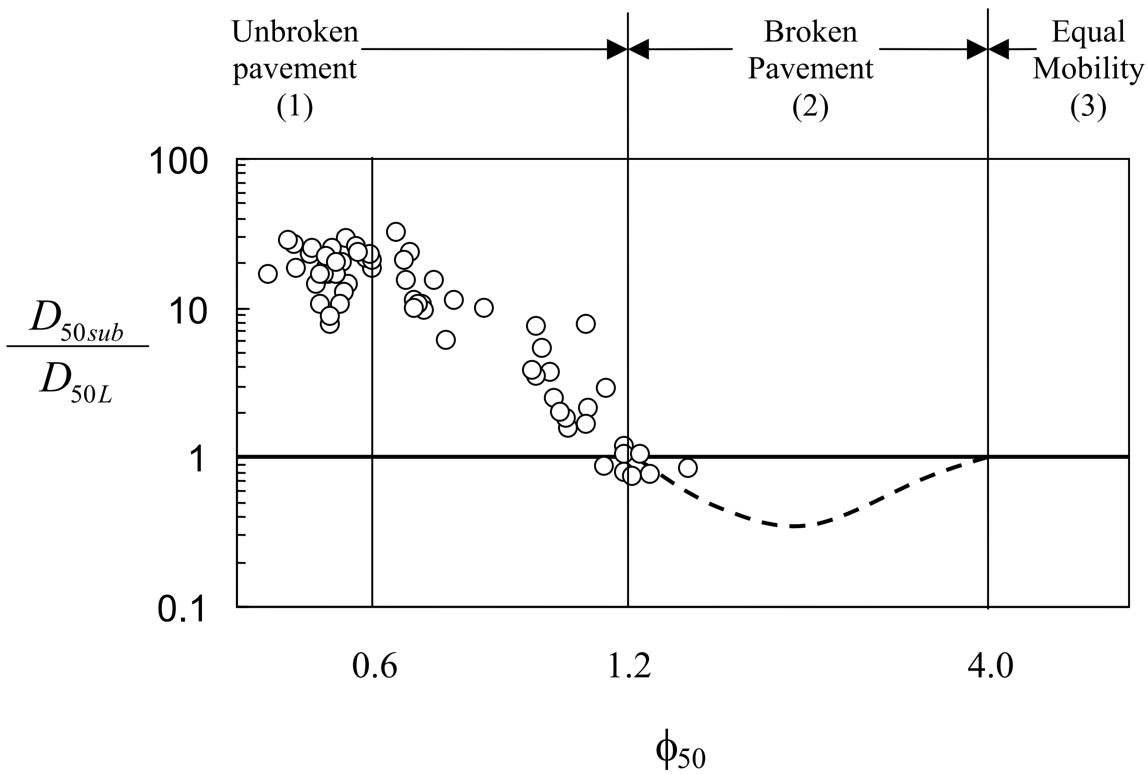

Figure 2.4 Variation of D_{50sub} / D_{50L} with the normalized Shields stress, ϕ_{50}. The circle points represent 66 bedload measurements of Oak Creek [*Milhous*, 1973]. The dashed line represents the trend suggested by *Diplas* [1987] for $1.2 < \phi_{50} < 4.0$.

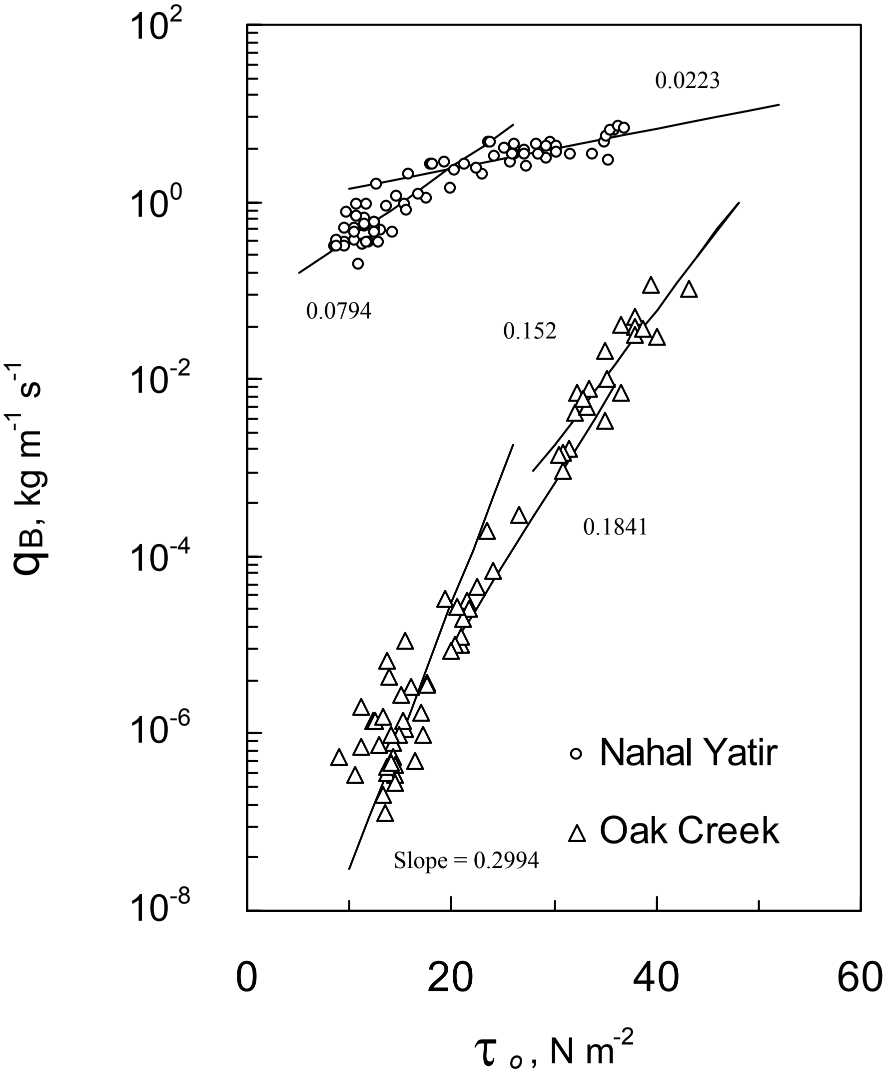

Figure 2.5 Measured bedload transport versus average cross-sectional bed shear stress. The solid line represents the fitted trend to a portion of bedload data. The slope of each trend was estimated as $\Delta \log(q_B)/\Delta\tau_0$. Data source for Oak Creek is *Milhous* [1973] and for Nahal Yatir is *Reid et al.* [1995].

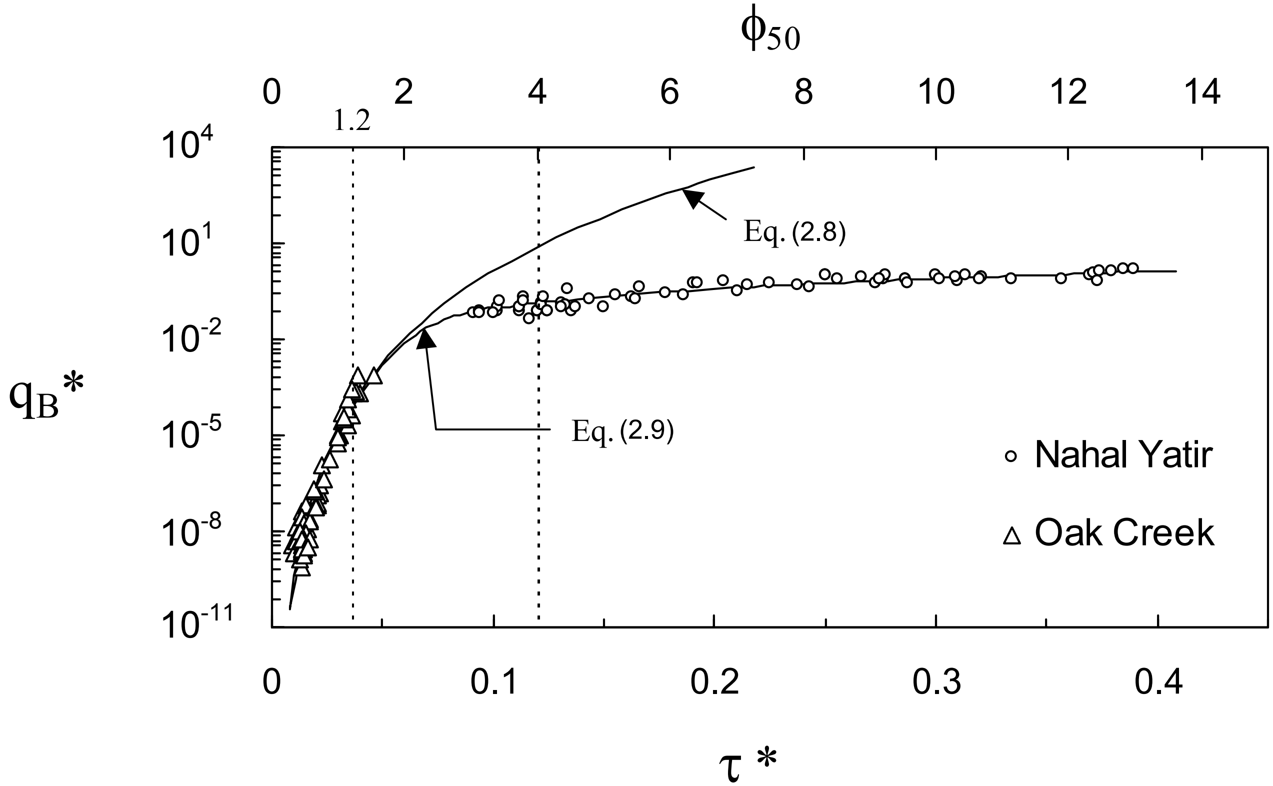

Figure 2.6 Plot of q_B^* versus τ^* based on the data of Oak Creek [*Milhous*, 1973] and Nahal Yatir [*Reid et al.*, 1995].

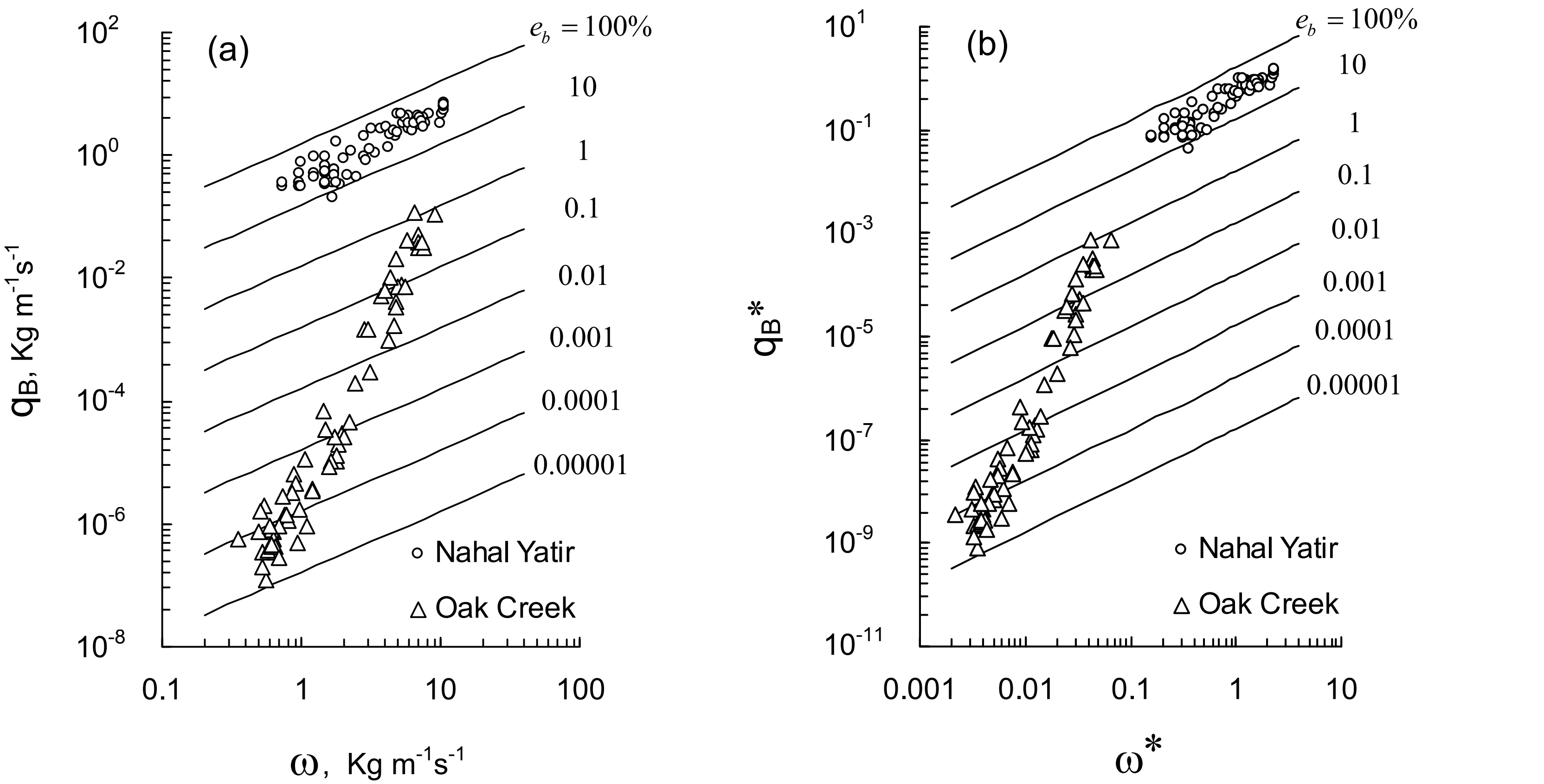

Figure 2.7 Bedload transport efficiency of Oak Creek [*Milhous*, 1973] and Nahal Yatir [*Reid et al.*, 1995]. (a) Dimensional presentation of the data similar to that performed by *Reid and Laronne* [1995]; (b) dimensionless presentation of the data.

Chapter 3: Bedload Transport in Gravel-Bed Streams with Unimodal sediment

3.1 Abstract

Bedload transport in many gravel-bed streams becomes highly complicated because of the nonuniformity of the grain size and the vertical stratification of channel bed material. A new relation for computing bedload transport rates in gravel-bed streams is proposed here. In an effort to account for the variation of the make-up of the surface material within a wide range of Shields stresses, the relation employs a two-parameter approach, one related to the material in the pavement and the other to that in the subpavement layers. The mode is used to represent the grain sizes of each layer. Available bedload transport data from gravel-bed streams with unimodal sediment are used to test the accuracy of the relation. A comparison with other bedload transport relations is also considered.

3.2 Introduction

Gravel streambeds typically possess a relatively thin surface layer, called pavement, which is coarser and better sorted than the immediate subsurface material [*Parker*, 1980; *Parker et al.*, 1982; *Diplas*, 1987]. Both surface and subsurface materials have a nonuniform grain size distribution. This condition causes the smaller particles to become sheltered by the larger ones, thereby exposing more of the larger grains to hydrodynamic forces [*Einstein*, 1950; *Parker and Klingeman*, 1982]. Consequently, a higher (lower) shear stress is required to entrain the small (large) particles than would be required to entrain a uniform material of the same particle size [e.g., *Rakoczi*, 1975; *Parker et al.*, 1982; *White and Day*, 1982; *Wiberg and Smith*, 1987].

Predicting bedload transport in gravel-bed streams is a difficult task. Despite the plethora of available bedload transport relations, there is still considerable controversy over their performance [*Gomez and Church*, 1989; *Bravo-Espinosa*, 1999]. For example, *Gomez and Church* [1989] evaluated many bedload transport relations developed for gravel-bed streams and found that not a single one of them performs well consistently. Most of them tend to be applicable strictly for those flow and sediment conditions represented in the data from which these relations were derived.

One of the most important parameters influencing the prediction of bedload transport in gravel-bed streams is the choice of the representative grain size [e.g., *Einstein*, 1950; *Misri et al.*, 1984]. In some cases, the choice is based on the range of particle sizes expected to be entrained by the flow [e.g., *Einstein*, 1950]. For gravel streambeds though, it has been shown that the make-up of the bedload material changes as the Shields stress does [e.g., *Milhous*, 1973; *Diplas*, 1987]. This suggests that it would be more appropriate to choose a grain size that describes the source of bedload, the bed material.

An important feature of gravel-bed streams is the complex variation of the make-up of the bed surface material with varying Shields stress values. For low stresses, selective particle entrainment renders the surface layer coarser than the subsurface material [*Milhous*, 1973]. For very high Shields stress values, the coarser surface layer is obliterated, exposing the subsurface material to the flow. For the intermediate values, the degree of coarseness of the surface layer declines as the Shields stress increases [*Diplas*, 1987]. This variation of the bed surface layer is expected to influence the bedload transport rates and thus it should be taken into account.

The present study proposes a new formula capable of predicting bedload transport rates in gravel-bed streams and for a wide range of Shields stresses. This formula is based on the following two premises: First, depending on the magnitude of the bed shear stress, either the surface or the subsurface material, or both contribute towards the bedload. Therefore, two particle diameters should be used, one to represent the surface (pavement) and another the subsurface (subpavement) materials. Second, the mode size is the most suitable single parameter for describing a bed material for bedload transport calculations. The accuracy of the relation is examined using available bedload transport data sets from gravel-bed streams with unimodal sediment. A comparison with other gravel bedload transport relations that employ a single representative particle diameter of either the surface or subsurface material is also considered.

3.3 Representative Particle Size

It has been reasonably well documented that fractional-based bedload transport rate calculations are preferable for poorly sorted sediments, as in the case of gravel-bed streams [*Parker et al.*, 1982; *Diplas*, 1987]. However, there is an advantage in calculations based on a single grain diameter due to the simplicity of the procedure. In the latter case, it is important to determine the most appropriate particle size to represent the entire sediment deposit. Choosing such a particle diameter is rather difficult and the opinions of various authors differ widely. *Meyer-Peter et al.* [1934], *Haywood* [1940], *Einstein* [1950], and *Ackers and White* [1973] adopted D_{35} as representative particle diameter, the size for which 35% of the particle size distribution is finer. *Schoklitsch* [1949] used a larger value equal to D_{40}. *Meyer-Peter and Muller* [1948] employed an effective diameter D_a; where $D_a = \sum_i f_i D_i$, D_i is the mean grain size of the *i*th fraction of bed material, and f_i is its percentage. For the bed materials used in their laboratory experiments, D_a varies from D_{50} to D_{60}.

The median grain size, D_{50}, is the particle diameter most widely adopted to represent a sediment mixture [e.g., *Shields*, 1936; *Rottner*, 1959; *Yalin*, 1963; *Parker*, 1979; *Bagnold*, 1980; *Diplas*, 1987]. The median size is a suitable choice for lognormally distributed grain sizes, an assumption commonly employed for natural sediments, because it coincides with the geometric mean and mode sizes of such a distribution.

Nevertheless, the grain size distribution for many fluvial gravel deposits is not lognormal; instead, it tends to be skewed towards the finer particles (negatively skewed) [*Kondolf and Wolman*, 1993; *Bunte and Abt*, 2001]. Thus, the median grain size may not be the most appropriate parameter to describe the grain size distribution for many gravel-bed materials.

An alternative statistical parameter proposed here is the mode. Although the mode plays a rather minor role in the sediment transport literature, it has been shown to be a useful parameter in many applications [e.g., *Dalenius*, 1965]. The mode has the advantage of always having the highest percentage of particles by weight. It also covers the largest portion of the bed surface area compared to any other size class. Additional reasons for choosing the mode will be discussed by examining its behavior in gravel-bed materials in terms of percentile variability, relative particle size, and stability.

3.3.1 Mode percentile variability

The histogram in Figure (3.1) presents the percentile corresponding to the mode of the grain size distribution for bed material samples collected from 125 gravel-bed streams having unimodal sediment, as reported by *Kondolf* [1988]. Most of the data are from USA rivers that have steep gradients and bed materials with a variety of particle sizes, ranging from sand to very large boulders. Figure (3.1) shows a wide variability of the mode percentile, from the 45th to 85th percentile. This could explain the different choices of representative particle size made by various researchers in an effort to obtain empirical curves that best fit the bedload transport data. At the same time, this variability may raise questions regarding the validity of using a fixed particle percentile to characterize the size distribution of gravel-bed materials.

It is interesting to note that the data in Figure (3.1) is well described by a lognormal distribution, having the following parameters: mode = 68.8%, median = 67%, arithmetic mean = 66.9%, and geometric mean = 64.3%. The location of these parameters implies that the materials included in Figure (3.1) represent negatively skewed grain size distributions, which is indeed the case for many fluvial gravel deposits. The mode value (68.8%) suggests that if one had to choose a fixed percentile to represent the bed material for bedload transport calculations, that should be close to D_{70}, a view that is not shared currently in the sediment transport literature. It is worth mentioning that the effective diameter D_a of *Meyer-Peter and Muller*, which varies in the *Kondolf* data from about D_{50} to D_{65}, lies closer to D_{70}, compared to other adopted diameters, e.g., D_{35}, D_{40}, and D_{50}. This may, to some extent, explain the popularity of the bedload transport relation of *Meyer-Peter and Muller* for applications with gravel- and cobble-bed streams [*Simons and Senturk*, 1992].

3.3.2 Relative particle size, D_m/D_{50}

While the mode percentile is widely variable in gravel-bed materials, it is useful to examine the mode particle size, D_m, relative to the median particle size, D_{50}. For the same 125 samples of bed material, the histogram in Figure (3.2) shows D_m / D_{50} ratios ranging from 0.96 to 2.75. The mode value of the histogram, D_m / D_{50}, is equal to 1.59 and represents about 20.8% of the data points. Under these circumstances, the distinction between the mode and median grain sizes in gravel materials is very important. Bedload relations employing D_m will calculate considerably different transport rates than those using D_{50}.

3.3.3 Mode stability

The mode grain size of the pavement material is expected to be stable during flows with low bed shear stress, when only the finer grains are mobilized. This behavior of the mode can be demonstrated using the laboratory data of *Proffitt* [1980].

Proffitt used four sediment mixtures as bed materials, each with different median size and geometric standard deviation σ_g. He performed four flume experiments for each case, each with a different bed shear stress (Table 3.1). Two numbers are used to designate each experiment. The first refers to the bed material series and the second to the experiment within that series. For example, 2-3 represents the third experiment of the second sediment mixture used as bed material. Initially, the material was thoroughly mixed and placed within a laboratory flume 27.5 m long and 0.61 m wide. Water was then introduced into the flume and a flow established. The bed material was sampled 20 to 95 hours later depending on the applied bed shear stress and initial bed-material grading [*Proffitt*, 1980].

As in natural gravel-bed streams, the sediment in the flume was segregated into surface and subsurface materials. Table (3.1) shows that both the subsurface median grain size, D_{50sub}, and the subsurface mode grain size, D_{msub}, remained constant during all the experiments, most likely because the subsurface material was protected from the fluid forces by the surface material. The surface median grain size, D_{50s}, however, changed with bed shear stress, τ_0. The surface mode grain size, D_{ms}, though, remained constant, except for the experiments of the first series.

The trends of $D_{ms} / \overline{D_{ms}}$ and $D_{50s} / \overline{D_{50s}}$ as the normalized shear stress, τ_0 / τ_c, varies are shown in Figure (3.3); where τ_c is the critical shear stress estimated here as $\tau_c \approx 0.03g(\rho_s - \rho)D_{ms}$, g is the gravitational acceleration, ρ_s is the sediment density, ρ is the water density, $\overline{D_{ms}}$ is the average mode grain size of each bed material series, and $\overline{D_{50s}}$ is the average median grain size of each bed material series. Figure (3.3) shows that $D_{50s} / \overline{D_{50s}}$ is variable over the entire range of shear stresses. However, $D_{ms} / \overline{D_{ms}}$ is stable before reaching the critical shear stress value capable of entraining the surface mode ($\tau_0 / \tau_c < 1$).

The implication is that the mode particle size can be estimated in the field during low shear stresses more accurately than the median grain size, because the value of the former is relatively insensitive to the movement of smaller particles. The accurate estimation of the representative particle size is important because it affects the bedload transport calculations.

As a practical consideration, it is worth mentioning that the determination of the mode size will require a larger sample of bed material compared to the sample size necessary to determine other statistical characteristics of the grain size distribution, such as the mean and the median sizes.

3.4 Bedload Transport Relation Based on D_{ms} and D_{msub}

The surface mode grain size is stable at low shear stresses, and the subsurface mode size eventually becomes exposed to the surface during very high shear stresses; in between, however, the mode of the material exposed to the flow is expected to change. A bedload transport relation that takes into account the trend exhibited by the mode of the bed material would be pertinent for gravel-bed streams. Bedload transport data collected by *Milhous* [1973] from Oak Creek, a perennial gravel-bed stream in Oregon, and by *Reid et al.* [1995] from Nahal Yatir, an ephemeral gravel-bed stream in Israel, are used here to obtain a bedload transport formula suitable for a wide range of Shields stresses.

Oak Creek and Nahal Yatir data sets represent two limits of bedload transport [*Reid and Laronne*, 1995]. Oak Creek operates under low to moderate Shields stresses, incapable of entraining the coarsest grains from the surface material. Under these circumstances, the bedload transport condition is mostly within the unbroken pavement regime [*Milhous*, 1973]. In contrast, Nahal Yatir experiences very high Shields stresses, under which the condition of equal mobility prevails [*Reid and Laronne*, 1995]. It is suggested here that the two data sets might be parts of the same overall curve relating bedload transport with Shields stress.

The bedload transport data of Oak Creek and Nahal Yatir are plotted in Figure (3.4) in terms of

$$W^* = \frac{R_s q_B}{\sqrt{g}\,(dS)^{1.5}} \tag{3.1}$$

and

$$\tau^* = \frac{\tau_0}{g(\rho_s - \rho)D_{mr}} \tag{3.2}$$

where W^* is the dimensionless bedload parameter, τ^* is the Shields stress parameter, q_B is the volumetric bedload transport rate per unit channel width, D_{mr} is the representative mode grain size of the material exposed to the flow, R_s is the submerged specific gravity, d is the flow depth, and S is the energy slope. In expression (3.2), the particle size is denoted as D_{mr}, referring to a variable mode diameter changing from D_{ms} to D_{msub} for a wide range of Shields stresses.

An empirical relation can be fitted by log-linear regression for the Oak Creek data as

$$W^*_{oak} = 10^{9.59}\,{\tau^*_{ms}}^{7.95} \tag{3.3}$$

with the correlation coefficient equal to $r = 0.944$. Here, the Shields stress parameter is denoted as τ^*_{ms} to refer to the constant D_{ms} value of the unbroken pavement regime. Likewise, an empirical relation can be fitted by log-linear regression for the Nahal Yatir data

$$W^*_{yatir} = 7.59\,{\tau^*_{msub}}^{0.35} \tag{3.4}$$

with correlation coefficient equal to $r = 0.912$. The Shields stress parameter τ^*_{msub} refers to a constant D_{msub} in the absence of a pavement layer. The data from the two streams together with the fitted trends are plotted in Figure (3.4).

One way to combine these two empirical relations into one general expression, having a smooth transition from one trend to the other, is to use the following expression

$$\frac{1}{W^*} = \frac{1}{W^*_{yatir}} + \frac{1}{W^*_{oak}} \tag{3.5}$$

The range of W^*_{oak} and W^*_{yatir} values differs widely in magnitude (Figure 3.4). The above expression renders W^* equal to W^*_{oak} or W^*_{yatir} when dealing with low or very high dimensionless shear stress values, respectively. However, in between, both parts contribute to W^*. Substituting Equations (3.3) and (3.4) into (3.5), the general relation of bedload transport obtained herein can be written as

$$W^* = \frac{1}{0.132\tau^{*\,-0.35}_{msub} + 10^{-9.59}\ \tau^{*\,-7.95}_{ms}} \tag{3.6}$$

This relation depends on the constants D_{ms} and D_{msub} rather than the variable D_{mr}, which is difficult to estimate in the field during the passage of floods. As expected, Equation (3.6) follows very closely the trends exhibited by the Oak Creek and Nahal Yatir bedload data (Figure 3.5).

3.5 Application to Bedload Data with Unimodal Sediment

Equation (3.6) is intended for use with gravel-bed streams having unimodal sediment. The presence of two modes in bimodal materials results in an additional degree of difficulty that the present approach cannot account for. To check its accuracy, it is preferable to test Equation (3.6) against measured bedload transport data collected from natural gravel-bed streams. Although many bedload transport data sets are available in the literature, it is difficult to find data that include the grain size distributions of both surface and subsurface materials. Such information is necessary for estimating the corresponding mode grain sizes.

3.5.1 Bedload data

Three bedload transport data sets that satisfy the above requirements are considered here:

Sagehen Creek. This creek drains the east flank of the Sierra Nevada, California [*Andrews*, 1994]. The reach average bankfull width is 4.85 m, and the corresponding channel depth is 0.41 m. The bedload transport measurements, reported by *Andrews* [1994], were taken with a Helley-Smith sampler. The Shields stress, τ^*_{ms}, values vary from 0.0268 to 0.0393. The mode of the surface and subsurface materials is equal to 61 mm and 54 mm, respectively, and the corresponding median grain sizes are 58 mm and 30 mm.

Elbow River. This river, located in Alberta, Canada [*Hollingshead*, 1971], has an average channel width of 43.5 m and average water depth of 0.75 m. The bedload samples, reported by *Hollingshead* [1971], were collected with Water Survey of Canada (WSC) basket type samplers during snowmelt periods of 1967, 1968, and 1969. τ^*_{ms} values range from 0.0424 to 0.0564. The mode grain size of the surface and subsurface materials is 76 mm and 28 mm, respectively, with identical corresponding median grain sizes.

Jacoby River. This river is located in the redwood forest of the Coast Range of northern California [*Lisle*, 1989]. The bankfull width is 17.2 m and the bankfull depth is 1 m. Bedload transport rates, reported by *Lisle* [1989], were measured using a Helley-Smith sampler. τ^*_{ms} values vary from 0.0147 to 0.081. The mode grain size of the surface and subsurface materials is equal to 28 mm and 12 mm, respectively, with the corresponding median grain sizes being 22 mm and 8 mm. Additional details about these three streams are included in Table (3.2).

3.5.2 Evaluation of proposed bedload formula

Each measured bedload data set is plotted separately, together with Equation (3.6), in Figure (3.6). The trend exhibited by the measured data is well represented by Equation (3.6).

To examine more closely the accuracy of Equation (3.6), the measured bedload transport rates from all three streams are plotted in Figure (3.7) against the corresponding predicted values. In this figure, the solid line represents the condition of perfect agreement, and the dashed lines represent discrepancy ratios, $q_{predicted}/q_{measured}$, of 0.05, 0.5, 2, and 20. The percentage of the overall data having a discrepancy ratio between 0.05 and 20 is about 97%; the percentage for each stream is 98% for Sagehen Creek, 100% for Elbow River, and 94% for Jacoby River. Also, the percentage of the overall data having a discrepancy ratio between 0.5 and 2 is about 67%: Sagehen Creek, 75%, Elbow River, 95%, and Jacoby River, 31%.

3.5.3 Mode- versus median-based bedload transport predictions

The bed materials of Oak Creek and Nahal Yatir are well represented by lognormal distributions. Therefore, the median grain sizes for both streams coincide with the corresponding mode values (Table 3.2). As a result, regression Equation (3.6) would not change if median sizes, D_{50s} and D_{50sub}, were used in place of the mode sizes for calculating the Shields stresses of the data shown in Figure (3.4). A comparison between the mode- and median-based approaches is necessary to determine which of the two is more appropriate. This is performed by using the data of Sagehen Creek, Elbow River, and Jacoby River to generate Figure (3.8), which is similar to Figure (3.7) except for the use of Equation (3.6) in terms of D_{50s} and D_{50sub}.

The bed material of Jacoby River is the only one that has median grain sizes distinctly different from the corresponding mode sizes. Therefore, this data set is the most suitable for comparing the mode- and median-based predictions obtained from Equation (3.6). Comparison of Figure (3.7) with (3.8) highlights the advantage of using the mode over the median. The bedload values predicted by using the median sizes are consistently higher than the corresponding measured values and 73% of them fall outside the discrepancy range of 0.05 to 20 (Figure 3.8). This percentage is considerably higher than that obtained by the mode-based approach for Jacoby River (6%). A Mean Absolute Standard Error (MASE) expression is proposed here as a quantitative criterion for testing the accuracy of both approaches in an objective manner

$$\mathsf{MASE} = \frac{\sum_{i=1}^{n} q_{ri}}{n} \tag{3.7}$$

where

$$q_{ri} = \begin{cases} \dfrac{q_{i\ measured}}{q_{i\ predicted}} & \text{if} \quad q_{i\ measured} > q_{i\ predicted} \\[2ex] \dfrac{q_{i\ predicted}}{q_{i\ measured}} & \text{if} \quad q_{i\ measured} < q_{i\ predicted} \end{cases}$$

and n is the total number of bedload samples. Equation (3.7) indicates that $\mathsf{MASE} \geq 1$. The closer the MASE value to one is, the better the accuracy of an equation will be, with $\mathsf{MASE} = 1$ representing the condition of perfect agreement. Using the median-based approach, the MASE value for the Jacoby River data is 69.68, while for the mode-based approach $\mathsf{MASE} = 5.23$.

For the bedload data of Elbow River, the performance of Equation (3.6) is the same regardless if the mode or median grain sizes are employed (Table 3.3). In both cases, the MASE value is equal to 1.49. This is also the case for the Sagehen Creek data, where MASE is equal to 2.52 and 2.53 for the mode- and median-based approaches, respectively. The result for Elbow River data is not surprising, since the mode and median grain sizes coincide for the surface bed material, as well as for the subsurface material (Table 3.2). For Sagehen Creek, however, the same is true only for the surface material, $D_{ms} / D_{50s} \approx 1.05$ (Table 3.2). It is interesting to note that the bedload transport data for Sagehen Creek were collected at low Shields stresses, ranging from $\tau^*_{ms} \approx 0.0268$ to 0.0393. Throughout this range, the pavement layer remains in place and becomes the main source of the material transported as bedload. This behavior explains the similar plots of the bedload data for Sagehen Creek shown in Figures (3.7) and (3.8).

3.6 Comparison with other Bedload Relations

To examine whether a two-parameter approach results in improved predictions, Equation (3.6) is compared against several bedload transport relations that employ a single representative particle size, based either on the surface or subsurface material. The bedload data from Sagehen Creek, Elbow River, and Jacoby River are used for this purpose. The following four bedload transport relations were chosen for the comparison: *Meyer-Peter and Muller* [1948], *Einstein-Brown* [*Brown*, 1950], *Parker* [1979], and *Parker et al.* [1982].

The equation proposed by *Meyer-Peter and Muller* [1948] is written as follows:

$$q_B^* = 8\left(\tau^* - 0.047\right)^{1.5} \tag{3.8}$$

where $q_B^* = q_B / \sqrt{R_s g D^3}$ is the Einstein bedload parameter.

The *Einstein-Brown* [*Brown*, 1950] equation is expressed as:

$$
q_B^* = \begin{cases} 40Y\tau^{*3} \ldots\ldots\ldots\ldots\ldots\ldots\ldots\ldots\ldots\tau^* \geq 0.182 \\ \dfrac{Y \exp\left(\dfrac{-0.391}{\tau^*}\right)}{0.465} \ldots\ldots\ldots\ldots\tau^* < 0.182 \end{cases} \tag{3.9}
$$

where $Y = \left(2/3 + 36v^2 / gD^3R_s\right)^{1/2} - \left(36v^2 / gD^3R_s\right)^{1/2}$, and v is the kinematic viscosity.

The equation proposed by Parker [1979] is written as:

$$
q_B^* = 11.2 \frac{\left(\tau^* - 0.03\right)^{4.5}}{\tau^{*3}} \tag{3.10}
$$

The bedload transport formula proposed by Parker et al. [1982] is:

$$
q_B^* = \begin{cases} 0.0025\tau_{50sub}^{*1.5} \exp\left[14.2\left(\dfrac{\tau_{50sub}^*}{0.0876} - 1\right) - 9.28\left(\dfrac{\tau_{50sub}^*}{0.0876} - 1\right)^2\right] \ldots\ldots 0.08322 < \tau_{50sub}^* < 0.1445 \\ 11.2\tau_{50sub}^{*1.5}\left(1 - \dfrac{0.072}{\tau_{50sub}^*}\right)^{4.5} \ldots\ldots\ldots\ldots\ldots\ldots\ldots\ldots 0.1445 < \tau_{50sub}^* \end{cases} \tag{3.11}
$$

These bedload transport relations were selected, because they are commonly used for gravel-bed streams and have been mentioned extensively in the literature. The equation of *Meyer-Peter and Muller* [1948] is based on laboratory data. Both uniform and nonuniform bed materials, having D_a values from 0.4 mm to 30 mm, were used in the experiments. Here, the equation will be used for the calculations once in terms of D_a of the surface material and a second time in terms of the subsurface material. The equation of *Einstein-Brown* [*Brown*, 1950] is based on laboratory data with median grain sizes from 0.3 mm to 28.6 mm. The equation of *Parker* [1979] was derived from laboratory and field data, all in the gravel range. Both *Einstein-Brown* and *Parker* use the median size to describe the bed material. Two sets of bedload transport calculations will be obtained from Equations (3.9) and (3.10). For the first set, the surface material will be used as the basis for estimating the median grain size for each equation, while for the second set the subsurface material is employed. The equation of *Parker et al.*

[1982] is based on the idea of equal mobility and the Oak Creek bedload transport data. This relation employs D_{50sub} as the representative diameter.

Box plots, shown in Figure (3.9), are used to explore the distribution characteristics of the discrepancy ratio $q_{predicted}/q_{measured}$ obtained from Equation (3.6), based on the mode, together with the selected bedload transport relations. Apparently, Equation (3.6) provides the best bedload predictions for Sagehen Creek, Elbow River, and Jacoby River, with the median values of the discrepancy ratio equal to 1.2, 0.97, and 2.03, respectively. For the other selected relations, the box plots indicate an obvious overestimation of the Jacoby River bedload data, with median discrepancy ratios ranging from 13 (for *Einstein-Brown* surface) to 2119 (*Meyer-Peter and Muller* subsurface). However, for Sagehen Creek and Elbow River, some of the selected relations overestimate, and others underestimate, the bedload transport rate measurements.

The relation of *Parker et al.* underestimates the bedload transport for Sagehen Creek and Elbow River, with median discrepancy ratios equal to 0.006 and 0.56, respectively. The corresponding MASE values are equal to 218 and 2.2 (Table 3.3). The surface-based *Parker* and *Einstein-Brown* calculations underestimate the measured bedload transport rates of the two data sets, while the subsurface-based calculations overestimate them. The subsurface-based relation of *Meyer-Peter and Muller* overestimates the data of Elbow River, with median discrepancy and MASE values of 16.5 and 27, respectively; however, the relation is unable to calculate bedload transport rates for Sagehen Creek, because $\tau^* < 0.047$. The surface-based relation of *Meyer-Peter and Muller* is also unable to calculate any bedload rates for Sagehen Creek and most of the Elbow River Shields stress values.

3.7 Conclusion

A new bedload transport relation for gravel-bed streams has been proposed. The relation is an empirical fit to the data of Oak Creek and Nahal Yatir, which are considered to represent the two limits of the spectrum of bedload transport rate observed in the field and laboratory. This relation has two new features: It employs the mode as a representative particle size of bed material, and it considers a two parameter approach, the first representing the pavement material while the second represents the subpavement. The latter feature accounts, in a simple way, for the variation of the make-up of the surface bed material over a wide range of Shields stresses. It also reflects the resulting changes in the contributions made by the surface and subsurface layers to the material transported as bedload.

The accuracy of the new relation has been tested using bedload transport data obtained from the literature for Sagehen Creek, Elbow River, and Jacoby River, with τ_{ms}^{*} values ranging from 0.0147 to 0.081. The last data set, in particular, demonstrated the advantage of using the mode- over the median-based approach. A comparison with other, single-parameter bedload transport relations, employing either a surface or subsurface representative particle diameter, has shown that the relation proposed here provides more accurate bedload transport rate predictions. Additional testing will be necessary though to examine the validity of the new relation, especially for τ_{ms}^{*} values larger than 0.081. The application of Equation (3.6) is limited to gravel streambeds having unimodal sediment.

References

Ackers, P., and W. R. White, Sediment transport: New approach and analysis, *J. Hydraul. Div. Am. Soc. Civ. Eng.*, *99*(11), 2041-2060, 1973.

Andrews, E. D., Marginal bed load transport in a gravel bed stream, Sagehen Creek, California, *Water Resour. Res.*, *30*(7), 2241-2250, 1994.

Bagnold, R. A., An empirical correlation of bed load transport rates in flumes and natural rivers, Proc. Roy. Soc. of London, A372, 453-473, 1980.

Bravo-Espinosa, M., Prediction of bedload discharge for alluvial channels, Ph.D. thesis, Univ. of Arizona, Tucson, 1999.

Brown, C. B., Sediment transportation, in *engineering hydraulics*, ed. H. Rouse, 771 pp., John Wiley, New York, 1950.

Bunte, K., and S. R. Abt, Sampling surface and subsurface particle-size distributions in wadable gravel- and cobble-bed streams for analyses in sediment transport, hydraulics, and streambed monitoring, *Technical Rep. RMRS-GTR-74*, 482 pp., U.S.D.A. Forest Service, Rocky Mountain Research Station, 2001.

Dalenius, T., The mode—a neglected statistical parameter, *J. of Roy. Stat. Soc.*, *Series A (General)*, *128*(1), 110-117, 1965.

Diplas, P., Bedload transport in gravel-bed streams, *J. Hydraul. Engng., Am. Soc. Civ. Eng.*, *113*(3), 277-292, 1987.

Einstein, H. A., The bed-load function for sediment transportation in open channel flows, U.S. Department of Agriculture, Soil Conservation Service, Technical Bulletin no. 1026, 1950.

Gomez, B., and M. Church, An assessment of bed load sediment transport formulae for gravel bed rivers, *Water Resour. Res.*, *25*(6), 1161-1186, 1989.

Haywood, O. G., Flume experiments on the transportation by water of sand and light-weight materials, Ph.D. thesis, Mass. Inst. of Tech., Cambridge, 1940.

Hollingshead, A. B., Sediment transport measurements in gravel river, *J. Hydraul. Div. Am. Soc. Civ. Eng.*, 1817-1834, 1971.

Kondolf, G. M., Salmonid spawning gravels: a geomorphic perspective on their size distribution, modification by spawning fish, and criteria for gravel, Ph.D. thesis, The Johns Hopkins Univ., Baltimore, Maryland, 1988.

Kondolf, G. M., and M. G. Wolman, The sizes of salmonid spawning gravels, *Water Resour. Res.*, *29*(7), 2275-2285, 1993.

Lisle, T. E., Sediment transport and resulting deposition in spawning gravels, north Coastal California, *Water Resour. Res.*, *25*(6), 1303-1319, 1989.

Meter-Peter, E., H. Favre, and A. Einstein, Neuere Versuchsresultate uber den Geschiebetried, Schweiz Bauzeitung, *103*(13), 1934.

Meyer-Peter, E., and Muller, R., Formula for bedload transport, *Proc. Int. Assoc. of Hydr. Struct. Res.*, 39-64, 1948.

Misri, R. L., R. J. Garde, K. G. Ranga Raju, Bed load transport of coarse nonuniform sediment, *J. Hydraul. Engng., Am. Soc. Civ. Eng.*, *110*(3), 312-328, 1984.

Milhous, R. T., Sediment transport in a gravel-bottomed stream, unpublished Ph.D. thesis, Oregon State Univ., Corvallis, 1973.

Parker, G., Hydraulic geometry of active gravel rivers, *J. Hydraul. Div. Am. Soc. Civ. Eng.*, *105*(HY9), 1185-1201, 1979.

Parker, G., Armored versus paved gravel beds, Discussion, *J. Hydraul. Div. Am. Soc. Civ. Eng., 106*(HY11), 1120-1121, 1980.

Parker, G., and P.C. Klingeman, On why gravel bed streams are paved, *Water Resour. Res.*, *18*(5), 1409-1423, 1982.

Parker, G., P. C. Klingeman, and D. G. McLean, Bedload and size distribution in paved gravel bed streams, J. Hydraul. Div. Am. Soc. Civ. Eng., 108(HY4), 544-569, 1982.

Proffitt, G. T., Selective transport and armouring of non-uniform alluvial sediments, *Report no. 80/22*, 203 pp., Department of Civil Engineering, University of Canterbury, New Zealand, 1980.

Rakoczi, L., Influence of grain-size composition on the incipient motion and self-pavement of bed materials, *Proc. of the 16th congress of the Int. Assoc. for Hydraul. Res.*, Sao Paulo, Brazil, Vol. 2, July, 150-157, 1975.

Reid, I., and J. B. Laronne, Bed load sediment transport in an ephemeral stream and a comparison with seasonal and perennial counterparts, *Water Resour. Res.*, *31*(3), 773-781, 1995.

Reid, I., J. B. Laronne, and D. M. Powell, The Nahal Yatir bedload database sediment dynamics in a gravel-bed ephemeral stream, *Earth Surf. Processes Landforms*, *20*, 845-857, 1995.

Rottner, J., A formula for bed-load transportation, *La Houille Blanche*, *14*(3), 285-307, 1959.

Schoklitsch, A., Berechnung der Geschiebefracht, Wasser und Energiewirtscaft, Nr. 1, 1949.

Shields, A., Application of similarity principles and turbulence research to bed-load movement, Berlin; English Trans. By W.P. Ott and J.C. Van Uchelen, Soil Conservation Service, Cal. Inst. Tech. Publ. No. 167, 1936.

Simons, D. B., and F. Senturk, Sediment transport technology: water and sediment dynamics, 897 pp., Water Resources Publications, Littleton, 1992.

White, W. R., and T. J. Day, Transport of graded gravel bed material, in *Gravel-Bed Rivers: Fluvial processes, Engineering, and Management*, edited by R. D. Hey, J. C. Bathurst, and C. R. Thorne, pp. 181-213, John Wiley, New York, 1982.

Wiberg, P. L., and J. D. Smith, Calculations of the critical shear stress for motion of uniform and heterogeneous sediments, *Water Resour. Res.*, *23*(8), 1471-1480, 1987.

Yalin, M. S., An expression for bed-load transportation, Proc. of the American Society of Civil Engineers, J. Hydraul. Div. Am. Soc. Civ. Eng., 89(HY3), 221-250, 1963.

Notation

B	Channel width, [L]
D	Particle grain size, [L]
D_{35}	Particle grain size that 35 percent of all particles are smaller, [L]
D_{40}	Particle grain size that 40 percent of all particles are smaller, [L]
D_{50}	Particle grain size that 50 percent of all particles are smaller, [L]
D_{60}	Particle grain size that 60 percent of all particles are smaller, [L]
D_{50s}	Median grain size of the surface, [L]
$\overline{D_{50s}}$	Average median grain size of surface, [L]
D_{50sub}	Median grain size of the subsurface, [L]
D_a	Effective diameter, [L]
D_i	Mean grain size of the *i*th grain size range, [L]
D_m	Mode grain size of bed material, [L]
D_{mr}	Representative mode grain size, [L]
D_{ms}	Mode grain size of the surface, [L]
$\overline{D_{ms}}$	Average mode grain size of surface, [L]
D_{msub}	Mode grain size of the subsurface, [L]
d	Flow depth, [L]
g	Gravitational acceleration, [L/T^2]
p_i	Fraction of bedload in *i*th grain size range
q_B	Volumetric bedload transport rate per unit channel width, [L^2/T]
q_B^*	Einstein bedload parameter
R_s	Submerged specific gravity of the sediment
S	Energy slope
W^*	Dimensionless bedload parameter
v	Kinematic viscosity, [L^2/T]

ρ	Water density, $[M/L^3]$
ρ_s	Grain density, $[M/L^3]$
τ_0	Bed shear stress, $[M/LT^2]$
τ_c	Critical shear stress, $[M/LT^2]$
τ^*	Shields stress parameter
τ^*_{ms}	Shields stress based on a constant D_{ms}
τ^*_{msub}	Shields stress based on a constant D_{msub}

Table 3.1 Geometric standard deviation, representative particle size of surface and subsurface materials, and shear stress conditions for the laboratory data of *Proffitt* [1980].

Run no.	σ_g	τ_0 N m^{-2}	τ_0/τ_c	D_{50sub} mm	D_{50s} mm	$\overline{D_{50s}}$ mm	D_{msub} mm	D_{ms} mm	$\overline{D_{ms}}$ mm
1-2	2.26	4.308	1.57	2.9	6.85	5.56	2.84	15.55	9.15
1-3		2.94	1.07	2.9	4.68		2.84	5.5	
1-4		3.731	1.37	2.9	5.7		2.84	7.78	
1-7		3.297	1.19	2.9	5		2.84	7.78	
2-1	3.24	3.676	0.47	3.25	6.4	8.42	3.99	15.55	15.55
2-2		4.336	0.56	3.25	6.9		3.99	15.55	
2-3		5.133	0.66	3.25	8.7		3.99	15.55	
2-4		6.826	0.88	3.25	11.7		3.99	15.55	
3-1	2.78	5.598	0.72	3.07	8.3	9.92	3.99	15.55	15.55
3-2		6.107	0.78	3.07	10.7		3.99	15.55	
3-3		7.224	0.93	3.07	11.7		3.99	15.55	
3-4		4.831	0.62	3.07	9		3.99	15.55	
4-1	1.95	3.646	1.33	4.2	4.95	5.09	5.5	5.5	5.5
4-2		3.069	1.12	4.2	4.65		5.5	5.5	
4-3		3.996	1.45	4.2	5.3		5.5	5.5	
4-4		4.492	1.63	4.2	5.45		5.5	5.5	

Table 3.2 Hydrologic, hydraulic, and sedimentary characteristics of the examined gravel-bed streams.

Characteristics	Oak Creek	Nahal Yatir	Sagehen Creek	Elbow River	Jacoby River
Stream type	Perennial	Ephemeral	Perennial	Perennial: snowmelt	Perennial
Number of bedload data samples	66	74	55	19	100
Surface median grain size D_{50s}, mm	54	6	58	76	22
Subsurface median grain size D_{50sub}, mm	20	10	30	28	8
Coarseness ratio D_{50s}/D_{50sub}	2.7	0.6	1.933	2.714	2.75
Surface mode grain size D_{ms}, mm	≈54	≈6	61	≈76	28
Subsurface mode grain size D_{msub}, mm	≈20	≈10	54	≈28	12
Coarseness ratio D_{ms}/D_{msub}	2.7	0.6	1.13	2.717	2.33
Slope S	[a]0.0083-0.0108	[b]0.007-0.0101	[c]0.0095-0.012	[b]0.00745	[a]0.0063
Flow depth d, m	0.11-0.45	0.10-0.47	0.275-0.418	0.61-0.811	0.13-0.6
Shields stress τ^*_{msub}	0.0237-0.1145	0.055-0.234	0.03-0.0444	0.115-0.153	0.0343-0.189
Shields stress τ^*_{ms}	0.00877-0.0424	0.092-0.39	0.0268-0.0393	0.0424-0.0564	0.0147-0.081
Shear stress τ_0, N m^{-2}	8.93-43.22	8.67-36.92	29.67-43.48	47.88-63.85	8.1-36.5

[a]Channel bed slope
[b]Water surface slope
[c]Total energy slope

Table 3.3 Fitting accuracy of the bedload transport relations.

Stream	Number of data utilized	Mean Absolute Standard Error ([a]MASE)								
		MPM		Einstein-Brown		Parker		Parker et al.	Equation (3.6)	
		Surface	Subsurface	Surface	Subsurface	Surface	Subsurface	Subsurface	Mode approach	Median approach
Sagehen Creek	55	[b]N	N	3.3	65	1554	171	218	2.52	2.53
Elbow River	19	N	27	8.6	11.7	4.54	23	2.2	1.49	1.49
Jacoby River	100	1975	6227	21	496	62	978	102	5.23	69.68

[a]MASE = Calculated from Equation (3.7).
[b]N = The relation is unable to calculate either all or most of the bedload transport rates because of difficulty in identifying the critical conditions.

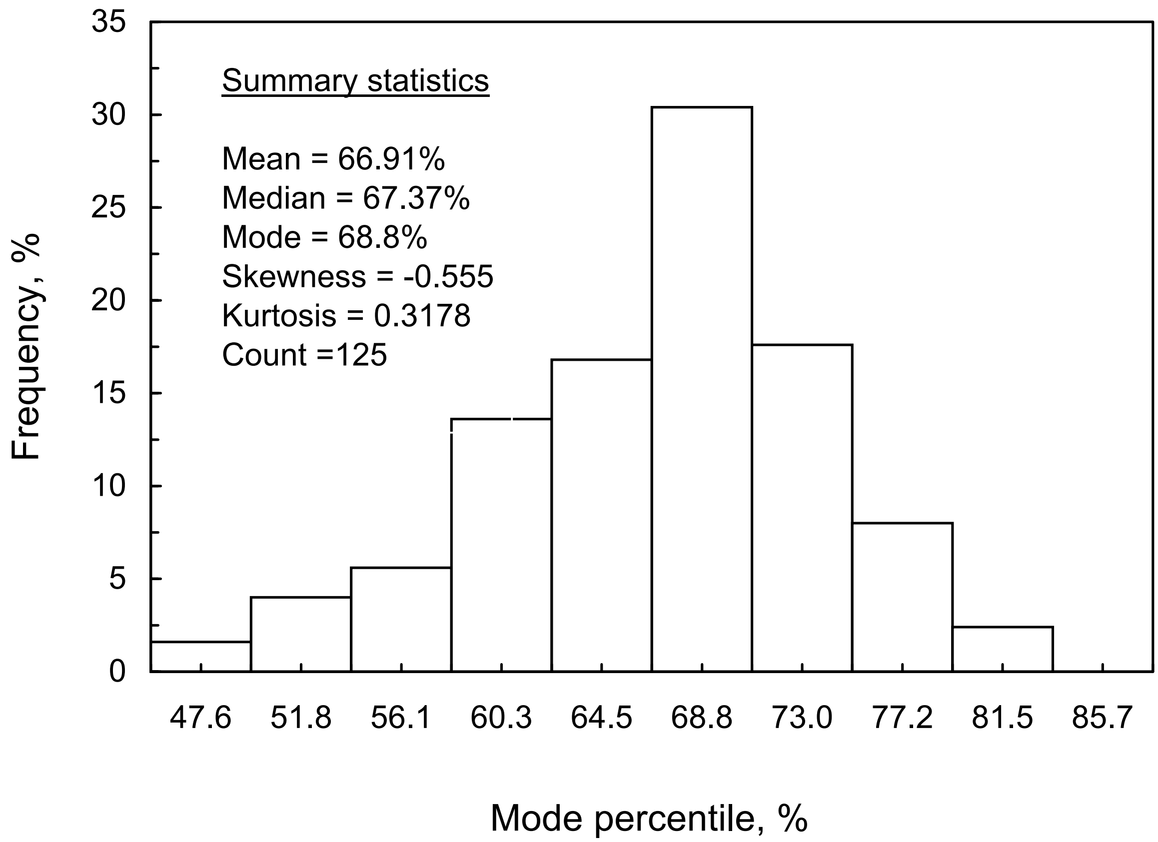

Figure 3.1 Mode percentiles for 125 fluvial gravel beds with unimodal sediment. The grain size distributions of the gravel materials were obtained from *Kondolf* [1988].

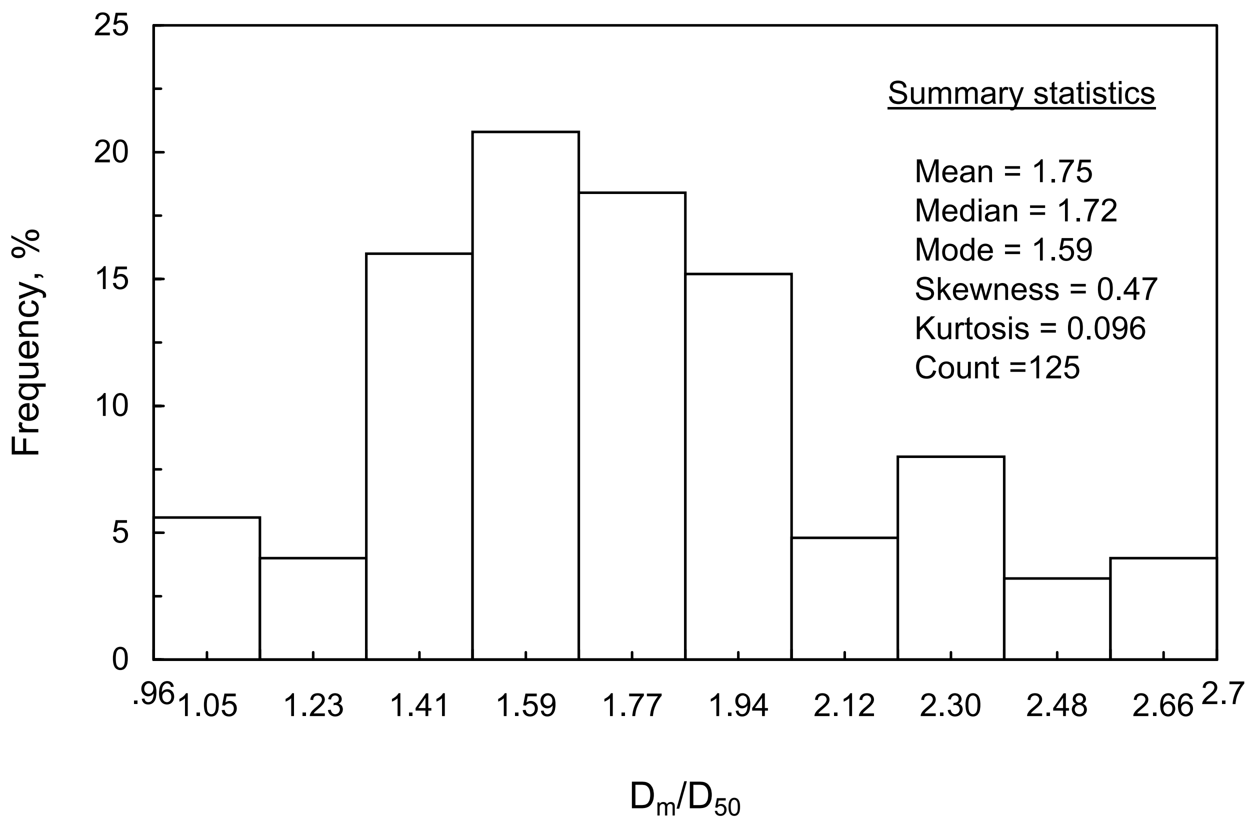

Figure 3.2 Variation of D_m / D_{50} for the 125 fluvial gravel sediments.

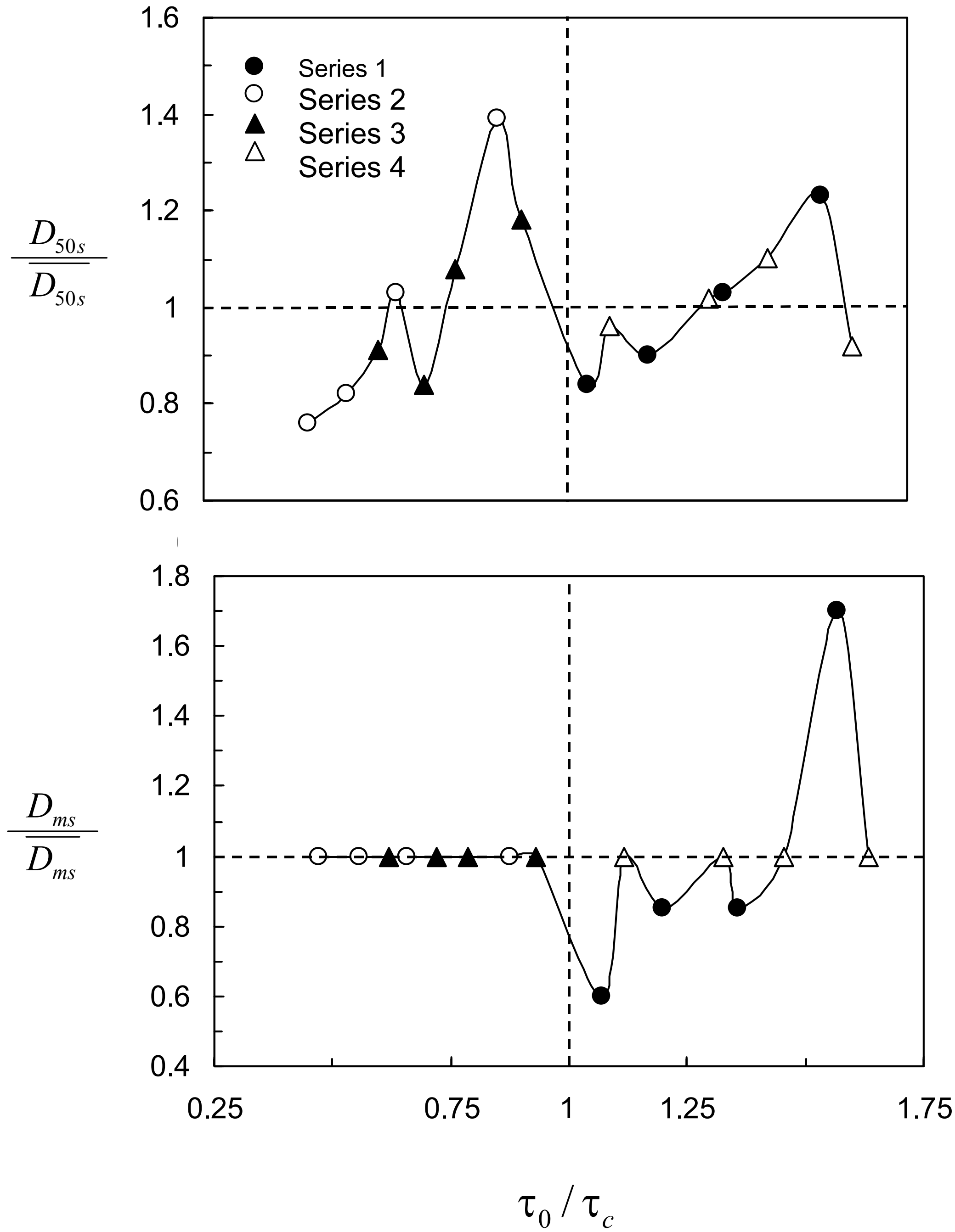

Figure 3.3 Comparison of $D_{ms} / \overline{D_{ms}}$ and $D_{50s} / \overline{D_{50s}}$ with the normalized shear stress τ_0 / τ_c.

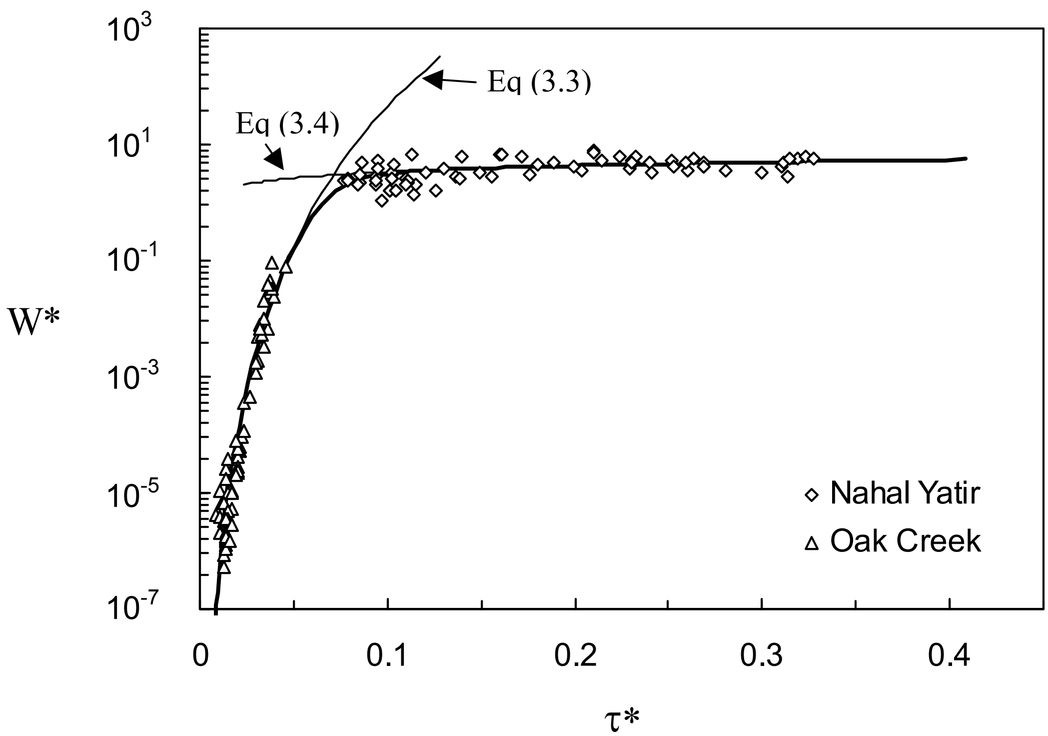

Figure 3.4 Dimensionless plot of bedload transport versus Shields stress based on the data of Oak Creek [*Milhous*, 1973] and Nahal Yatir [*Reid et al.*, 1995].

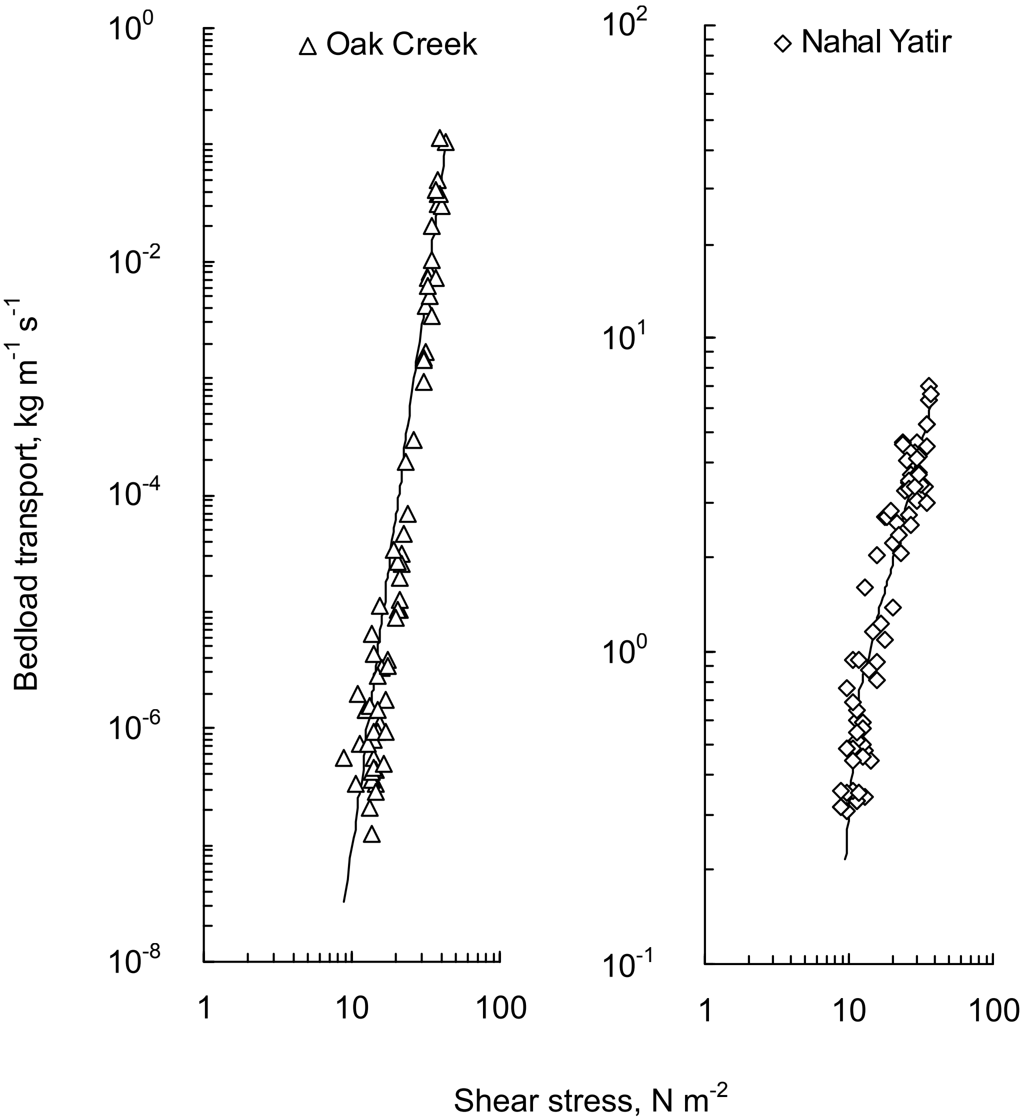

Figure 3.5 Bedload transport rate plotted against shear stress for the data of Oak Creek [*Milhous*, 1973] and Nahal Yatir [*Reid et al.*, 1995]. The solid line represents Equation (3.6).

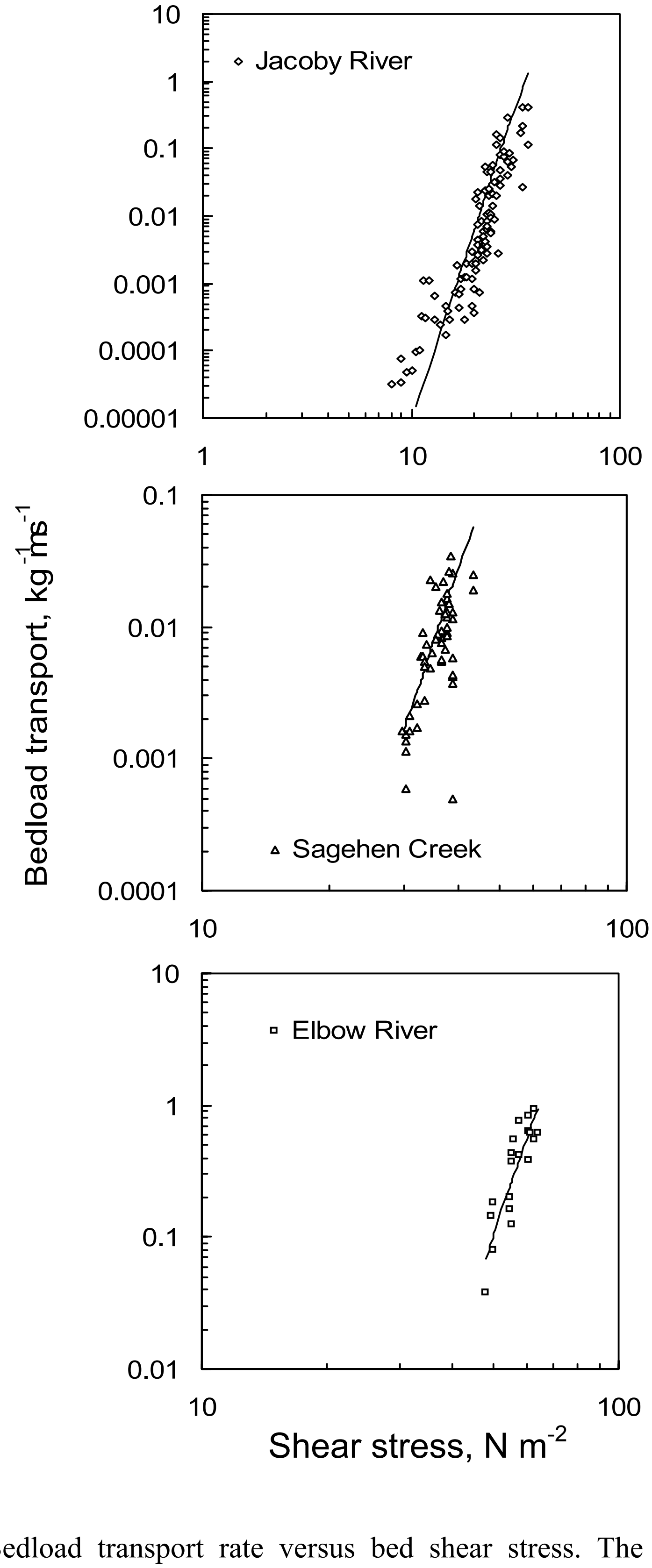

Figure 3.6 Bedload transport rate versus bed shear stress. The solid line represents bedload transport rates predicted by Equation (3.6).

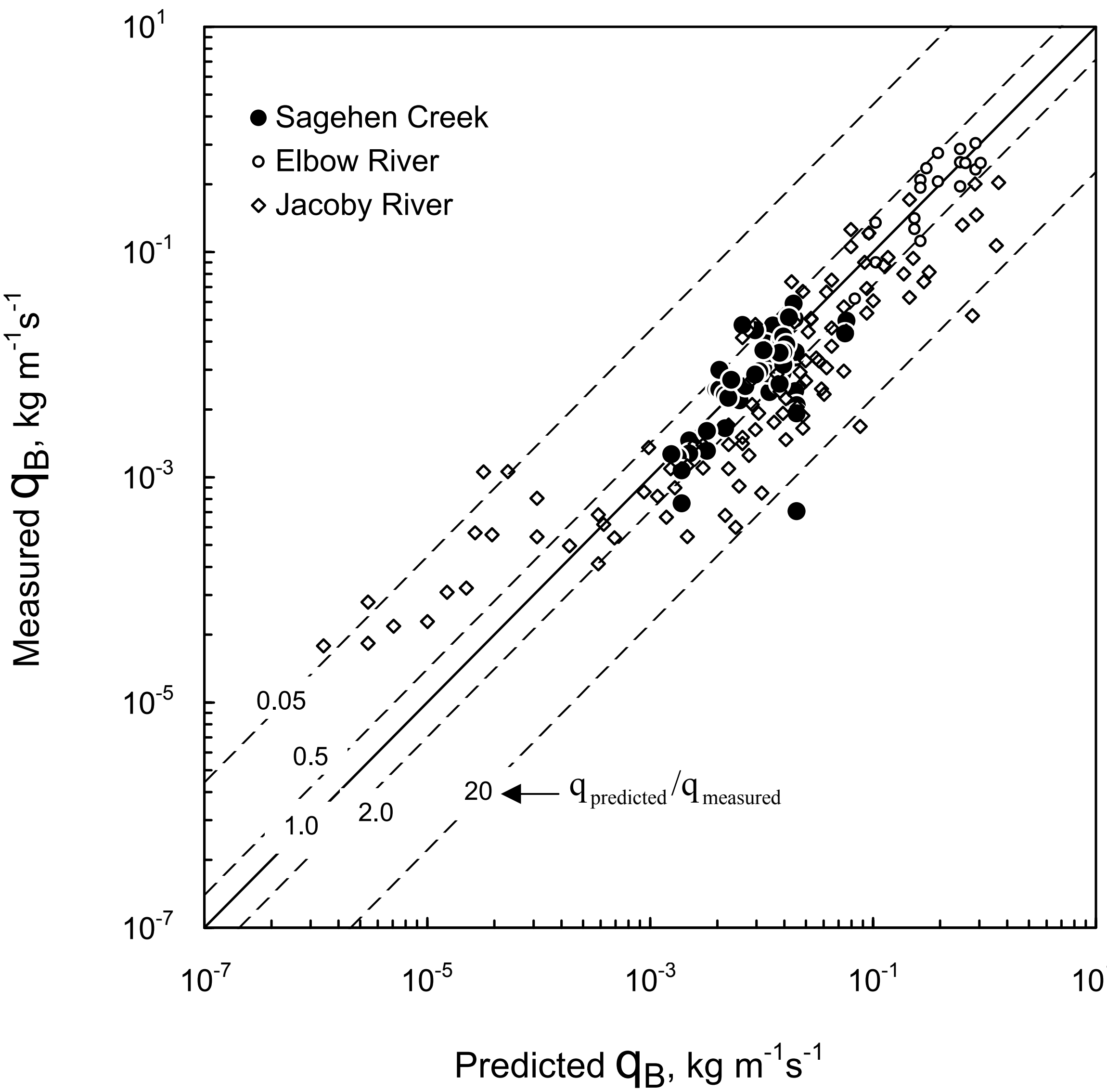

Figure 3.7 Measured versus predicted bedload transport rates based on the mode approach.

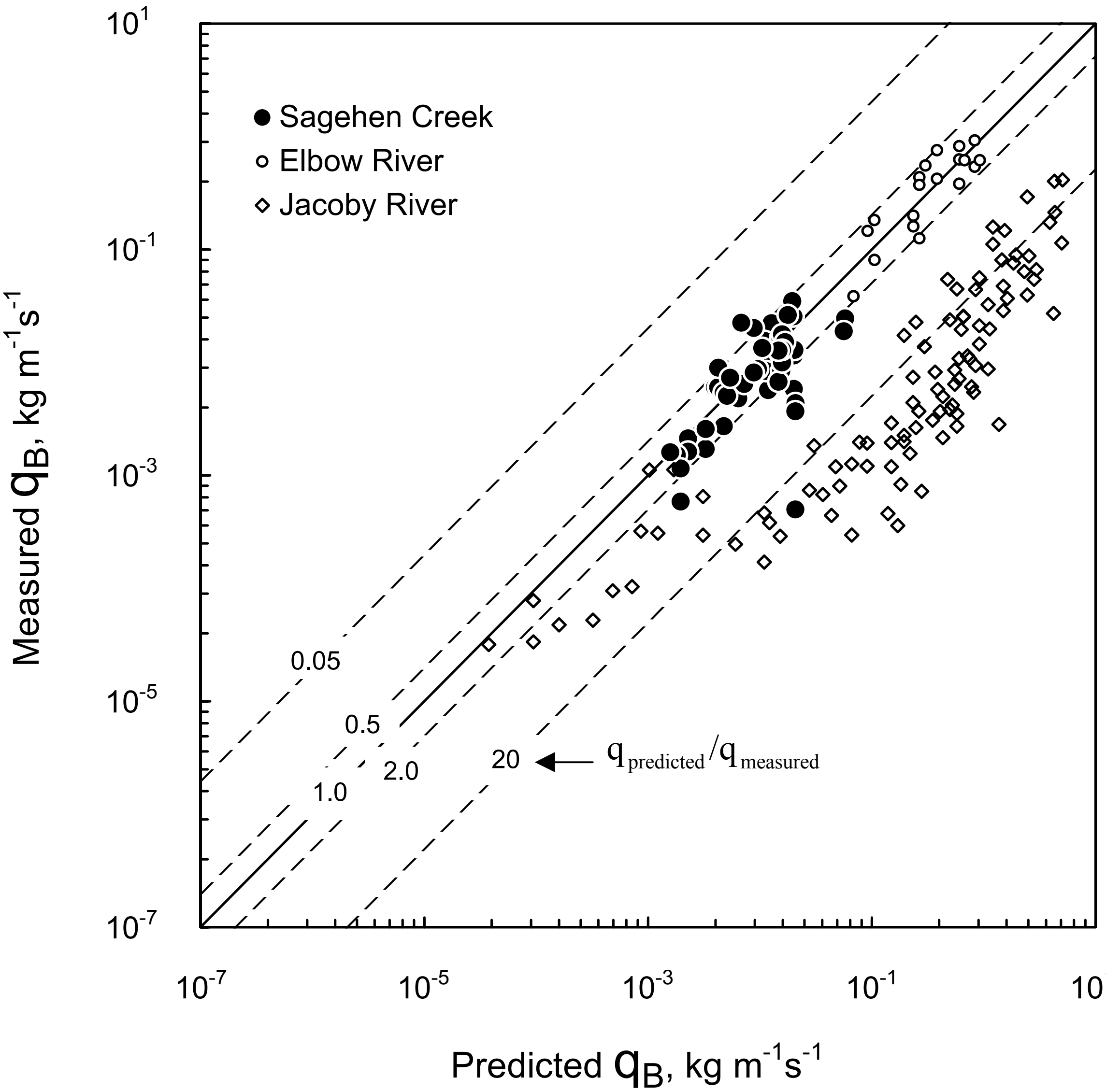

Figure 3.8 Measured versus predicted bedload transport rates based on the median approach.

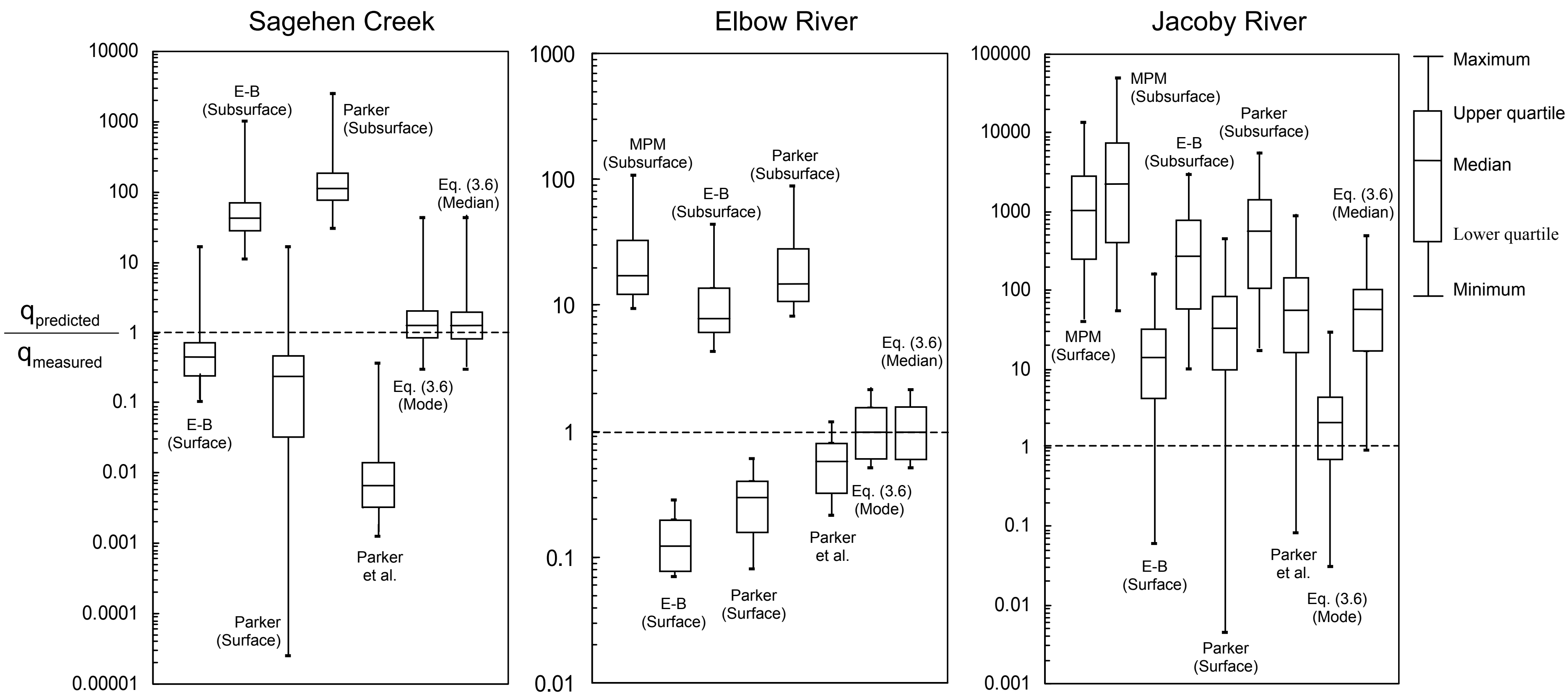

Figure 3.9 Box plots showing the distribution characteristics of the discrepancy ratio, $q_{predicted}/q_{measured}$, for the examined bedload transport relations.

Chapter 4: Bedload Transport Analysis in Gravel-Bed Streams with Bimodal Sediment

4.1 Abstract

The prediction of bedload transport rate in gravel-bed streams with bimodal sediment becomes highly complicated because of the presence of two representative mode grain sizes that may interact with each other, thus affecting the amount of bedload contributed by each one. An approach is proposed here for rendering the bimodal sediment into two independent unimodal fractions, one for sand and another for gravel. The approach relies on scaling the measured reference Shields stresses of sand and gravel modes to match the reference value of the mode of bed material having unimodal sediment. Subsequently, the contribution of each mode to bedload can be estimated by using a transport formula that has been previously proposed for unimodal sediment. Experimental and field bedload transport data sets collected by *Kuhnle* for the case of bimodal sediment are used to examine the validity of the overall approach.

4.2 Introduction

The material in gravel streambeds is either unimodal or bimodal [*Kondolf*, 1988]. In the second case, the presence of two modes, typically one of sand size and the other of gravel, complicates the bedload transport rate predictions [e.g., *Kuhnle*, 1993a; *Powell*, 1998; *Wilcock*, 1993; *Wilcock*, 2001; *Klingeman and Emmett*, 1982; *Ferguson et al.*, 1982]. The traditional approach for calculating bedload transport using a single characteristic grain size, such as the median, may not be appropriate in this case. This will be especially evident when the median falls in the gap between the two modes and, therefore, represents a size class containing a small percentage of the overall sediment [*Sambrook Smith et al.*, 1997].

One approach for estimating bedload transport rates in gravel-bed streams with bimodal sediment consists of dividing the material into two unimodal fractions, each with a representative particle diameter [e.g., *Bagnold*, 1980; *Kuhnle*, 1992; *Wilcock*, 1998]. *Bagnold* [1980] suggested using the corresponding mode grain size to represent each of the two unimodal fractions. For this case, the simplest possible approach for calculating bedload transport rates would be to carry out two separate computations, one for each mode grain size.

However, such an approach treats the mobility of the sand and gravel components as completely independent of each other, which is contrary to what one might expect, and has been reported in the literature [e.g., *Bagnold*, 1980], for most cases of bimodal mixtures. In some cases, the sand mode tends to hide around the gravel mode and requires a higher shear stress value to be entrained compared to that required for the same size in uniform material. In contrast, the gravel mode becomes more exposed to the hydrodynamic fluid forces and, therefore, requires a lower shear stress value to be entrained compared to that required for the same size in uniform material.

This study was carried out with the objective of presenting a new way for estimating bedload transport rates in gravel-bed streams with bimodal sediment. An approach for decoupling the sand from gravel fractions and thus rendering the bimodal sediment into two independent unimodal fractions is proposed. The computation of bedload transport for each sediment fraction is then performed using a suitable relation for unimodal sediments. The validity of the approach is examined using experimental and field bedload transport data from *Kuhnle*, with bed materials having 90%, 75%, 55%, and 25% of sand.

4.3 Two Fractions of Bedload Transport

During flow events capable of transporting sediment, the sand and gravel fractions of a bimodal bed material may interfere with each other, thus affecting the amount of bedload contributed by each one. This interference is influenced by several factors, including the percentage of sediment in each fraction and in each mode, and the separation between the two modes [*Wilcock*, 1992; *Wilcock*, 1993; *Kuhnle*, 1993b]. Data collected from a laboratory flume study by *Kuhnle* [1993b] are used here to examine the behavior of the two sediment fractions during bedload transport events.

The experiments were conducted in a flume 15.2 m long, 0.356 m wide, and 0.457 m deep. The slope of the channel was adjustable, and both water and sediment were recirculated. Three bed materials were employed, SG10, SG25, and SG45 (Figure 4.1); where the letter S refers to sand fraction, G to gravel fraction, and the two-digit number to the percentage of gravel in the original mixture—that is, the original sediment mixture designed as SG45 consists of 45% of gravel and 55% of sand [*Kuhnle*, 1993b]. For each material, with the mode grain size of sand, D_s, and gravel, D_g, being shown in Table (4.1), six runs were performed and bedload transport rates were measured. As reported by *Kuhnle* [1993b], vertical segregation of the channel bed material similar to that in natural gravel streambeds, with a surface layer overlying a finer subsurface, is absent during all the bimodal experiments.

In Figure (4.2), the grain size distributions of the bedload samples collected by *Kuhnle* [1993b] are arranged for each material in terms of bed shear stress, τ, from the lowest (starting at the left) to the highest available shear stress value. As can be seen, at low shear stresses, only sand is transported downstream. This is most evident in plots SG10-4, SG25-4, and SG45-3. At higher shear stresses, part of the gravel component starts appearing in the transported bedload. As shear stress continues to increase, the gravel amount increases progressively. At the highest available shear stress value, the proportions of gravel and sand appear to be similar to those available in the original sediment mixtures (see SG10-6, SG25-6, and SG45-5).

The results reported by *Kuhnle* [1993b] (Figures 4.1 and 4.2) indicate that, once the whole size range for one fraction is set in motion, the mode grain size of bedload material is similar to that of the original sediment mixture. For example, the original sediment mixture for SG45 has values of $D_s = 0.42$ mm and $D_g = 5.657$ mm that are similar to the corresponding values for SG45-4, -5, and -6 (Figure 4.2). However, the contribution of each sediment fraction to bedload is different from that present in the bed material (Table 4.1). Thus, a practical approach for calculating the total bedload transport rate would be to divide the original sediment mixture into sand, f_s, and gravel fractions, f_g, and then calculate separately the amount of bedload contributed from each sediment fraction. However, a correction will be necessary to account for the degree of influence that the presence of one fraction exerts on the mobility of the other.

4.4 Error from Independence Assumption

For the SG materials, in an effort to determine the influence that one fraction has on the mobility of the other, each sediment fraction is treated like an independent unimodal sediment, then the total bedload transport rate is calculated, and finally a comparison is made between the calculated and measured bedload transport rates.

Assuming two independent unimodal fractions, the total calculated bedload transport rate from sand and gravel, q_B, can be expressed as

$$q_B = f_s q_s + f_g q_g \tag{4.1}$$

where q_s is the calculated bedload transport rate of sand, and q_g is the calculated bedload transport rate of gravel. This can be written in dimensionless form as follows:

$$W^* = f_s W_s^* + f_g W_g^* \tag{4.2}$$

where $W^* = R_s q_B / \sqrt{g}\,(dS)^{1.5}$ is the total dimensionless bedload transport rate, R_s is the submerged specific gravity of the sediment, g is the gravitational acceleration , d is the flow depth, S is the energy slope, and $W_s^* = R_s q_s / \sqrt{g}\,(dS)^{1.5}$ and $W_g^* = R_s q_g / \sqrt{g}\,(dS)^{1.5}$ are the dimensionless bedload transport rates of sand and gravel, respectively.

To determine W^* from Equation (4.2), W_s^* and W_g^* are calculated separately by using a suitable formula that is appropriate for unimodal sediment. The formula proposed by *Almedeij and Diplas* [2002, in review] will be used here, which is an empirical fit to bedload data sets considered to represent a wide range of dimensionless Shields stresses. This formula can be written for sand and gravel, respectively, as

$$W_s^* = \frac{1}{0.132\tau_{ss}^{*\,-0.35} + 10^{-9.59}\,\tau_s^{*\,-7.95}} \tag{4.3}$$

and

$$W_g^* = \frac{1}{0.132\tau_{sg}^{*\,-0.35} + 10^{-9.59}\,\tau_g^{*\,-7.95}} \tag{4.4}$$

where τ_s^* is the Shields stress based on the surface sand mode, τ_{ss}^* is the Shields stress based on the subsurface sand mode, τ_g^* is the Shields stress based on the surface gravel mode, and τ_{sg}^* is the Shields stress based on the subsurface gravel mode. The Shields stress parameter τ_{xx}^* is expressed as $\tau_{xx}^* = dS / R_s D_{xx}$, corresponding to the mode of $xx = s$, ss, g, and sg. In Equations (4.3) and (4.4), the absence of the vertical segregation in the SG materials suggests that the surface and subsurface sand modes, as well as gravel modes, are identical.

Figure (4.3a) shows the trends obtained from Equation (4.2) and the total bedload transport rates measured by *Kuhnle* [1993b] during the flume experiments. It appears that the trends of Equation (4.2) fit the bedload data of SG10 and SG25 more closely than that of SG45. The overall fitting accuracy for each case can be determined by calculating the Mean Absolute Standard Error (MASE), with the results shown in Table (4.2),

$$\mathrm{MASE} = \frac{\sum_{i=1}^{n} q_{ri}}{n} \tag{4.5}$$

where

$$q_{ri} = \begin{cases} \dfrac{q_{i\ measured}}{q_{i\ predicted}} & \text{if} \quad q_{i\ measured} > q_{i\ predicted} \\[2ex] \dfrac{q_{i\ predicted}}{q_{i\ measured}} & \text{if} \quad q_{i\ measured} < q_{i\ predicted} \end{cases}$$

and n is the total number of bedload samples. Equation (4.5) indicates that $\mathsf{MASE} \geq 1$. The closer the MASE value to one is, the better the accuracy of an equation will be, with $\mathsf{MASE} = 1$ representing the condition of perfect agreement. From Table (4.2), the MASE value for SG10 and SG25 is equal to 2.2 and 2.8, respectively, while that of SG45 is 11.7. Although the sample is statistically small, a trend can be observed between the MASE values and the percentage of sand in the SG materials. This correlation is resulted from calculating the total bedload transport rates using Equation (4.2), which ignores the interference between the two sediment fractions.

4.4.1 Reference Shields stress

To examine separately the influence of one sediment fraction on the mobility of the other, it is appropriate to determine the reference Shields stress of sand and gravel modes. The technique of fractional transport analysis of *Parker et al.* [1982] is used for this purpose.

Initially, each SG material is divided into sand and gravel fractions, as suggested by *Wilcock* [1998]. The particle size that is typically considered to separate sand from gravel is $D = 2$ mm. Each fraction is then divided into N grain size ranges, with each size range having a representative grain size diameter, D_i, and a fraction, f_i. The volumetric bedload transport rate of each size range, q_{Bi}, is calculated from the total volumetric bedload discharge, q_B, by $q_{Bi} = p_i q_B$, where p_i is the fraction of bedload material. Transport-shear relations can be plotted using the parameters

$$W_i^* = \frac{R_s q_{Bi}}{f_i \sqrt{g}\,(dS)^{1.5}} \tag{4.6}$$

and

$$\tau_i^* = \frac{dS}{R_s D_i} \tag{4.7}$$

where W_i^* is the dimensionless bedload transport rate for the *i*th grain size, and τ_i^* is the Shields stress for the *i*th grain size. A plot of W_i^* versus τ_i^* for the sand and gravel components is shown in Figure (4.4). The reference Shields stresses of the corresponding modes, estimated at a reference transport rate $W_r^* = 0.002$ [*Parker et al.*, 1982], are shown in Table (4.3).

As can be seen, the estimated reference values of Shields stress capture the degree of interference between the two sediment fractions. When the sand material of the channel bed decreases from 90% to 55%, the reference value of sand, τ_{rs}^*, increases from 0.032 to 0.0687 and of gravel, τ_{rg}^*, from 0.0068 to 0.0078. Moreover, Table (4.3) shows that the estimated references are not analogous to the reference Shields stress value of unimodal sediment, equal to 0.03 at $W_r^* = 0.002$ [e.g., *Paintal*, 1971; *Parker et al.*, 1982; *Diplas*, 1987]. However, for SG10 and SG25, the corresponding values $\tau_{rs}^* \approx 0.032$ and $\tau_{rs}^* \approx 0.036$ are not that difference from 0.03, given the variability typically observed in sediment data. This finding indicates that for a sufficiently large percentage of sand, the sand is not affected in a major way by the presence of gravel; hiding effects become pronounced when the gravel component represents a sizable percentage of the bed material [*Iseya and Ikeda*, 1987].

4.5 Transformation Approach

The calculations of the total bedload transport rate in the SG materials are reconsidered here by accounting for the interaction of sand and gravel components during motion. An approach for transforming the bimodal sediment into two independent unimodal fractions is proposed in this section.

4.5.1 Similarity hypothesis

In Figure (4.4), it can be seen that for each SG material, the trends exhibited by the measured bedload transport rate with shear stress for the sand fraction resemble in shape those for the gravel fraction. The only obvious difference is that the trends for the finer grain sizes are shifted more to the right. Therefore, the trends can possibly be collapsed into a single curve with the aid of an appropriate transformation similar to that used by *Parker et al.* [1982] and *Diplas* [1987].

The transformation is based on similarity analysis and stands on plotting W_i^* in terms of the normalized Shields stress parameter, ϕ_i; where $\phi_i = \tau_i^* / \tau_{ri}^*$, and τ_{ri}^* is the reference Shields stress for the ith grain size. Figure (4.5) shows the similarity collapse for the bimodal materials, with the solid line representing the unimodal trend of bedload transport proposed by *Almedeij and Diplas* [2002, in review] in terms of ϕ_i, calculated using the 0.03 reference Shields stress value. As expected, the fractional bedload transport rates plotted in this form nearly collapse onto the unimodal trend.

It is suggested here that the same similarity concept can be used to collapse rather the two sediment fractions, sand and gravel. That is $\phi = \tau_s^* / \tau_{rs}^* = \tau_g^* / \tau_{rg}^*$. This expression can be written in terms of sand and gravel, each involving the normalized Shields stress of unimodal sediment, respectively, as

$$\frac{\tau_s^{**}}{0.03} = \frac{\tau_s^*}{\tau_{rs}^*} \Rightarrow \tau_s^{**} = 0.03 \times \frac{\tau_s^*}{\tau_{rs}^*} \tag{8}$$

and

$$\frac{\tau_g^{**}}{0.03} = \frac{\tau_g^*}{\tau_{rg}^*} \Rightarrow \tau_g^{**} = 0.03 \times \frac{\tau_g^*}{\tau_{rg}^*} \tag{9}$$

where τ_s^{**} and τ_g^{**} are the scaled Shields stress parameters based on the surface sand and gravel modes, respectively. The scaled parameters τ_s^{**} and τ_g^{**} are expected to behave in the material as if their corresponding modes have mobility characteristics that are independent of each other. For example, for the sand fraction of SG45, if τ_s^* is equal to 0.08, then Equation (4.8) suggests that τ_s^{**} will be equal to 0.035.

Figure (4.6a) shows the similarity collapse for the two sediment fractions using the scaled Shields stress parameters. Here, in the expression of W_i^*, f_i (p_i) represents the entire sediment fraction of sand or gravel in the bed (bedload) material. As can be seen, by using the scaled Shields stress parameters, the W_i^* values for the sand and gravel components nearly collapse onto the unimodal trend. It is interesting to perform the same analysis rather using the non-scaled Shields stress parameters (Figure 4.6b). Here, most of the plotted W_i^* values by the non-scaled parameters did not collapse. The W_i^* values for the gravel fractions fall above the unimodal trend, while the W_i^* values for the sand fraction of SG45 fall below the trend. It is worth mentioning that the W_i^* values for the sand fractions of SG10 and SG25, which have τ_{rs}^* values very close to 0.03, follow nearly the unimodal trend.

4.5.2 Approach and results

It is possible now to use the scaled Shields stress parameters to calculate the bedload transport rate of sand and gravel, respectively, as follows:

$$W_s^{**} = \frac{1}{0.132\left(0.03\times\tau_{ss}^* / \tau_{rs}^*\right)^{-0.35} + 10^{-9.59}\left(0.03\times\tau_s^* / \tau_{rs}^*\right)^{-7.95}} = \frac{1}{0.132\tau_{ss}^{**\,-0.35} + 10^{-9.59}\,\tau_s^{**\,-7.95}} \tag{4.10}$$

and

$$W_g^{**} = \frac{1}{0.132\left(0.03\times\tau_{sg}^* / \tau_{rg}^*\right)^{-0.35} + 10^{-9.59}\left(0.03\times\tau_g^* / \tau_{rg}^*\right)^{-7.95}} = \frac{1}{0.132\tau_{sg}^{**\,-0.35} + 10^{-9.59}\,\tau_g^{**\,-7.95}} \tag{4.11}$$

where $W_s^{**} = R_s q_s / \sqrt{g}\,(dS)^{1.5}$ and $W_g^{**} = R_s q_g / \sqrt{g}\,(dS)^{1.5}$ are the transformed dimensionless bedload transport of sand and gravel, respectively, and τ_{ss}^{**} and τ_{sg}^{**} are the scaled Shields stress parameters based on the subsurface sand and gravel modes, respectively. Obviously, the only difference between the transformed parameters, W_s^{**}

and W_g^{**}, and the corresponding non-transformed parameters, W_s^{*} and W_g^{*}, is that the transformed parameters are calculated using the scaled Shields stresses, which decouple the sand from gravel fractions, thus rendering the bimodal material into two independent unimodal fractions. The total bedload transport rate can be determined as

$$W^{**} = f_s W_s^{**} + f_g W_g^{**} \tag{4.12}$$

where $W^{**} = R_s q_B / \sqrt{g}\,(dS)^{1.5}$ is the total transformed dimensionless bedload transport rate.

Figure (4.3b) presents the trend of Equation (4.12) and the total measured bedload transport rates of SG10, SG25, and SG45. This figure indicates the advantage of the scaled approach (Equation 4.12) over the non-scaled approach (Equation 4.2). More than 83% of the total bedload transport rates calculated by the former approach fall within a range of discrepancy ratio, $q_{predicted}/q_{measured}$, between 0.5 and 2 (Figure 4.7), compared to 55% from the latter. Table (4.2) indicates significant improvement for the overall fitting accuracy, especially for the bedload transport data of SG45. The new MASE value for SG45 is equal to 1.78, which is about 6.6 times smaller than the one obtained from Equation (4.2). For SG10 and SG25, the calculated MASE values are 2 and 1.37, respectively, which are 1.1 and 2 times smaller than the corresponding values obtained from Equation (4.2).

Figure (4.8) shows an example of bedload transport rate computations for each sediment fraction, sand and gravel, of the SG45 material. In this figure, the measured bedload transport rates of sand, as well as of gravel, were plotted with the bedload transport rates calculated by the scaled and non-scaled approaches. The scaled calculations were performed using the expressions $f_s W_s^{**}$, for sand, and $f_g W_g^{**}$, for gravel, while the corresponding non-scaled calculations from $f_s W_s^{*}$ and $f_g W_g^{*}$. For the non-scaled approach, the MASE value for the sand and gravel fractions is equal to 11.4 and 3015, respectively. The scaled approach, however, shows significant improvement, which compares with a value for the sand fraction of 1.71 and for the gravel of 37.

4.6 Application to Goodwin Creek

The preceding analyses imply that if the sand content of the bed material has been reduced significantly, the dependency between the mobility of sand and gravel components would continue to increase until the movement of the sand mode requires the movement of the gravel mode. This is a typical situation when the sand material tends to settle between the gravel grains, leaving little or no sand exposed to the flow [*Wilcock*, 1998]. Goodwin Creek, located in north central Mississippi [*Kuhnle*, 1992], constitutes a good example.

Goodwin Creek is a gravel-bed stream with a weakly bimodal sediment, where the sand amount is about 25% of the surface and 32% of the subsurface material. The channel, which is about 25 m wide and 3 m deep, drains 17.9 km^2 of the watershed and is characterized by relatively steep slopes with a mean value equal to 0.0033. Bedload transport measurements, reported by *Kuhnle* [1992], were collected using a modified version of the Helley-Smith sampler. The channel bed possesses a surface material coarser than the underlying material, with corresponding median grain sizes equal to 11.7 mm and 8.3 mm. Notwithstanding the coarser surface layer, both surface and subsurface materials have similar mode grain sizes at $D_g = 26.9$ mm and $D_s = 0.5$ mm (Figure 4.9).

To examine the behavior of the two sediment fractions in Goodwin Creek, the same criterion of fractional transport analysis can be followed to estimate the reference Shields stresses of the sand and gravel modes. Owing to the vertical segregation of the channel bed material, the reference Shields stresses for the surface sand and gravel modes, as well as those of the subsurface material, should be estimated, because for low shear stresses the former material dominates bedload transport, while for sufficiently high shear stresses the latter dominates. A plot of W_i^* versus τ_i^* suggests estimated reference values for the surface material equal to $\tau_{rs}^* \approx 1.79$ and $\tau_{rg}^* \approx 0.0332$, and similar corresponding values for the subsurface material (Figure 4.10).

On the one hand, the estimated $\tau_{rg}^* \approx 0.0332$ of Goodwin Creek is very close to 0.03, suggesting that the material is approaching a unimodal sediment mixture dominated by gravel [*Iseya and Ikeda*, 1987; *Wilcock*, 1993]. The slightly higher magnitude of τ_{rg}^*, however, has possibly resulted from the amount of sand in the surface, 25%, and subsurface materials, 32%. Laboratory experiments performed by *Diplas and Parker* [1985] suggest that a small amount of sand stabilizes the bimodal sediment by creating a seal that reduces the mobility of the coarser grains.

On the other hand, $\tau_{rs}^* \approx 1.79$ of Goodwin Creek is very high, compared to τ_{rs}^* values of the SG materials (Table 4.3). This higher value might reflect the increased dependency between the mobility of sand and gravel components. *Rakoczi* [1975] and *Wilcock* [1998] suggested that when the mobility of the sand fraction depends completely on that of gravel, the threshold motion for the two sediment fractions will take place roughly at the same dimensional shear stresses—that is $\tau_{rs} \approx \tau_{rg}$; where τ_{rs} and τ_{rg} are the dimensional reference shear stresses of sand and gravel modes, respectively. Consequently, from the expression of the Shields stress parameter, the reference Shields stress of sand and gravel modes will be related to each other as

$$\tau_{rs}^* \approx \tau_{rg}^* \left(D_g / D_s\right) \tag{4.13}$$

It is interesting to check this relation for the determined references of Goodwin Creek. Given the estimated reference of gravel $\tau_{rg}^* \approx 0.0332$, the reference Shields stress of sand mode calculated by Equation (4.13) is equal to 1.7862, which is very close to $\tau_{rs}^* \approx 1.79$.

Figure (4.11) presents a dimensional comparison of the measured bedload transport rates of Goodwin Creek with the trends obtained from the scaled (Equation 4.12) and non-scaled approaches (Equation 4.2). Although the measured bedload transport rates present a very complicated pattern, the scaled approach yields better bedload transport rate predictions than the non-scaled approach. The latter provides MASE value of 450, which compares with a value of 11 from the scaled approach.

4.7 Conclusion

The amount of sand in a bimodal streambed material has an important influence on the initial bedload motion and complicates the bedload transport rate predictions. An approach for transforming the bimodal sediment into two independent unimodal fractions, sand and gravel, has been proposed in order to use for the bedload transport rate computations a suitable relation developed for unimodal sediments. The validity of the approach was examined using available bedload transport data with bed materials having 90%, 75%, 55%, and 25% of sand.

References

Almedeij, J., and Diplas, P., (in review), Bedload transport in gravel-bed streams with unimodal sediment.

Bagnold, R. A., An empirical correlation of bed load transport rates in flumes and natural rivers, *Proc. Roy. Soc. of London, A372*, 453-473, 1980.

Diplas, P., Bedload transport in gravel-bed streams, *J. Hydraul. Engng., Am. Soc. Civ. Eng.*, *113*(3), 277-292, 1987.

Diplas, P., and G. Parker, Pollution of gravel spawning grounds due to fine sediment, *Project Report No. 240*, St Anthony Fall Hydraulic Laboratory, University of Minnesota, Minneapolis, MN, 1985.

Ferguson, R. I., K. L. Prestegaard, P. J. and Ashworth, Influence of sand on hydraulics and gravel transport in a braided gravel bed river, *Water Resour.*, *25*(4), 635-643, 1989.

Iseya, F., and H. Ikeda, Pulsations in bedload transport rates induced by a longitudinal sediment sorting: a flume study using sand and gravel mixtures, *Geogr. Ann.*, *69*, 15-27, 1987.

Klingeman, P. C., and W. W. Emmett, Gravel bedload transport processes, in *Gravel-bed Rivers*, edited by R. D. Hey, J. C. Bathurst, and C. R. Thorne, pp. 141-179, John Wiley & Sons, New York, 1982.

Kondolf, G. M., Salmonid spawning gravels: a geomorphic perspective on their size distribution, modification by spawning fish, and criteria for gravel, Ph.D. thesis, The Johns Hopkins Univ., Baltimore, Maryland, 1988.

Kuhnle, R. A., Fractional transport rates of bed load on Goodwin Creek, in *Dynamics of gravel-bed rivers*, edited by P. Billi, R. D. Hey, C. R. Thorne, and P. Tacconi, pp. 141-155, John Wiley & Sons, Chichester, U.K., 1992.

Kuhnle, R. A., Fluvial transport of sand and gravel mixtures with bimodal size distributions, *Sediment. Geol.*, *85*, 17-24, 1993a.

Kuhnle, R. A., Incipient motion of sand-gravel sediment mixtures, *J. Hydraul. Engng.,* *Am. Soc. Civ. Eng.*, *119*(12), 1400-1415, 1993b.

Paintal, A. S., Concept of critical shear stress in loose boundary open channels, *J. Hydraul. Res.*, *9*(1), 91-113, 1971.

Parker, G., P. C. Klingeman, and D. G. McLean, Bedload and size distribution in paved gravel bed streams, , *J. Hydraul. Div. Am. Soc. Civ. Eng.*, *108*(HY4), 544-569, 1982.

Powell, D. M., Patterns and processes of sediment sorting in gravel-bed rivers, *Prog. Phys. Geog.*, *22*(1), 1-32, 1998.

Rakoczi, L., Influence of grain-size composition on the incipient motion and self-pavement of bed materials, *Proc. of the 16th congress of the Int. Assoc. for Hydraul. Res.*, Sao Paulo, Brazil, Vol. 2, July, 150-157, 1975.

Sambrook Smith, G. H., A. P. Nicholas, and R. I. Ferguson, Measuring and defining bimodal sediments: Problems and implications, *Water Resour. Res.*, *33*(5), 1179-1185, 1997.

Wilcock, P. R., Bed-load transport of mixed-size sediment, in *Dynamics of gravel-bed rivers*, edited by P. Billi, R. D. Hey, C. R. Thorne, and P. Tacconi, pp. 109-131, John Wiley & Sons, Chichester, U.K., 1992.

Wilcock, P. R., Critical shear stress of natural sediments, *J. Hydraul. Engng., Am. Soc. Civ. Eng.*, *119*(4), 491-505, 1993.

Wilcock, P. R., Two-fraction model of initial sediment motion in gravel-bed rivers, *Science*, *280*, 410-412, 1998.

Wilcock, P. R., Toward a practical method for estimating sediment-transport rates in gravel-bed rivers, *Earth Surf. Processes Landforms*, *26*, 1395-1408, 2001.

Notation

D_g	Mode grain size of gravel, [L]
D_i	Mean grain size of the *i*th grain size range, [L]
D_s	Mode grain size of sand, [L]
d	Flow depth, [L]
f_g	Fraction of gravel in surface material
f_i	Fraction of the material in *i*th grain size range
f_s	Fraction of sand in surface material
g	Gravitational acceleration, [L/T^2]
p_i	Fraction of bedload in *i*th grain size range
q_B	Volumetric bedload transport rate per unit channel width, [L^2/T]
q_{Bi}	Volumetric bedload per unit width in *i*th grain size range, [L^2/T]
q_g	Volumetric bedload transport rate of gravel, [L^2/T]
q_s	Volumetric bedload transport rate of sand, [L^2/T]
R_s	Submerged specific gravity of the sediment
S	Energy slope
W^*	Dimensionless bedload parameter
W^{**}	Transformed dimensionless bedload transport
W_g^*	Dimensionless bedload transport of gravel
W_g^{**}	Transformed dimensionless bedload transport of gravel
W_i^*	Dimensionless bedload transport of *i*th grain size range
W_r^*	Reference dimensionless bedload transport
W_s^*	Dimensionless bedload transport of sand
W_s^{**}	Transformed dimensionless bedload transport of sand

τ	Bed shear stress, [M/LT^2]
τ_g^*	Shields stress of surface gravel mode
τ_g^{**}	Scaled Shields stress of surface gravel mode
τ_i^*	Shields stress of *i*th grain size range
τ_{rg}^*	Reference Shields stress of gravel mode
τ_{rs}^*	Reference Shields stress of sand mode
τ_s^*	Shields stress of surface sand mode
τ_s^{**}	Scaled Shields stress of surface sand mode
τ_{sg}^*	Shields stress of subsurface gravel mode
τ_{sg}^{**}	Scaled Shields stress of subsurface gravel mode
τ_{ss}^*	Shields stress of subsurface sand mode
τ_{ss}^{**}	Scaled Shields stress of subsurface sand mode

Table 4.1 Bedload material, original sediment mixture, and exposed shear stress conditions.

Experimental Run	Original sediment mixture D_s mm	Original sediment mixture D_g mm	Bedload material D_s mm	Bedload material D_g mm	Bedload material Sand %	Bedload material Gravel %	τ N m^{-2}	τ_s^*	τ_g^*
SG10-4	0.42	4.757	0.42	N[a]	99.99	0.01	0.2496	0.0367	0.0032
SG10-3			0.42	N	99.99	0.01	0.3756	0.0553	0.0049
SG10-2			0.42	N	99.9	0.1	0.5439	0.08	0.0071
SG10-1			0.42	N	99.66	0.34	0.7347	0.108	0.0095
SG10-5			0.42	4.757	96.64	3.36	1.6165	0.2378	0.021
SG10-6			0.42	4.757	92.76	7.24	2.4281	0.357	0.0315
SG25-4	0.5	5.657	0.5	N	99.999	0.001	0.3036	0.0375	0.0033
SG25-3			0.5	N	99.987	0.013	0.4806	0.0594	0.0052
SG25-2			0.5	N	99.93	0.07	0.6568	0.0812	0.0072
SG25-1			0.5	N	99.75	0.25	0.7645	0.0945	0.0084
SG25-5			0.5	5.657	91.397	8.603	1.4554	0.1799	0.0159
SG25-6			0.5	5.657	76.84	23.16	2.5776	0.3185	0.0282
SG45-3	0.42	5.657	0.42	N	99.99	0.01	0.5966	0.0878	0.0065
SG45-2			0.42	N	99.97	0.03	0.8009	0.1178	0.0088
SG45-1			0.42	N	99.95	0.05	1.0378	0.153	0.0113
SG45-4			0.42	5.657	85.5	14.5	1.7311	0.255	0.0189
SG45-6			0.42	5.657	67.147	32.853	2.2486	0.331	0.0246
SG45-5			0.42	5.657	56.137	43.863	2.6456	0.389	0.0289

[a]N = No enough material in motion to identify clear mode size.

Table 4.2 Fitting accuracy of total bedload transport calculated based on scaled and non-scaled approaches.

Data set	Sand of surface %	$MASE = \frac{\sum_{i=1}^{n} q_{ri}}{n}$	
		Scaled	Non-scaled
SG10	90	2	2.2
SG25	75	1.37	2.8
SG45	55	1.78	11.7
Goodwin Creek	25	11	450

Table 4.3 Reference Shields stresses of sand and gravel modes estimated at $W_r^* = 0.002$.

Bed material	τ_{rg}^*	τ_{rs}^*	$0.03/\tau_{rg}^*$	$0.03/\tau_{rs}^*$
SG10	0.0068	0.032	4.412	0.938
SG25	0.0072	0.036	4.167	0.833
SG45	0.0078	0.0687	3.846	0.437

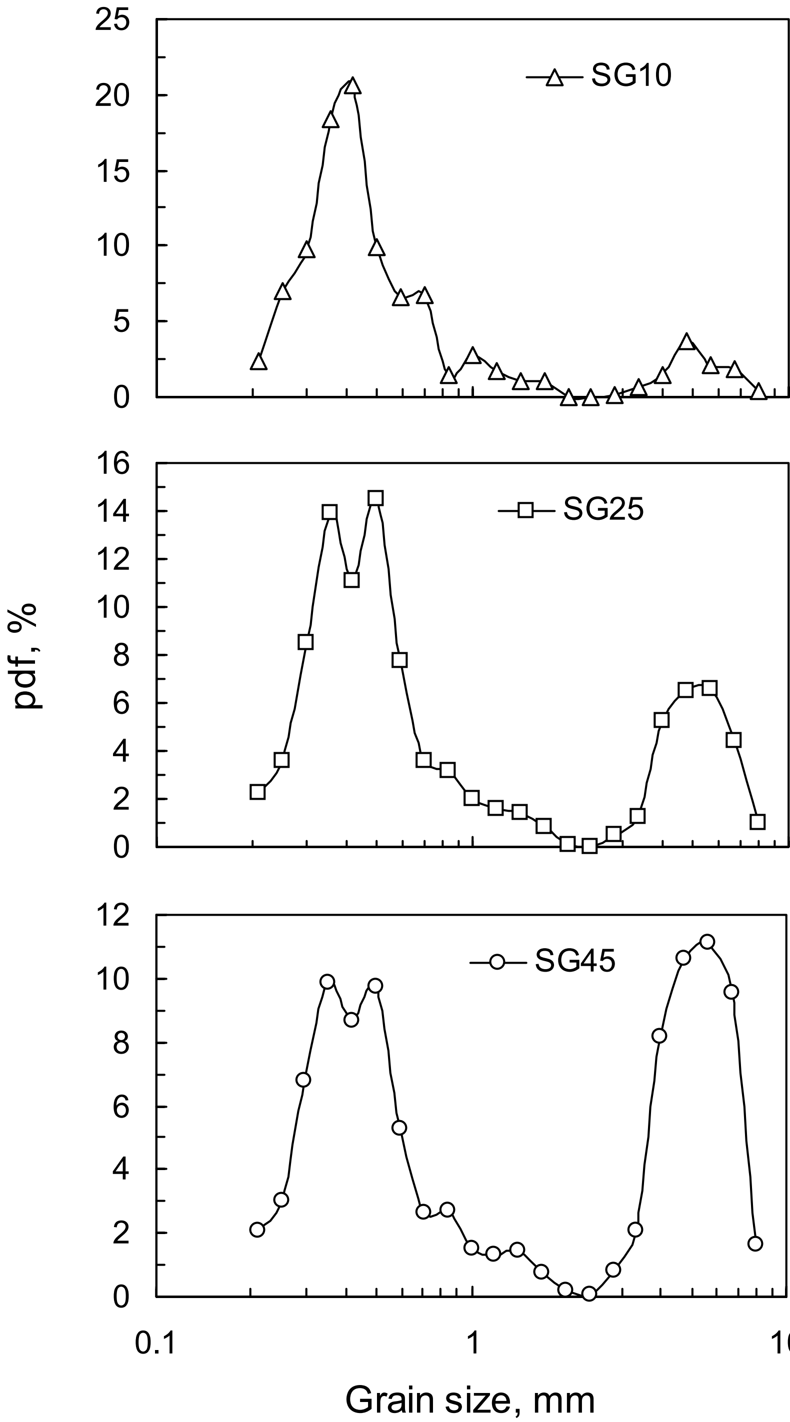

Figure 4.1 Grain size distribution of SG bed materials. Data source is from *Kuhnle* [1993b].

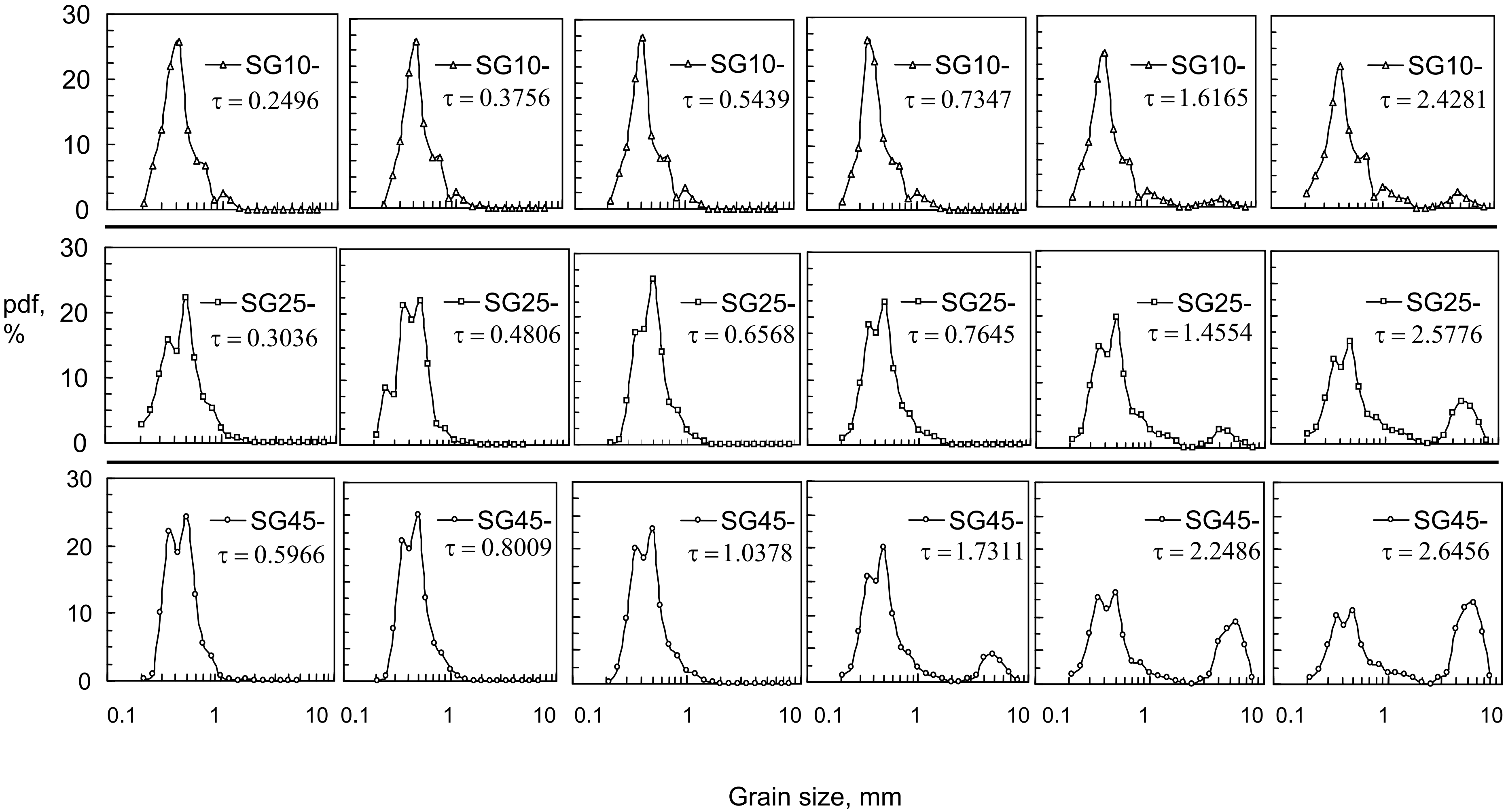

Figure 4.2 Grain size distributions of bedload materials, arranged from the left to the right based on the bed shear stresses, τ ($\mathrm{N\,m^{-2}}$), from the lowest to the highest available shear stress values. Data source is from *Kuhnle* [1993b].

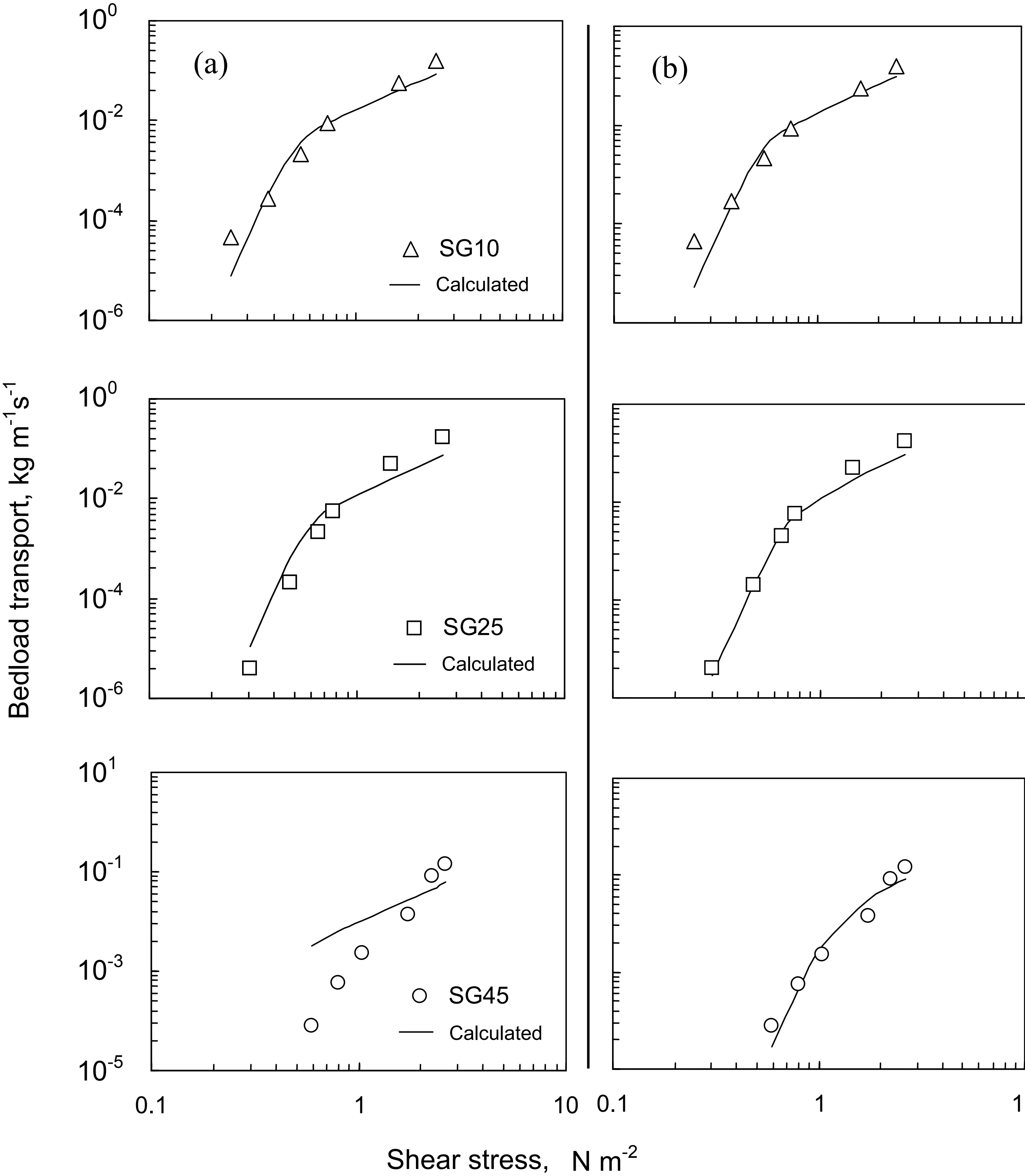

Figure 4.3 Bedload transport versus bed shear stress, with the solid line representing the calculated bedload transport rates. (a) Bedload calculation is based on the non-scaled approach of Equation (4.2); (b) bedload calculation is based on the scaled approach of Equation (4.12).

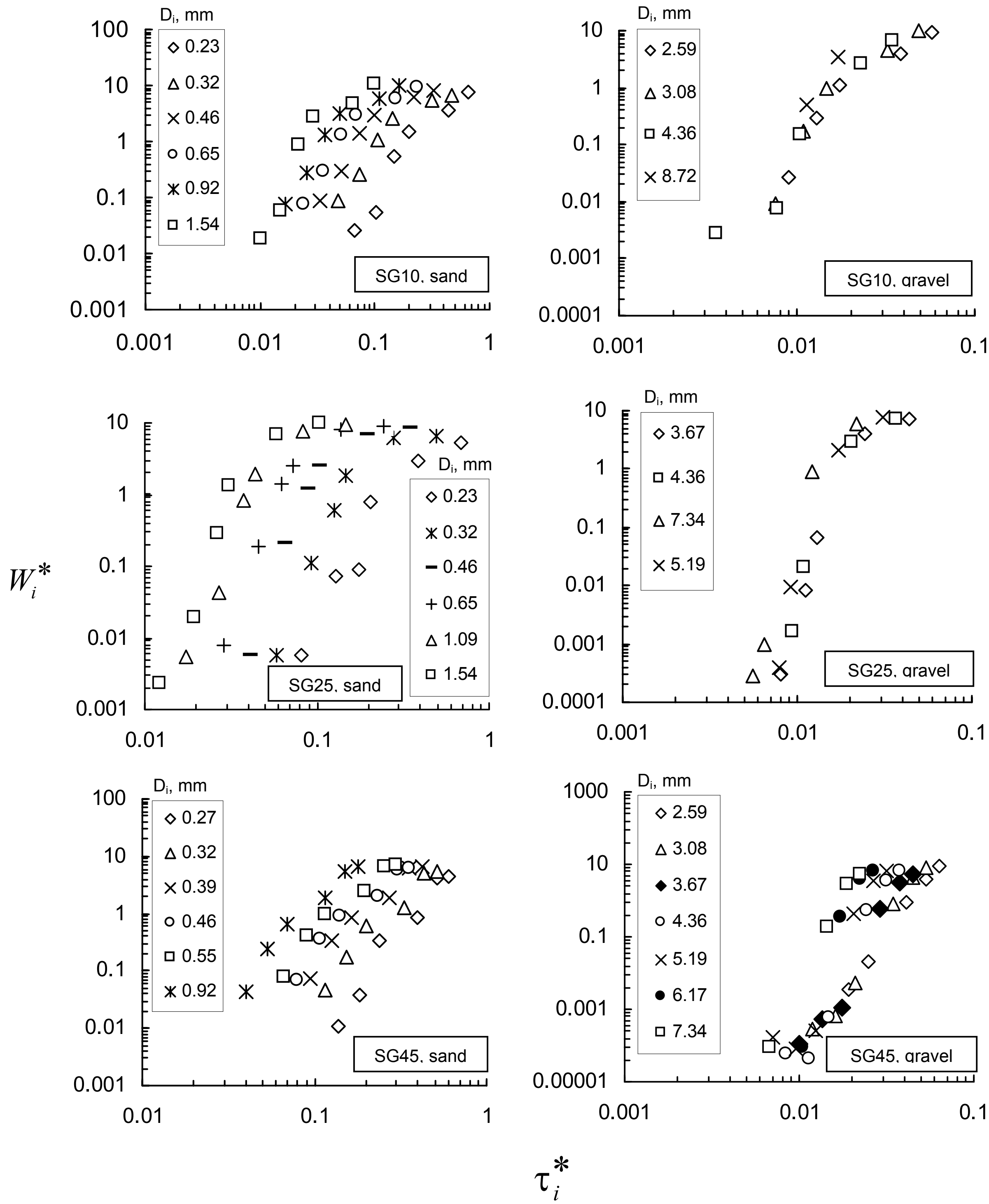

Figure 4.4 Plot of W_i^* versus τ_i^* for the sand and gravel fractions of SG materials. Data source is from *Kuhnle* [1993b].

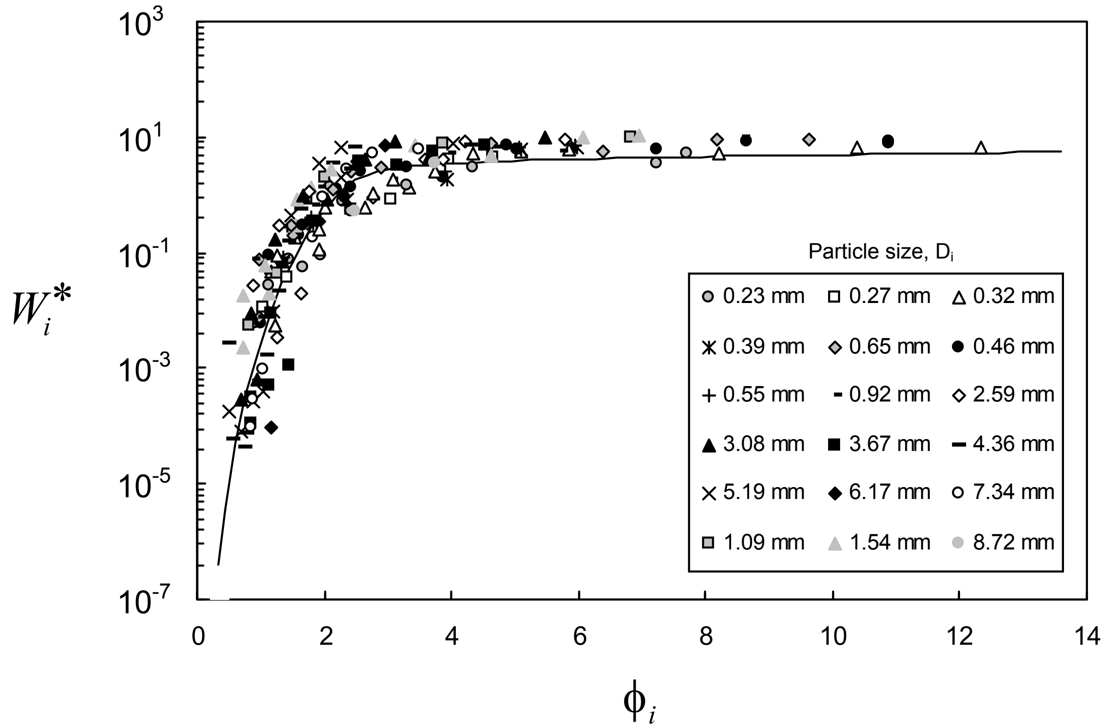

Figure 4.5 Similarity collapse for the SG data of *Kuhnle* [1993b], with D_i sizes indicated. The solid line represents the trend of bedload transport of *Almedeij and Diplas* [2002, in review] in terms of ϕ_i, calculated using a reference Shields stress value equal to 0.03.

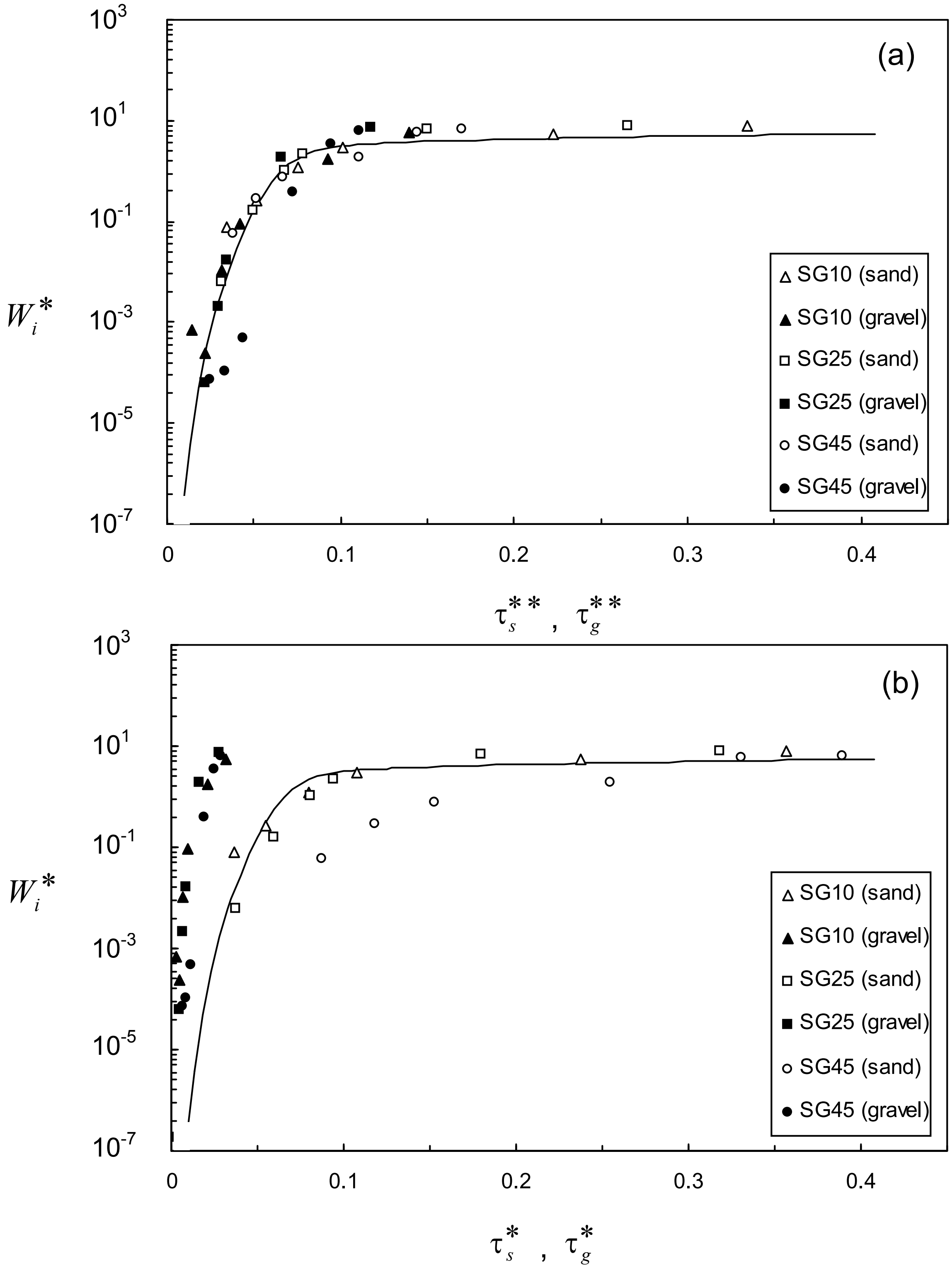

Figure 4.6 Dimensionless bedload transport versus Shields stress for the sand and gravel fractions of SG materials of *Kuhnle* [1993b], with the solid line representing the unimodal trend of *Almedeij and Diplas* [2002, in review] in terms of Shields stress. (a) Analysis is based on the scaled approach; (b) analysis is based on the non-scaled approach.

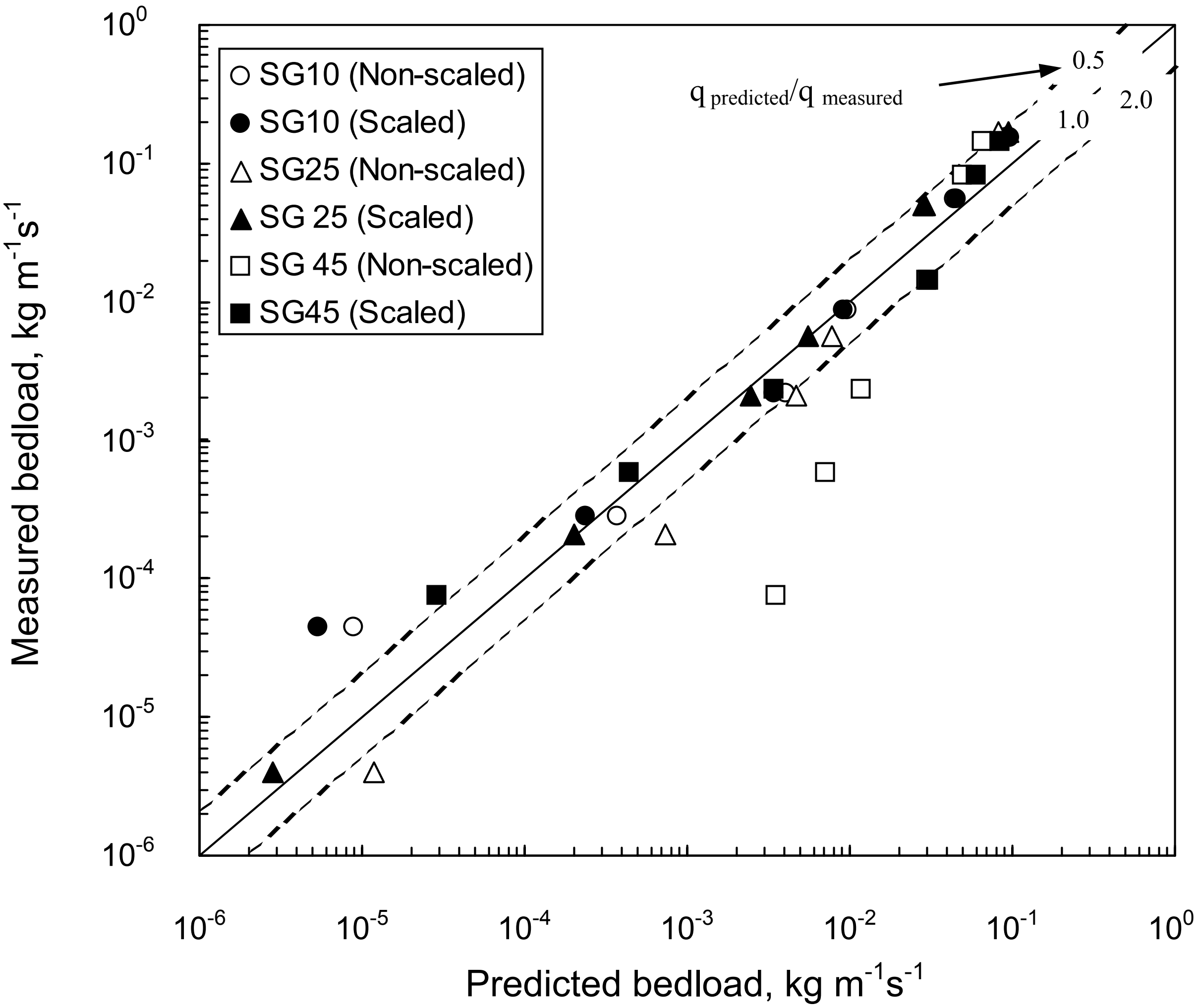

Figure 4.7 Measured versus predicted bedload transport rate for the SG data of *Kuhnle* [1993b].

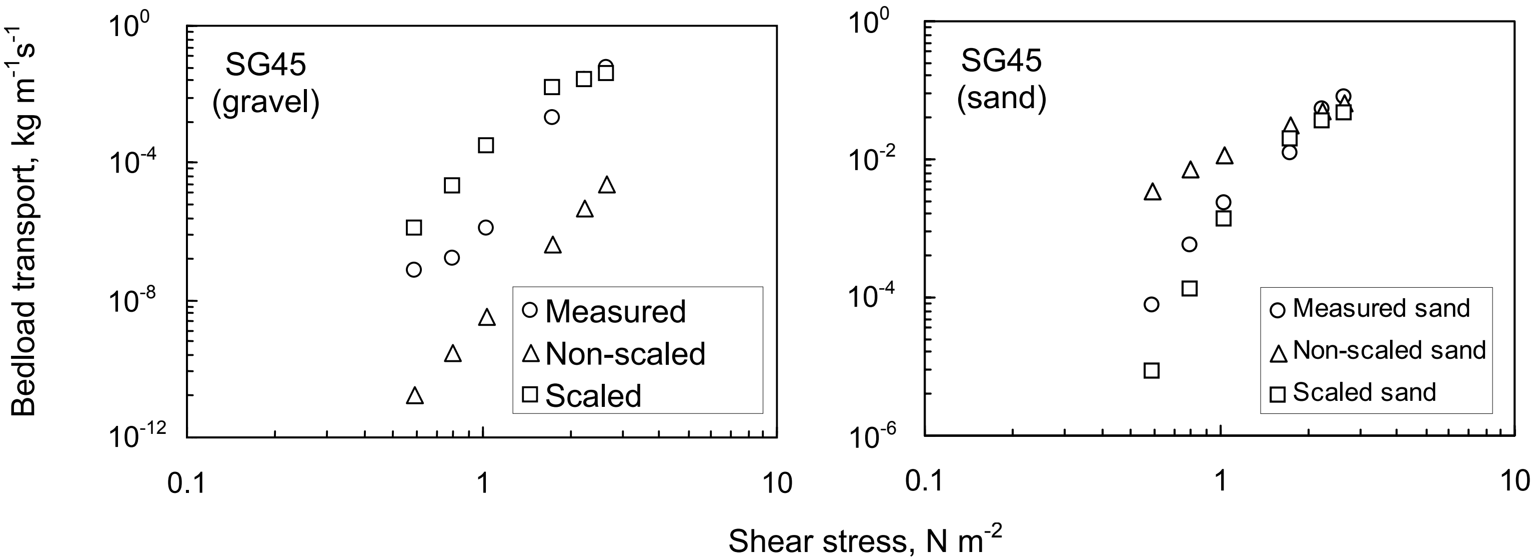

Figure 4.8 Calculated and measured bedload transport versus bed shear stress for the sand and gravel fractions of SG45.

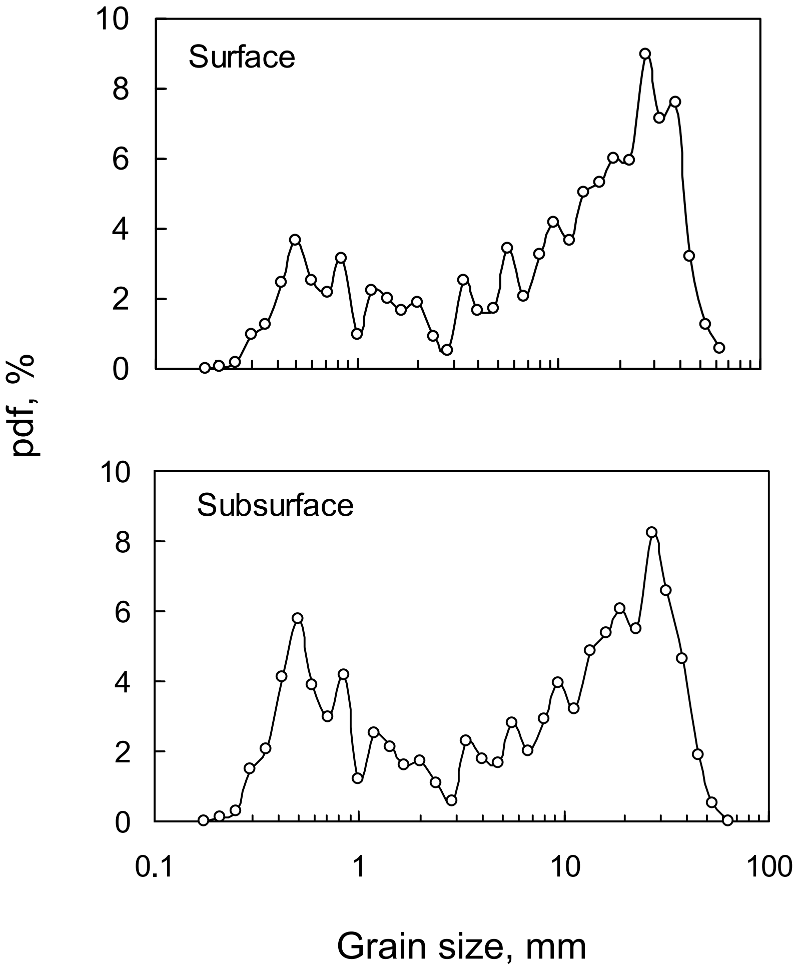

Figure 4.9 Grain size distribution for the surface and subsurface materials of Goodwin Creek. Data source is from *Kuhnle* [1992].

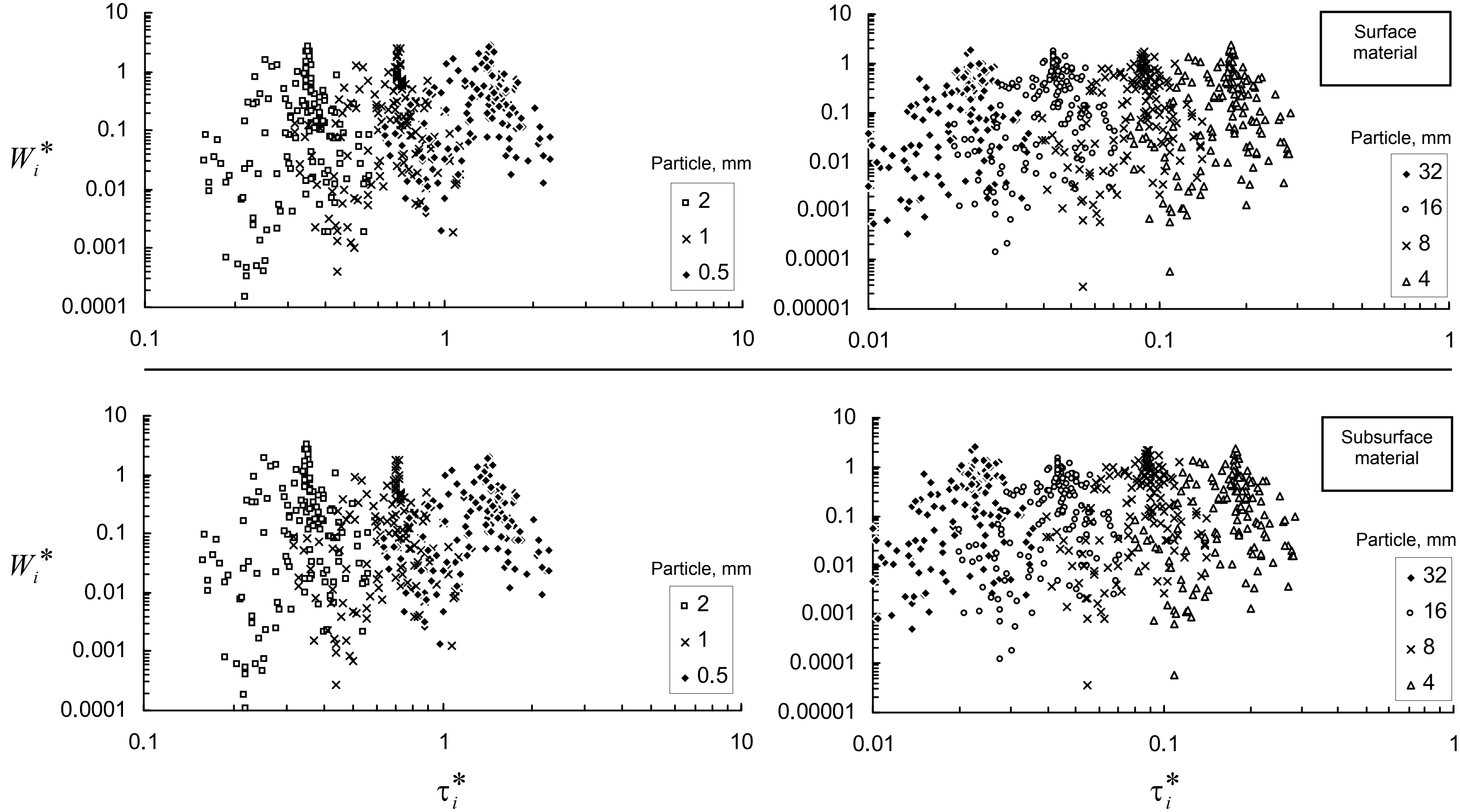

Figure 4.10 Plot of W_i^* versus τ_i^* for the surface and subsurface materials of Goodwin Creek. Data source is from *Kuhnle* [1992].

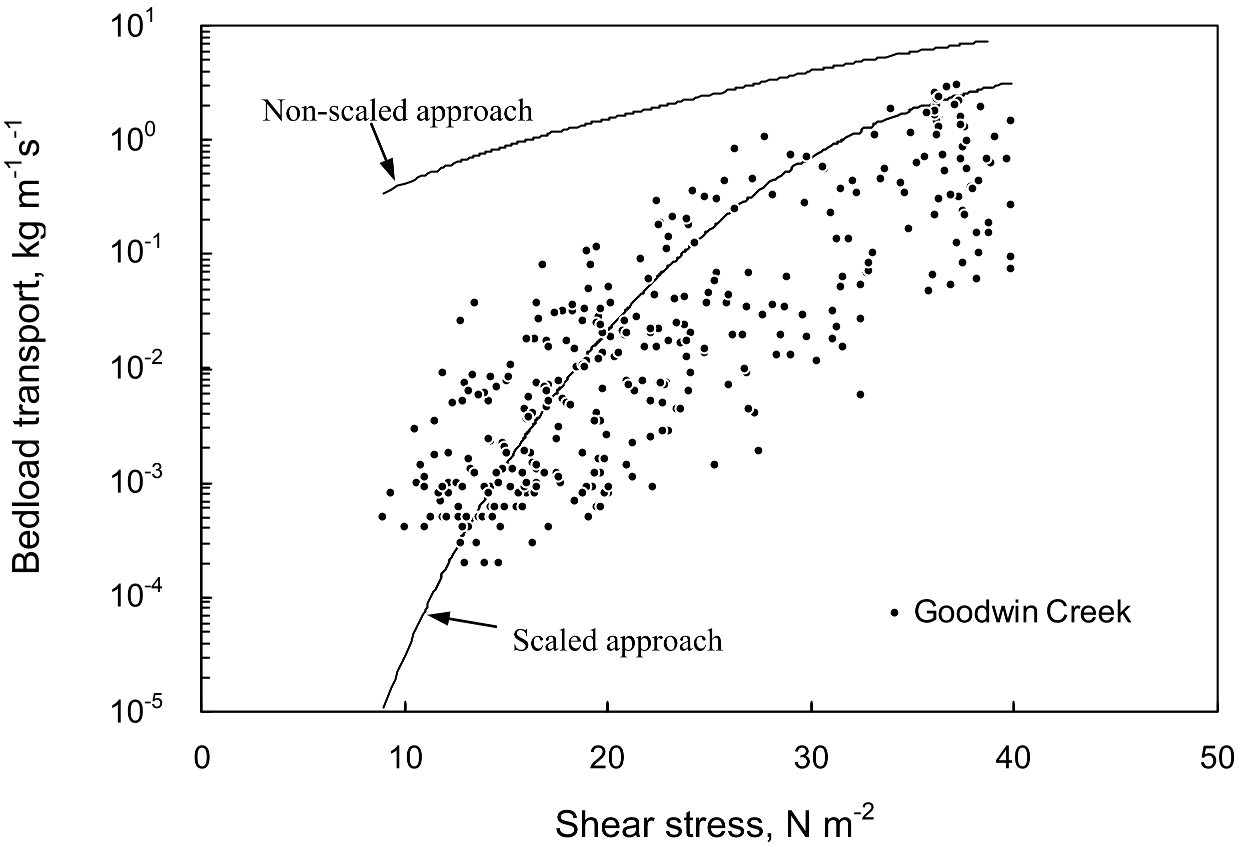

Figure 4.11 Comparison between measured and predicted bedload transport rates for Goodwin Creek. The solid line represents the predicted values. Only the bedload transport data points with $\tau < 40\ \mathrm{N\,m^{-2}}$ are used in this comparison, as recommended by *Kuhnle* [1992].

Chapter 5: Overall Summary and Conclusions

Investigating bedload transport in perennial and ephemeral gravel-bed streams has proved important, because the lower magnitudes of flow strengths encountered in the ephemeral Nahal Yatir appear to coincide with the higher magnitudes of flow strengths in the perennial Oak Creek. This finding suggests that bedload transport data might actually be parts of the same overall curve relating bedload transport rate to increasing bed shear stress.

The investigation was used to propose an empirical bedload transport relation that accommodates the mode grain size of the surface and subsurface materials and accounts for the variation of the surface make-up within a wide range of Shields stresses. The accuracy of the relation was tested using available bedload data from unimodal sediment, which are Sagehen Creek, Elbow River, and Jacoby River data. The relatively high discrepancies between predicted and measured bedload transport rates may have resulted from using for the computations a single particle size, rather than the entire range of sizes, of bed material. Indeed, fractional-based bedload transport rate predictions are more preferable for a poorly sorted sediment material, as in the case of gravel-bed streams. Notwithstanding the relatively high discrepancies, a comparison with commonly used bedload transport relations that employ either a surface or subsurface representative particle revealed that the relation of this study provides the most accurate predictions.

The presence of the two modes in a bimodal sediment was found to complicate further the bedload transport rate predictions. This is because, during flow events capable of transporting sediment, one mode may influence the mobility of the other, thus affecting the amount of bedload contributed by each one. An approach for transforming the bimodal material into two independent unimodal sediment fractions has been proposed. The approach relies on scaling the measured reference Shields stresses of sand and gravel modes to match the reference Shields stress value of the mode of unimodal sediment. The validity of the approach was examined using the data of SG materials, with 90%, 75%, and 55% of sand bed surface, and the weakly bimodal Goodwin Creek, with 25% of sand.

Appendix A: Bedload Transport Data

- Oak Creek

No.	Water depth m	Water discharge m^3/s	Hydraulic radius ft	Energy slope %	Shear stress N/m^2	Bedload discharge kg/hour
1	0.12	0.153	0.36	0.83	8.934	0.0071
2	0.14	0.238	0.44	0.84	11.051	0.025
3	0.16	0.337	0.48	0.86	12.343	0.018
4	0.18	0.391	0.55	0.83	13.650	0.082
5	0.20	0.447	0.59	0.87	15.348	0.14
6	0.18	0.382	0.54	0.86	13.886	0.056
7	0.16	0.323	0.49	0.86	12.600	0.018
8	0.14	0.275	0.44	0.85	11.183	0.0092
9	0.14	0.227	0.42	0.84	10.549	0.0043
10	0.51	2.605	1.31	0.97	37.995	641
11	0.51	2.605	1.31	0.97	37.995	484
12	0.51	2.633	1.31	0.97	37.995	392
13	0.54	2.832	1.37	0.98	40.145	385
14	0.59	3.398	1.46	0.99	43.219	1362
15	0.42	1.897	1.12	1	33.489	101
16	0.40	1.812	1.08	1	32.293	91
17	0.28	0.906	0.8	0.98	23.442	2.41
18	0.26	0.736	0.74	0.97	21.463	0.39
19	0.26	0.765	0.75	0.97	21.753	0.33
20	0.25	0.680	0.72	0.97	20.883	0.13
21	0.25	0.708	0.73	0.97	21.173	0.25
22	0.25	0.680	0.72	0.97	20.883	0.16
23	0.40	1.756	1.07	1	31.994	53
24	0.39	1.699	1.05	1	31.396	21
25	0.38	1.529	1.03	1	30.798	12
26	0.32	1.161	0.9	0.99	26.642	3.7
27	0.27	0.821	0.77	0.98	22.563	0.59
28	0.24	0.623	0.7	0.97	20.303	0.13
29	0.21	0.453	0.61	0.96	17.510	0.048
30	0.20	0.368	0.59	0.96	16.936	0.022
31	0.19	0.331	0.56	0.96	16.075	0.042
32	0.18	0.283	0.53	0.95	15.055	0.035
33	0.17	0.232	0.5	0.95	14.203	0.01
34	0.17	0.241	0.5	0.95	14.203	0.007
35	0.25	0.651	0.71	0.97	20.593	0.34
36	0.21	0.453	0.61	0.96	17.510	0.044
37	0.18	0.311	0.54	0.96	15.501	0.014
38	0.17	0.252	0.51	0.95	14.487	0.0043
39	0.16	0.221	0.49	0.94	13.772	0.0046
40	0.17	0.252	0.51	0.95	14.487	0.0056

41	0.15	0.193	0.46	0.94	12.929	0.0093
42	0.16	0.198	0.47	0.94	13.210	0.02
43	0.16	0.218	0.48	0.94	13.491	0.0016
44	0.16	0.235	0.49	0.94	13.772	0.0053
45	0.16	0.204	0.47	0.94	13.210	0.0026
46	0.17	0.238	0.5	0.94	14.053	0.0058
47	0.18	0.300	0.53	0.96	15.214	0.018
48	0.17	0.269	0.52	0.95	14.771	0.012
49	0.17	0.232	0.5	0.94	14.053	0.012
50	0.17	0.263	0.51	0.95	14.487	0.0036
51	0.23	0.566	0.67	0.97	19.433	0.43
52	0.24	0.600	0.69	0.97	20.013	0.11
53	0.20	0.419	0.6	0.96	17.223	0.012
54	0.19	0.362	0.57	0.96	16.362	0.0062
55	0.29	0.538	0.83	0.97	24.073	0.86
56	0.44	1.756	1.17	1	34.984	43
57	0.46	2.039	1.21	1.01	36.542	90
58	0.49	2.605	1.27	1.02	38.734	480
59	0.47	2.209	1.22	1.08	39.397	1460
60	0.42	1.529	1.12	1.05	35.163	130
61	0.40	1.331	1.07	1.04	33.274	63
62	0.37	1.019	1.01	1.02	30.804	19
63	0.37	1.076	1	1.02	30.499	18
64	0.41	1.444	1.1	1	32.891	78
65	0.44	1.756	1.17	1	34.984	260
66	0.47	2.095	1.22	1	36.479	523

- Nahal Yatir

No.	Water depth m	Hydraulic radius m	Water surface slope %	Water discharge m^3/s	Shear stress N/m^2	Bedload discharge kg/ms
1	0.46	0.38	0.7	3.7	27.1	3.69
2	0.5	0.41	0.71	4.1	29.7	4.66
3	0.58	0.46	0.72	4.8	33.8	3.37
4	0.6	0.47	0.73	5	35.0	4.54
5	0.6	0.47	0.75	5	36.0	6.32
6	0.59	0.46	0.75	4.9	35.2	5.33
7	0.6	0.47	0.74	5	35.5	6.33
8	0.59	0.47	0.76	4.9	36.4	7.05
9	0.59	0.47	0.77	4.9	36.9	6.62
10	0.2	0.18	0.84	1.2	15.4	0.92
11	0.2	0.18	0.85	1.2	15.6	0.81
12	0.15	0.14	0.83	0.7	11.9	0.35
13	0.14	0.13	0.83	0.7	11.0	0.2
14	0.16	0.15	0.84	0.8	12.9	0.34
15	0.17	0.15	0.85	0.9	13.0	0.48
16	0.17	0.16	0.87	1	14.2	0.45
17	0.21	0.19	0.91	1.3	17.6	1.09
18	0.24	0.21	0.93	1.6	19.9	1.38
19	0.27	0.24	0.94	1.8	23.0	2.06
20	0.29	0.25	0.95	2	24.2	3.25
21	0.31	0.27	0.94	2.2	25.9	2.73
22	0.32	0.27	0.95	2.3	26.2	3.44
23	0.33	0.28	0.95	2.4	27.1	3.47
24	0.34	0.29	0.96	2.5	28.4	4.33
25	0.34	0.3	0.96	2.6	29.4	3.03
26	0.36	0.31	0.96	2.7	30.4	3.75
27	0.37	0.31	0.96	2.8	30.4	4.19
28	0.37	0.32	0.97	2.8	31.7	3.41
29	0.13	0.13	0.86	0.6	11.4	0.33
30	0.13	0.13	0.86	0.6	11.4	0.33
31	0.14	0.13	0.87	0.7	11.5	0.6
32	0.15	0.14	0.88	0.7	12.6	0.5
33	0.15	0.14	0.87	0.7	12.4	0.59
34	0.15	0.14	0.88	0.7	12.6	0.57
35	0.14	0.14	0.87	0.7	12.4	0.46
36	0.14	0.13	0.87	0.6	11.5	0.65
37	0.14	0.13	0.87	0.6	11.5	0.52
38	0.13	0.12	0.87	0.6	10.7	0.36
39	0.13	0.12	0.87	0.5	10.7	0.49
40	0.12	0.12	0.87	0.5	10.7	0.45
41	0.12	0.11	0.86	0.4	9.7	0.35
42	0.12	0.11	0.86	0.4	9.7	0.49
43	0.11	0.11	0.85	0.4	9.5	0.31
44	0.11	0.1	0.85	0.3	8.7	0.32

45	0.25	0.23	1.01	1.7	23.7	4.68
46	0.29	0.26	0.98	2.1	26.0	3.52
47	0.29	0.26	0.99	2.1	26.3	4.35
48	0.29	0.25	0.99	2	25.3	4.08
49	0.3	0.26	0.98	2.1	26.0	3.33
50	0.31	0.27	0.99	2.2	27.3	2.52
51	0.32	0.28	1	2.3	28.6	3.37
52	0.33	0.29	0.99	2.5	29.3	4.16
53	0.34	0.3	0.99	2.6	30.3	3.65
54	0.35	0.35	0.99	2.7	35.4	2.98
55	0.11	0.1	0.87	0.3	8.9	0.36
56	0.11	0.1	0.87	0.4	8.9	0.32
57	0.12	0.11	0.87	0.4	9.8	0.76
58	0.13	0.12	0.88	0.5	10.8	0.94
59	0.13	0.12	0.88	0.6	10.8	0.69
60	0.14	0.13	0.87	0.6	11.5	0.55
61	0.14	0.13	0.88	0.6	11.7	0.94
62	0.14	0.13	0.89	0.7	11.8	0.35
63	0.15	0.14	0.89	0.7	12.7	1.6
64	0.16	0.15	0.89	0.8	13.6	0.87
65	0.17	0.16	0.9	0.9	14.7	1.15
66	0.19	0.17	0.91	1.1	15.8	2.02
67	0.2	0.18	0.92	1.2	16.9	1.23
68	0.2	0.19	0.93	1.2	18.0	2.69
69	0.22	0.19	0.94	1.4	18.2	2.68
70	0.23	0.2	0.95	1.5	19.4	2.79
71	0.24	0.21	0.95	1.6	20.4	2.21
72	0.25	0.22	0.95	1.7	21.3	2.58
73	0.26	0.23	0.96	1.8	22.5	2.35
74	0.27	0.24	0.97	1.9	23.8	4.55

- Sagehen Creek

No.	Water depth m	Water discharge m^3/s	Hydraulic radius m	Energy slope	Shear stress N/m^2	Bedload discharge kg/ms x 10^{-3}
1	0.518	2.18	0.369	0.012	43.48	24.5
2	0.501	2.04	0.361	0.0104	36.80	5.529
3	0.501	2.04	0.361	0.0104	36.80	7.586
4	0.521	2.2	0.371	0.0101	36.73	9.266
5	0.536	2.33	0.378	0.0099	36.74	5.696
6	0.407	1.34	0.309	0.011	33.34	2.727
7	0.498	2.02	0.359	0.0105	37.01	22.28
8	0.538	2.35	0.379	0.0098	36.47	15.48
9	0.557	2.51	0.388	0.0096	36.58	8.37
10	0.617	3.09	0.417	0.0095	38.86	11.55
11	0.617	3.09	0.417	0.0095	38.86	5.817
12	0.618	3.1	0.417	0.0095	38.90	12.94
13	0.619	3.11	0.418	0.0095	38.95	4.245
14	0.62	3.12	0.418	0.0095	39.00	4.365
15	0.62	3.12	0.418	0.0095	38.98	0.4988
16	0.62	3.12	0.418	0.0095	38.98	3.694
17	0.616	3.08	0.417	0.0095	38.83	25.54
18	0.614	3.06	0.416	0.0095	38.73	34.9
19	0.605	2.97	0.411	0.0095	38.34	26.31
20	0.598	2.91	0.409	0.0095	38.07	14.94
21	0.595	2.87	0.407	0.0095	37.91	8.984
22	0.592	2.85	0.406	0.0095	37.81	8.445
23	0.591	2.83	0.405	0.0095	37.73	16.5
24	0.587	2.8	0.403	0.0095	37.57	12.56
25	0.591	2.83	0.405	0.0095	37.73	11.74
26	0.594	2.86	0.406	0.0095	37.87	17.77
27	0.587	2.8	0.403	0.0095	37.57	6.758
28	0.594	2.86	0.406	0.0095	37.87	9.991
29	0.599	2.92	0.409	0.0095	38.11	15.11
30	0.594	2.86	0.406	0.0095	37.87	12.91
31	0.587	2.8	0.403	0.0095	37.57	12.71
32	0.584	2.77	0.402	0.011	43.35	18.88
33	0.443	1.6	0.330	0.011	35.60	20.21
34	0.428	1.48	0.321	0.011	34.63	22.47
35	0.367	1.1	0.286	0.011	30.85	2.128
36	0.36	1.05	0.281	0.011	30.35	1.378
37	0.386	1.21	0.297	0.011	32.05	1.715
38	0.424	1.46	0.319	0.011	34.41	4.81
39	0.446	1.62	0.331	0.011	35.76	8.541
40	0.431	1.51	0.323	0.011	34.85	6.428
41	0.386	1.21	0.297	0.011	32.05	2.575
42	0.367	1.1	0.286	0.011	30.85	1.624
43	0.356	1.03	0.279	0.011	30.09	1.512
44	0.36	1.05	0.281	0.011	30.35	1.152

45	0.35	0.99	0.275	0.011	29.67	1.601
46	0.36	1.05	0.281	0.011	30.35	0.5868
47	0.4	1.23	0.303	0.011	32.71	6.03
48	0.4	1.3	0.305	0.011	32.94	6.03
49	0.449	1.64	0.333	0.011	35.93	8.724
50	0.4	1.3	0.305	0.011	32.94	8.968
51	0.407	1.34	0.309	0.011	33.34	5.393
52	0.41	1.37	0.311	0.011	33.58	5.076
53	0.414	1.39	0.313	0.011	33.80	7.325
54	0.443	1.6	0.330	0.011	35.60	8.143
55	0.455	1.68	0.336	0.011	36.26	13.42

- Elbow River

No.	Water depth m	Water Width m	Water discharge m^3/s	Hydraulic radius m	Slope	Shear stress N/m^2	Bedload discharge kg/ms
1	0.8	45.8	82.0736	0.773	0.00745	60.81	0.3832
2	0.66	40.1	46.05084	0.639	0.00745	50.17	0.0808
3	0.66	39.7	44.5434	0.639	0.00745	50.17	0.1823
4	0.65	39.3	42.66015	0.629	0.00745	49.41	0.1462
5	0.63	38.7	39.49722	0.610	0.00745	47.88	0.0385
6	0.8	45.8	82.0736	0.773	0.00745	60.81	0.6272
7	0.83	46.8	90.89496	0.802	0.00745	63.09	0.54
8	0.76	43.8	68.57328	0.735	0.00745	57.77	0.7558
9	0.73	43	62.1522	0.706	0.00745	55.49	0.437
10	0.74	43.2	63.936	0.715	0.00745	56.25	0.555
11	0.84	47.4	95.16024	0.811	0.00745	63.85	0.617
12	0.83	46.8	90.50652	0.802	0.00745	63.09	0.9242
13	0.81	46.1	84.76407	0.783	0.00745	61.57	0.6175
14	0.8	45.8	82.0736	0.773	0.00745	60.81	0.8234
15	0.76	44	69.5552	0.735	0.00745	57.77	0.4234
16	0.73	43	62.1522	0.706	0.00745	55.49	0.373
17	0.72	42.5	59.364	0.696	0.00745	54.73	0.1606
18	0.72	42.5	59.364	0.696	0.00745	54.73	0.1995
19	0.73	43	62.1522	0.706	0.00745	55.49	0.1256

- Jacoby River

No.	Water depth m	Water discharge m^3/s	Hydraulic radius m	Shear stress N/m^2	Bedload discharge kg/ms
1	0.133	0.603	0.131	8.09	3.18E-05
2	0.147	0.749	0.144	8.91	7.79E-05
3	0.147	0.749	0.144	8.91	3.36E-05
4	0.155	0.848	0.152	9.42	4.76E-05
5	0.167	1.000	0.164	10.15	5.22E-05
6	0.175	1.101	0.171	10.59	9.53E-05
7	0.183	1.209	0.179	11.05	0.0001036
8	0.186	1.262	0.182	11.26	0.0003211
9	0.190	1.315	0.186	11.47	0.0011147
10	0.193	1.370	0.189	11.68	0.0003085
11	0.200	1.481	0.196	12.10	0.0011225
12	0.214	1.708	0.209	12.89	0.0006508
13	0.214	1.708	0.209	12.89	0.0002957
14	0.230	2.002	0.224	13.83	0.0002454
15	0.245	2.308	0.238	14.74	0.0001709
16	0.245	2.308	0.238	14.74	0.000465
17	0.248	2.370	0.241	14.91	0.0003817
18	0.254	2.498	0.247	15.26	0.0002893
19	0.272	2.889	0.263	16.28	0.0007387
20	0.275	2.956	0.266	16.45	0.0018346
21	0.280	3.089	0.271	16.77	0.0006775
22	0.286	3.227	0.277	17.10	0.0004416
23	0.289	3.296	0.279	17.26	0.0011939
24	0.291	3.365	0.282	17.41	0.0008056
25	0.300	3.577	0.289	17.89	0.0012629
26	0.300	3.577	0.289	17.89	0.0002965
27	0.305	3.721	0.295	18.20	0.0019735
28	0.310	3.867	0.300	18.52	0.0019349
29	0.310	3.867	0.300	18.52	0.001209
30	0.326	4.315	0.314	19.43	0.0004589
31	0.329	4.391	0.317	19.58	0.0019538
32	0.329	4.391	0.317	19.58	0.002905
33	0.329	4.391	0.317	19.58	0.0011937
34	0.334	4.547	0.322	19.88	0.0003592
35	0.337	4.623	0.324	20.03	0.000834
36	0.339	4.703	0.327	20.18	0.017383101
37	0.339	4.703	0.327	20.18	0.0022634
38	0.339	4.703	0.327	20.18	0.0019896
39	0.345	4.860	0.331	20.48	0.0015605
40	0.347	4.940	0.334	20.62	0.0044113
41	0.347	4.940	0.334	20.62	0.0073841
42	0.350	5.020	0.336	20.77	0.0227311
43	0.350	5.020	0.336	20.77	0.002643
44	0.352	5.101	0.338	20.91	0.0037009

45	0.355	5.183	0.341	21.06	0.0007245
46	0.357	5.264	0.343	21.21	0.0137984
47	0.365	5.512	0.350	21.64	0.0030779
48	0.367	5.593	0.352	21.78	0.0082332
49	0.370	5.678	0.355	21.92	0.0057766
50	0.372	5.761	0.357	22.06	0.003688
51	0.375	5.846	0.359	22.20	0.0021564
52	0.375	5.846	0.359	22.20	0.0049912
53	0.380	6.018	0.364	22.48	0.054420799
54	0.382	6.105	0.366	22.63	0.003822
55	0.382	6.105	0.366	22.63	0.023871599
56	0.385	6.191	0.368	22.77	0.0042028
57	0.387	6.280	0.371	22.91	0.0085717
58	0.387	6.280	0.371	22.91	0.0064241
59	0.390	6.367	0.373	23.05	0.0027256
60	0.390	6.367	0.373	23.05	0.003523
61	0.390	6.367	0.373	23.05	0.044711399
62	0.392	6.455	0.375	23.18	0.0071946
63	0.392	6.455	0.375	23.18	0.0108274
64	0.395	6.544	0.377	23.32	0.0195819
65	0.397	6.634	0.380	23.46	0.0253822
66	0.397	6.634	0.380	23.46	0.025715799
67	0.402	6.813	0.384	23.74	0.0114228
68	0.404	6.903	0.386	23.87	0.0108121
69	0.407	6.995	0.389	24.01	0.0060872
70	0.409	7.087	0.391	24.15	0.0054502
71	0.412	7.179	0.393	24.28	0.0093751
72	0.412	7.179	0.393	24.28	0.044101101
73	0.417	7.365	0.397	24.56	0.0211602
74	0.417	7.365	0.397	24.56	0.0145548
75	0.417	7.365	0.397	24.56	0.056452702
76	0.429	7.838	0.408	25.23	0.0325201
77	0.429	7.838	0.408	25.23	0.0087588
78	0.431	7.933	0.410	25.36	0.019823999
79	0.436	8.126	0.415	25.63	0.158214294
80	0.436	8.126	0.415	25.63	0.1116082
81	0.445	8.517	0.423	26.16	0.0028301
82	0.450	8.715	0.428	26.42	0.080854202
83	0.452	8.816	0.430	26.55	0.028692499
84	0.452	8.816	0.430	26.55	0.047376301
85	0.455	8.915	0.432	26.68	0.147376297
86	0.459	9.119	0.436	26.95	0.036867699
87	0.471	9.634	0.446	27.59	0.075888802
88	0.476	9.845	0.451	27.85	0.089324699
89	0.494	10.700	0.467	28.87	0.063937698
90	0.501	11.029	0.473	29.25	0.292502106
91	0.501	11.029	0.473	29.25	0.039535801
92	0.505	11.250	0.477	29.51	0.087908798
93	0.519	11.926	0.490	30.26	0.054464001
94	0.526	12.271	0.496	30.63	0.066369499
95	0.573	14.804	0.537	33.20	0.174229294

96	0.588	15.695	0.551	34.04	0.0271763
97	0.593	15.953	0.555	34.28	0.402078888
98	0.595	16.082	0.557	34.40	0.213156097
99	0.630	18.229	0.587	36.28	0.114121696
100	0.634	18.505	0.591	36.52	0.413460907

- Goodwin Creek

No.	Water depth m	Water discharge m^3/s	Water width m	Hydraulic radius m	Water surface slope	Shear stress N/m^2	Bedload discharge kg/ms
1	0.366	1.37	11.13	0.505	0.0021	10.40	0.0014
2	0.43	1.99	11.21	0.526	0.0022	11.35	0.0005
3	0.457	2.29	11.34	0.557	0.0021	11.47	0.0005
4	0.488	2.66	11.45	0.585	0.0022	12.63	0.0004
5	0.515	3.02	11.56	0.611	0.0022	13.19	0.0005
6	0.524	3.14	11.60	0.622	0.0021	12.81	0.0012
7	0.524	3.14	11.61	0.624	0.0022	13.47	0.0002
8	0.527	3.18	11.60	0.62	0.0022	13.38	0.0005
9	0.518	3.06	11.58	0.617	0.0022	13.32	0.0005
10	0.509	2.94	11.55	0.608	0.0021	12.53	0.0005
11	0.491	2.70	11.49	0.593	0.0021	12.22	0.0005
12	0.475	2.51	11.45	0.584	0.0022	12.60	0.0005
13	0.463	2.36	11.42	0.578	0.0022	12.47	0.0002
14	0.445	2.16	11.36	0.563	0.0022	12.15	0.0006
15	0.427	1.96	11.32	0.553	0.0021	11.39	0.0007
16	0.415	1.83	11.29	0.544	0.0022	11.74	0.0008
17	0.411	1.80	11.28	0.544	0.0021	11.21	0.0008
18	0.418	1.86	11.29	0.544	0.0022	11.74	0.001
19	0.439	2.09	11.34	0.557	0.0021	11.47	0.0009
20	0.485	2.62	11.48	0.591	0.0021	12.18	0.001
21	0.506	2.90	11.54	0.607	0.0023	13.70	0.0009
22	0.524	3.14	11.59	0.619	0.0021	12.75	0.0013
23	0.543	3.40	11.64	0.63	0.0021	12.98	0.0012
24	0.56	3.66	11.72	0.65	0.0022	14.03	0.0068
25	0.567	3.76	11.74	0.656	0.0022	14.16	0.0022
26	0.576	3.90	11.77	0.661	0.0022	14.27	0.0022
27	0.579	3.95	11.78	0.664	0.0022	14.33	0.002
28	0.588	4.09	11.80	0.67	0.0022	14.46	0.0018
29	0.586	4.06	11.79	0.666	0.0022	14.37	0.0013
30	0.582	4.00	11.78	0.664	0.0022	14.33	0.0006
31	0.567	3.76	11.73	0.652	0.0022	14.07	0.001
32	0.542	3.39	11.66	0.635	0.0022	13.70	0.0005
33	0.527	3.18	11.61	0.623	0.0022	13.45	0.0009
34	0.506	2.90	11.54	0.607	0.0023	13.70	0.0006
35	0.485	2.62	11.46	0.587	0.0021	12.09	0.001
36	0.46	2.33	11.40	0.573	0.0022	12.37	0.0009
37	0.445	2.16	11.36	0.563	0.0021	11.60	0.0005
38	0.927	11.62	12.93	0.927	0.0024	21.83	0.0049
39	0.949	12.27	13.14	0.971	0.0025	23.81	0.0138
40	0.957	12.52	13.20	0.985	0.0026	25.12	0.0193
41	0.944	12.13	13.17	0.977	0.0026	24.92	0.0072
42	0.909	11.12	13.01	0.943	0.0025	23.13	0.009
43	0.859	9.76	12.78	0.893	0.0024	21.02	0.0155
44	0.81	8.53	12.59	0.851	0.0023	19.20	0.0026

45	0.759	7.35	12.33	0.794	0.0024	18.69	0.0041
46	0.713	6.37	12.17	0.757	0.0022	16.34	0.0169
47	0.738	6.88	12.31	0.788	0.0024	18.55	0.0009
48	0.695	6.00	12.16	0.753	0.0023	16.99	0.001
49	0.671	5.53	12.05	0.728	0.0022	15.71	0.0015
50	0.637	4.91	11.95	0.704	0.0023	15.88	0.001
51	0.641	4.98	11.82	0.674	0.0016	10.58	0.0011
52	0.655	5.24	11.99	0.714	0.0022	15.41	0.0008
53	0.658	5.30	11.91	0.695	0.0015	10.23	0.001
54	0.649	5.13	11.95	0.705	0.0023	15.91	0.0013
55	0.616	4.54	11.78	0.663	0.0017	11.06	0.0017
56	0.853	9.62	12.56	0.845	0.0019	15.75	0.0179
57	0.935	11.86	13.03	0.947	0.0019	17.65	0.0145
58	1.031	14.85	13.52	1.052	0.0021	21.67	0.0216
59	1.085	16.70	13.80	1.112	0.0022	24.00	0.0447
60	1.097	17.14	13.89	1.13	0.0022	24.39	0.0677
61	1.093	17.00	13.88	1.127	0.0022	24.32	0.0581
62	1.068	16.09	13.78	1.106	0.0022	23.87	0.0149
63	1.015	14.33	13.52	1.053	0.0022	22.73	0.0164
64	0.938	11.95	13.15	0.975	0.0021	20.09	0.0256
65	0.835	9.15	12.68	0.872	0.002	17.11	0.0053
66	0.774	7.69	12.52	0.835	0.0026	21.30	0.0025
67	0.764	7.47	12.45	0.82	0.0025	20.11	0.0077
68	0.764	7.47	12.44	0.818	0.0025	20.06	0.0191
69	0.75	7.15	12.33	0.793	0.0021	16.34	0.0045
70	0.738	6.88	12.25	0.775	0.0019	14.45	0.0077
71	0.738	6.88	12.24	0.773	0.0018	13.65	0.0051
72	0.744	7.01	12.26	0.776	0.0018	13.70	0.0023
73	0.92	11.42	13.05	0.952	0.0019	17.74	0.0104
74	1.027	14.73	13.55	1.06	0.0022	22.88	0.0235
75	1.097	17.11	13.89	1.13	0.0024	26.60	0.029
76	1.143	18.82	14.19	1.19	0.0027	31.52	0.0666
77	1.158	19.40	14.26	1.205	0.003	35.46	0.0534
78	1.143	18.82	14.27	1.207	0.0031	36.71	0.0594
79	1.097	17.14	13.99	1.151	0.0028	31.62	0.0712
80	1.007	14.06	13.54	1.058	0.0025	25.95	0.0671
81	0.911	11.17	13.07	0.957	0.0023	21.59	0.015
82	0.856	9.70	12.84	0.906	0.0022	19.55	0.0125
83	0.827	8.94	12.63	0.861	0.002	16.89	0.0077
84	0.862	9.84	12.79	0.895	0.002	17.56	0.032
85	0.883	10.41	12.91	0.923	0.0021	19.01	0.0137
86	0.876	10.20	12.86	0.912	0.0021	18.79	0.028
87	0.845	9.41	12.74	0.886	0.0021	18.25	0.0117
88	0.837	9.21	12.70	0.877	0.0021	18.07	0.0105
89	0.832	9.08	12.71	0.879	0.0021	18.11	0.0101
90	0.787	7.99	12.53	0.838	0.002	16.44	0.0071
91	0.728	6.69	12.31	0.787	0.0019	14.67	0.0106
92	0.674	5.59	12.14	0.748	0.0017	12.47	0.0073
93	0.649	5.13	12.05	0.727	0.0018	12.84	0.0087
94	0.619	4.60	11.93	0.7	0.0018	12.36	0.0052
95	0.588	4.09	11.84	0.679	0.0019	12.66	0.0063

96	1.035	14.98	13.62	1.074	0.0027	28.45	0.0295
97	1.013	14.25	13.57	1.062	0.0029	30.21	0.0513
98	0.988	13.48	13.48	1.044	0.0027	27.65	0.0341
99	0.958	12.54	13.32	1.011	0.0026	25.79	0.0347
100	0.921	11.47	13.15	0.974	0.0025	23.89	0.0364
101	0.892	10.66	13.01	0.945	0.0025	23.18	0.0203
102	0.863	9.86	12.86	0.912	0.0024	21.47	0.0429
103	0.835	9.15	12.73	0.883	0.0023	19.92	0.0208
104	0.812	8.57	12.61	0.855	0.0023	19.29	0.0508
105	0.783	7.90	12.52	0.836	0.0022	18.04	0.0255
106	0.766	7.50	12.43	0.815	0.0022	17.59	0.0357
107	0.744	7.03	12.33	0.793	0.0022	17.11	0.0321
108	0.72	6.51	12.24	0.771	0.0021	15.88	0.0374
109	0.701	6.12	12.19	0.761	0.0022	16.42	0.0052
110	0.954	12.43	13.19	0.982	0.0018	17.34	0.005
111	0.969	12.89	13.23	0.991	0.0018	17.50	0.0048
112	0.988	13.45	13.30	1.007	0.0017	16.79	0.0024
113	0.991	13.55	13.32	1.011	0.0019	18.84	0.0016
114	0.997	13.74	13.35	1.016	0.0019	18.94	0.0035
115	1.003	13.93	13.40	1.028	0.002	20.17	0.0014
116	1.015	14.33	13.43	1.034	0.0019	19.27	0.0008
117	1.024	14.62	13.47	1.043	0.002	20.46	0.0011
118	1.021	14.53	13.45	1.038	0.0021	21.38	0.0009
119	1.012	14.23	13.39	1.025	0.0019	19.10	0.0008
120	0.991	13.55	13.28	1.002	0.0019	18.68	0.0006
121	0.963	12.70	13.16	0.977	0.0019	18.21	0.0009
122	0.936	11.89	13.02	0.947	0.0019	17.65	0.0007
123	0.905	11.02	12.90	0.92	0.002	18.05	0.0008
124	0.872	10.10	12.76	0.888	0.0018	15.68	0.0003
125	0.829	9.00	12.48	0.826	0.0016	12.96	0.0003
126	0.658	5.30	11.82	0.674	0.0016	10.58	0.0004
127	0.588	4.09	11.54	0.608	0.0015	8.95	0.0008
128	1.169	19.82	14.33	1.219	0.0032	38.27	0.0726
129	1.122	18.02	14.12	1.175	0.003	34.58	0.0659
130	1.039	15.10	13.73	1.097	0.0029	31.21	0.054
131	0.951	12.34	13.31	1.008	0.0028	27.69	0.0619
132	0.877	10.24	12.97	0.935	0.0025	22.93	0.0124
133	0.805	8.42	12.66	0.866	0.0025	21.24	0.0205
134	0.738	6.88	12.35	0.798	0.0024	18.79	0.0119
135	0.695	6.00	12.20	0.764	0.0022	16.49	0.015
136	0.783	7.90	12.45	0.819	0.0017	13.66	0.0024
137	0.832	9.08	12.64	0.863	0.0015	12.70	0.0016
138	0.911	11.19	13.00	0.941	0.0016	14.77	0.0013
139	0.954	12.43	13.18	0.981	0.0016	15.40	0.0019
140	1.073	16.27	13.71	1.093	0.0021	22.52	0.0044
141	1.097	17.14	13.84	1.119	0.0019	20.86	0.0078
142	1.17	19.87	14.22	1.196	0.0022	25.81	0.0091
143	1.192	20.72	14.28	1.209	0.0021	24.91	0.0369
144	1.186	20.47	14.31	1.215	0.0023	27.41	0.0194
145	1.198	20.96	14.36	1.225	0.0026	31.24	0.0268
146	1.198	20.96	14.36	1.224	0.0025	30.02	0.0229

147	1.131	18.36	14.33	1.219	0.0025	29.90	0.0315
148	1.18	20.23	14.32	1.216	0.0024	28.63	0.0188
149	1.167	19.76	14.23	1.199	0.0023	27.05	0.035
150	1.158	19.40	14.18	1.188	0.0022	25.64	0.0193
151	1.146	18.94	14.10	1.172	0.002	22.99	0.017
152	1.113	17.69	13.99	1.149	0.002	22.54	0.0243
153	1.088	16.81	13.88	1.127	0.002	22.11	0.0172
154	1	13.84	13.32	1.011	0.0016	15.87	0.0075
155	0.96	12.61	13.18	0.981	0.0016	15.40	0.0036
156	0.893	10.68	12.88	0.915	0.0015	13.46	0.0061
157	0.762	7.42	12.33	0.793	0.0013	10.11	0.0029
158	0.899	10.85	12.97	0.935	0.0024	22.01	0.0075
159	0.911	11.19	12.99	0.941	0.0023	21.23	0.0217
160	0.911	11.19	13.03	0.948	0.0022	20.46	0.0066
161	0.905	11.02	12.99	0.94	0.0021	19.36	0.0189
162	0.902	10.93	12.95	0.931	0.0022	20.09	0.0203
163	0.89	10.59	12.92	0.924	0.0021	19.04	0.0201
164	0.881	10.35	12.88	0.916	0.0021	18.87	0.0333
165	0.866	9.94	12.85	0.91	0.0021	18.75	0.025
166	0.914	11.25	12.90	0.92	0.0018	16.25	0.0068
167	0.885	10.45	12.79	0.897	0.0018	15.84	0.0014
168	0.838	9.23	12.58	0.849	0.0019	15.82	0.0008
169	0.771	7.62	12.28	0.782	0.0017	13.04	0.0003
170	1.164	19.64	14.33	1.218	0.003	35.85	0.316
171	1.173	19.99	14.38	1.229	0.003	36.17	0.5439
172	1.213	21.58	14.54	1.26	0.0031	38.32	1.4683
173	1.17	19.87	14.48	1.249	0.003	36.76	0.102
174	1.158	19.40	14.42	1.236	0.003	36.38	0.3797
175	1.155	19.29	14.41	1.235	0.0031	37.56	1.0592
176	1.152	19.17	14.37	1.227	0.003	36.11	1.2576
177	1.146	18.94	14.34	1.221	0.003	35.93	1.3624
178	1.146	18.94	14.34	1.221	0.003	35.93	1.5758
179	1.14	18.71	14.31	1.214	0.0032	38.11	0.6745
180	1.134	18.48	14.27	1.207	0.0031	36.71	0.154
181	1.125	18.14	14.26	1.204	0.003	35.43	0.3319
182	1.122	18.02	14.23	1.199	0.0031	36.46	0.3684
183	1.116	17.80	14.21	1.194	0.003	35.14	0.528
184	1.113	17.69	14.19	1.191	0.003	35.05	0.7183
185	1.109	17.58	14.16	1.185	0.003	34.87	1.5642
186	1.103	17.36	14.15	1.183	0.003	34.82	1.6306
187	1.103	17.36	14.14	1.181	0.003	34.76	1.4279
188	1.103	17.36	14.14	1.181	0.003	34.76	2.0262
189	1.103	17.36	14.14	1.18	0.003	34.73	1.6352
190	1.103	17.36	14.12	1.177	0.0031	35.79	2.1952
191	1.103	17.36	14.12	1.176	0.0031	35.76	2.9846
192	1.106	17.47	14.13	1.178	0.003	34.67	2.526
193	1.106	17.47	14.15	1.183	0.003	34.82	2.267
194	1.113	17.69	14.14	1.18	0.003	34.73	1.7476
195	1.106	17.47	14.14	1.18	0.0031	35.88	1.3223
196	1.109	17.58	14.15	1.182	0.0031	35.95	1.3435
197	1.109	17.58	14.15	1.183	0.0031	35.98	0.8667

198	1.109	17.58	14.17	1.186	0.0032	37.23	0.1846
199	1.109	17.58	14.16	1.184	0.0031	36.01	0.2317
200	1.109	17.58	14.18	1.187	0.0031	36.10	0.2182
201	1.113	17.69	14.17	1.186	0.0031	36.07	0.0825
202	1.106	17.47	14.17	1.187	0.0032	37.26	0.1535
203	1.106	17.47	14.18	1.189	0.0032	37.33	0.6147
204	1.106	17.47	14.16	1.185	0.003	34.87	1.308
205	1.109	17.58	14.17	1.186	0.003	34.90	2.33
206	1.1	17.25	14.15	1.183	0.0032	37.14	0.663
207	1.1	17.25	14.14	1.18	0.0031	35.88	0.6666
208	1.094	17.03	14.12	1.176	0.0032	36.92	1.9389
209	1.091	16.92	14.10	1.173	0.0031	35.67	2.0297
210	1.085	16.70	14.07	1.167	0.003	34.34	1.725
211	1.076	16.38	14.03	1.159	0.0031	35.25	2.9068
212	1.064	15.96	13.98	1.147	0.0029	32.63	1.8238
213	1.058	15.75	13.95	1.142	0.003	33.61	1.1385
214	1.049	15.44	13.90	1.131	0.0029	32.18	0.4441
215	1.042	15.23	13.87	1.125	0.003	33.11	0.4223
216	1.033	14.93	13.83	1.117	0.0029	31.78	0.1029
217	1.024	14.62	13.79	1.11	0.0029	31.58	0.0829
218	1.012	14.23	13.72	1.094	0.0028	30.05	0.1339
219	1	13.84	13.67	1.084	0.0029	30.84	0.4405
220	0.988	13.45	13.62	1.074	0.0028	29.50	0.546
221	0.981	13.26	13.57	1.063	0.0029	30.24	0.3711
222	0.972	12.98	13.51	1.052	0.0027	27.86	0.7241
223	0.957	12.52	13.47	1.042	0.0028	28.62	0.705
224	0.951	12.34	13.42	1.032	0.0029	29.36	0.5684
225	0.939	11.98	13.37	1.022	0.0027	27.07	0.327
226	0.93	11.71	13.30	1.006	0.0027	26.65	1.044
227	0.914	11.27	13.23	0.991	0.0026	25.28	0.8302
228	0.905	11.02	13.20	0.984	0.0027	26.06	0.4532
229	0.896	10.76	13.13	0.97	0.0025	23.79	0.3162
230	0.878	10.26	13.07	0.957	0.0026	24.41	0.296
231	0.875	10.18	13.03	0.948	0.0025	23.25	0.3556
232	0.869	10.02	13.00	0.942	0.0025	23.10	0.1786
233	0.863	9.86	12.98	0.936	0.0025	22.96	0.204
234	0.853	9.62	12.92	0.923	0.0024	21.73	0.1824
235	0.847	9.46	12.90	0.92	0.0024	21.66	0.1803
236	0.838	9.23	12.86	0.91	0.0025	22.32	0.2134
237	0.832	9.08	12.82	0.902	0.0025	22.12	0.1376
238	0.823	8.85	12.80	0.897	0.0025	22.00	0.1078
239	0.814	8.63	12.74	0.885	0.0024	20.84	0.0909
240	0.805	8.40	12.71	0.879	0.0025	21.56	0.2869
241	0.792	8.12	12.66	0.868	0.0022	18.73	0.1155
242	0.786	7.97	12.63	0.861	0.0023	19.43	0.037
243	0.774	7.69	12.54	0.84	0.0024	19.78	0.0136
244	0.768	7.55	12.52	0.836	0.0023	18.86	0.0233
245	0.756	7.28	12.47	0.825	0.002	16.19	0.0806
246	0.75	7.15	12.44	0.817	0.0023	18.43	0.0795
247	0.738	6.88	12.38	0.805	0.0023	18.16	0.0328
248	0.725	6.62	12.36	0.8	0.0022	17.27	0.0175

249	0.716	6.43	12.29	0.785	0.0022	16.94	0.003
250	0.692	5.94	12.18	0.758	0.0022	16.36	0.0063
251	0.671	5.53	12.11	0.743	0.0021	15.31	0.0044
252	0.646	5.08	12.02	0.722	0.0022	15.58	0.0018
253	0.631	4.81	11.94	0.702	0.0023	15.84	0.0009
254	0.61	4.44	11.83	0.677	0.0023	15.28	0.0019
255	0.573	3.85	11.73	0.652	0.0023	14.71	0.0009
256	0.546	3.44	11.65	0.634	0.0024	14.93	0.0006
257	0.521	3.10	11.58	0.616	0.0023	13.90	0.0006
258	0.5	2.82	11.50	0.597	0.0024	14.06	0.0002
259	0.475	2.51	11.44	0.582	0.0025	14.27	0.0004
260	0.802	8.33	12.44	0.818	0.0019	15.25	0.0012
261	0.893	10.68	12.90	0.92	0.0018	16.25	0.0012
262	0.936	11.89	13.12	0.967	0.0019	18.02	0.0018
263	0.969	12.89	13.28	1.002	0.0022	21.63	0.0074
264	0.972	12.98	13.35	1.017	0.0022	21.95	0.0071
265	0.969	12.89	13.31	1.008	0.0022	21.75	0.0073
266	0.957	12.52	13.26	0.997	0.0021	20.54	0.0062
267	0.945	12.15	13.19	0.982	0.0023	22.16	0.0028
268	0.927	11.62	13.12	0.967	0.0023	21.82	0.0028
269	0.905	11.02	13.03	0.948	0.002	18.60	0.0034
270	0.881	10.35	12.93	0.927	0.0021	19.10	0.0016
271	0.86	9.78	12.82	0.902	0.0019	16.81	0.0012
272	0.805	8.40	12.58	0.85	0.0018	15.01	0.0008
273	0.744	7.01	12.37	0.803	0.0018	14.18	0.0004
274	0.668	5.47	12.12	0.743	0.0017	12.39	0.0004
275	0.6	4.29	11.91	0.695	0.0018	12.27	0.0003
276	0.543	3.40	11.73	0.652	0.0017	10.87	0.0005
277	0.491	2.70	11.56	0.612	0.0016	9.61	0.0004
278	0.387	1.57	11.45	0.584	0.0015	8.59	0.0005
279	0.914	11.27	12.62	0.859	0.0024	20.22	0.0072
280	1.103	17.36	13.72	1.095	0.0032	34.37	0.0474
281	1.137	18.59	13.93	1.137	0.0032	35.69	0.1239
282	1.142	18.79	13.98	1.148	0.0034	38.29	0.0918
283	1.052	15.54	13.65	1.079	0.0033	34.93	0.2979
284	1.039	15.13	13.55	1.059	0.0032	33.24	0.3347
285	0.975	13.07	13.01	0.943	0.0027	24.98	0.0438
286	0.908	11.10	12.88	0.916	0.0026	23.36	0.1243
287	0.939	11.98	12.96	0.933	0.0025	22.88	0.0413
288	0.869	10.02	12.71	0.877	0.0024	20.65	0.0279
289	0.817	8.70	12.42	0.814	0.0023	18.37	0.0487
290	0.744	7.01	12.13	0.746	0.0021	15.37	0.0182
291	0.689	5.88	11.93	0.699	0.002	13.71	0.0085
292	0.637	4.91	11.76	0.659	0.002	12.93	0.037
293	0.604	4.34	11.62	0.627	0.002	12.30	0.0254
294	0.57	3.81	11.51	0.599	0.002	11.75	0.0018
295	1.067	16.06	13.74	1.099	0.0031	33.42	0.1641
296	1.015	14.33	13.45	1.038	0.0028	28.51	0.2819
297	0.945	12.15	13.14	0.971	0.0026	24.77	0.4359
298	0.85	9.54	12.81	0.901	0.0024	21.21	0.0602
299	0.881	10.35	12.57	0.847	0.0022	18.28	0.1039

300	0.805	8.40	12.43	0.814	0.0021	16.77	0.0298
301	0.701	6.12	12.25	0.774	0.0021	15.95	0.0266
302	0.732	6.75	12.11	0.743	0.002	14.58	0.0085
303	0.692	5.94	11.95	0.706	0.0019	13.16	0.0058
304	0.658	5.30	11.83	0.676	0.0018	11.94	0.005
305	0.628	4.75	11.72	0.65	0.0018	11.48	0.0089
306	0.6	4.29	11.61	0.624	0.0018	11.02	0.0035
307	0.567	3.76	11.50	0.597	0.0018	10.54	0.0009
308	1.183	20.35	14.33	1.219	0.0032	38.27	0.2636
309	1.143	18.82	14.10	1.173	0.0032	36.82	0.4405
310	1.125	18.14	14.01	1.153	0.0032	36.19	0.9819
311	1.109	17.58	13.95	1.143	0.0031	34.76	1.1114
312	1.097	17.14	13.87	1.125	0.0031	34.21	0.7078
313	1.082	16.59	13.84	1.12	0.0029	31.86	1.0846
314	1.076	16.38	13.80	1.112	0.0031	33.82	0.6152
315	1.067	16.06	13.74	1.098	0.003	32.31	0.5422
316	1.052	15.54	13.69	1.089	0.0029	30.98	0.3371
317	1.036	15.03	13.64	1.077	0.0029	30.64	0.134
318	1.03	14.83	13.59	1.068	0.0029	30.38	0.0624
319	1.018	14.43	13.53	1.054	0.0027	27.92	0.0128
320	0.997	13.74	13.39	1.026	0.0026	26.17	0.004
321	0.966	12.79	13.26	0.997	0.0027	26.41	0.0019
322	0.905	11.02	13.05	0.952	0.0026	24.28	0.0014
323	0.856	9.70	12.84	0.906	0.0026	23.11	0.0062
324	0.832	9.08	12.75	0.888	0.0026	22.65	0.0043
325	0.808	8.48	12.67	0.868	0.0024	20.44	0.0022
326	0.786	7.97	12.60	0.853	0.0023	19.25	0.0009
327	0.765	7.48	12.52	0.836	0.0023	18.86	0.0006
328	0.738	6.88	12.42	0.814	0.0023	18.37	0.0005
329	0.71	6.31	12.30	0.786	0.0022	16.96	0.0011
330	0.686	5.82	12.20	0.763	0.0022	16.47	0.0004
331	0.664	5.41	12.09	0.738	0.0021	15.20	0.0006
332	0.631	4.81	11.99	0.713	0.0021	14.69	0.0009
333	0.594	4.19	11.90	0.693	0.0021	14.28	0.0013
334	0.564	3.71	11.84	0.679	0.0023	15.32	0.0009
335	0.549	3.49	11.74	0.656	0.0024	15.44	0.001
336	0.527	3.18	11.68	0.64	0.0022	13.81	0.0005
337	0.512	2.98	11.64	0.631	0.0022	13.62	0.0008
338	0.494	2.74	11.59	0.619	0.0023	13.97	0.0012
339	0.838	9.23	12.73	0.882	0.0022	19.04	0.0066
340	0.951	12.34	13.21	0.986	0.0022	21.28	0.0051
341	1.012	14.23	13.50	1.049	0.0025	25.73	0.0097
342	1.052	15.54	13.75	1.1	0.0027	29.14	0.0117
343	1.079	16.49	13.89	1.13	0.0027	29.93	0.018
344	1.082	16.59	13.92	1.136	0.0028	31.20	0.0057
345	1.073	16.27	13.89	1.129	0.0027	29.90	0.018
346	1.045	15.33	13.77	1.105	0.0028	30.35	0.0154
347	1	13.84	13.59	1.066	0.0026	27.19	0.0131
348	0.951	12.34	13.35	1.017	0.0026	25.94	0.0044
349	0.789	8.04	12.53	0.837	0.0023	18.89	0.0012
350	0.732	6.75	12.32	0.79	0.0024	18.60	0.0012

351	0.655	5.24	12.04	0.725	0.0022	15.65	0.004
352	1.202	21.15	14.55	1.263	0.0028	34.69	0.2193
353	1.1	17.25	14.07	1.167	0.0026	29.77	0.2309
354	1	13.84	13.62	1.073	0.0024	25.26	0.2482
355	0.924	11.56	13.24	0.992	0.0023	22.38	0.0406
356	0.841	9.31	12.80	0.897	0.0018	15.84	0.0367
357	0.768	7.55	12.49	0.83	0.0019	15.47	0.0056
358	0.713	6.37	12.31	0.788	0.002	15.46	0.0038

- Kuhnle Data

Run number	Water depth m	Water discharge m^3/s	Hydraulic radius m	Water surface slope	Shear stress N/m^2	Bedload discharge kg/ms
SG10-1	0.1071	0.0178	0.0669	0.00112	0.764	0.00863
SG10-2	0.1049	0.015	0.0660	0.00084	0.566	0.00219
SG10-3	0.1079	0.0125	0.0672	0.00057	0.391	0.000282
SG10-4	0.1073	0.0104	0.0669	0.00038	0.260	0.000045
SG10-5	0.1067	0.023	0.0667	0.00247	1.681	0.05494
SG10-6	0.1058	0.0295	0.0664	0.00373	2.525	0.153
SG25-1	0.1036	0.0176	0.0655	0.00119	0.795	0.00572
SG25-2	0.1024	0.0148	0.0650	0.00103	0.683	0.00208
SG25-3	0.1054	0.0123	0.0662	0.00074	0.500	0.000206
SG25-4	0.1045	0.0104	0.0658	0.00047	0.316	0.000004
SG25-5	0.107	0.0231	0.0668	0.00222	1.514	0.05017
SG25-6	0.1013	0.0293	0.0646	0.00407	2.681	0.169
SG45-1	0.1052	0.0172	0.0661	0.0016	1.079	0.0023
SG45-2	0.1045	0.0146	0.0658	0.00124	0.833	0.000572
SG45-3	0.107	0.012	0.0668	0.00091	0.620	0.000076
SG45-4	0.1045	0.0229	0.0658	0.00268	1.800	0.01399
SG45-5	0.1012	0.0287	0.0645	0.00418	2.751	0.1422
SG45-6	0.1065	0.0259	0.0666	0.00344	2.339	0.08134

Vita

Jaber H. Almedeij was born on November 1, 1971, in Kuwait. He graduated from Kuwait University in 1995 with a Bachelor of Science in Civil Engineering. From 1995 to 1996, he worked for Kuwait National Petroleum Company (KNPC) as an engineer. In 1996, he joined the staff of Kuwait University as a teacher and research assistant in the Civil Engineering Department. In 1997, he was awarded a scholarship by Kuwait University to pursue his graduate studies in Civil Engineering. In 1998, he received a Master of Science in Civil Engineering from the University of Pittsburgh, Pittsburgh, PA. In 2002, he completed the requirements for the Doctor of Philosophy in Civil Engineering from Virginia Polytechnic Institute and State University, Blacksburg, VA.